Received: 15 May 2019 | Revised: 26 September 2019 | Accepted: 1 October 2019

DOI: 10.1002/adc2.20

ORIGINAL ARTICLE

WILEY

Adaptive digital PID control of first-order-lag-plus-dead-time dynamics with sensor, actuator, and feedback nonlinearities

Mohammadreza Kamaldar[1] | **Syed Aseem Ul Islam**[1] | **Sneha Sanjeevini**[1] | **Ankit Goel**[1] | **Jesse B. Hoagg**[2] | **Dennis S. Bernstein**[1]

[1]Department of Aerospace Engineering, University of Michigan, Ann Arbor, Michigan

[2]Department of Mechanical Engineering, University of Kentucky, Lexington, Kentucky

Correspondence
Dennis S. Bernstein, Department of Aerospace Engineering, 1320 Beal Avenue, University of Michigan, Ann Arbor, MI 48109.
Email: dsbaero@umich.edu

Funding information
AFOSR under DDDAS, Grant/Award Number: FA9550-18-1-0171; ONR, Grant/Award Number: N00014-18-1-2211 and N00014-19-1-2273

Abstract

Proportional-integral-derivative (PID) control is one of the most widely used feedback control strategies because of its ability to follow step commands and reject constant disturbances with zero asymptotic error, as well as the ease of tuning. This paper presents an adaptive digital PID controller for sampled-data systems with sensor, actuator, and feedback nonlinearities. The linear continuous-time dynamics are assumed to be first-order lag with dead time (ie, delay). The plant gain is assumed to have known sign but unknown magnitude, and the dead time is assumed to be unknown. The sensor and actuator nonlinearities are assumed to be monotonic, with known trend but are otherwise unknown, and the feedback nonlinearity is assumed to be monotonic, but is otherwise unknown. A numerical investigation is presented to support a simulation-based conjecture, which concerns closed-loop stability and performance. Numerical examples illustrate the effect of initialization on the rate of adaptation and investigate failure modes in cases where the assumptions of the simulation-based conjecture are violated.

KEYWORDS

autotuning, integral control, nonlinear system, time-delay process, process control

1 | INTRODUCTION

The enduring popularity of proportional-integral-derivative (PID) control as the most effective and widely used feedback control strategy is due to at least three reasons. First, one of the most common control objectives is to have the measured output of a process attain a setpoint while rejecting a constant disturbance. The internal model principle[1] implies that an integrator is needed to achieve this goal. Next, a PID controller, at least in its simplest form, entails only three numbers, each of which has a distinct effect on the closed-loop response, thus facilitating tuning. Finally, extensive practical experience with PID controllers helps to ensure that these controllers can be reliably implemented and maintained in applications ranging from a few PID loops to dozens or hundreds of interacting loops operating under changing and uncertain conditions.

The simplicity of PID control, however, is challenged by a multitude of real-world effects. As in all feedback applications, a PID controller must ensure closed-loop stability either by not destabilizing a stable plant or by stabilizing an unstable plant. In fact, the class of linear time-invariant continuous-time plants that can be stabilized by continuous-time PID controllers is a difficult and unsolved problem.[2]

For linear time-invariant continuous-time plants, continuous-time PID controller tuning has been extensively studied, and a vast number of tuning rules have been developed based on analytical models, simulation models, or the actual plant response.[3-9] Since all models are erroneous to some extent and the dynamics of a real system can change unexpectedly, the challenge is to tune the PID controller for reliable performance despite model errors and unpredictable plant changes. Although integral control implies asymptotic setpoint command following, this guarantee is predicated on closed-loop stability. Therefore, for plants whose dynamics change over time, PID tuning for closed-loop stability must be maintained through continual closed-loop identification and careful gain updating. In modern applications, PID controllers are typically implemented digitally,[10-13] and thus sampling analog-to-digital (A/D) and reconstruction digital-to-analog (D/A) effects may impact closed-loop stability and performance.

Beyond these considerations, virtually, all real plants contain nonlinearities, and the problem of stabilizability by PID control is more difficult, especially in the case where the plant nonlinearities are unmodeled, unknown, or uncertain.[14-17] For example, magnitude saturation, which is universal to all control applications, is a nonlinearity that requires antiwindup techniques to avoid divergence of the integrator state and degradation of the ability to follow changing setpoints.[18,19]

Adaptive PID control, also called autotuning, is an attractive extension of fixed-gain PID control. These techniques have been developed for continuous-time control[20-45] and for discrete-time control.[11,12,46-54] Adaptive PID control has the potential to allow PID controllers to continually adjust their gains due to changing plant dynamics with little or no manual intervention.

This paper develops an adaptive digital PID controller based on the approach developed in the work of Rahman et al.[55] The plant is assumed to have linear dynamics with sensor, actuator, and feedback nonlinearities, thus forming a Hammerstein-Wiener-Lur'e system.[56] The linear continuous-time dynamics are assumed to be first-order lag with dead time (ie, delay); these dynamics have been extensively considered in the literature, especially for Ziegler-Nichols PID tuning.[57-71] In this paper, the plant gain is assumed to have known sign but unknown magnitude, and the dead time is assumed to be unknown. The sensor and actuator nonlinearities are assumed to be monotonic, with known trend, but are otherwise unknown, and the feedback nonlinearity is assumed to be monotonic, but is otherwise unknown. Since the controller is digital, the closed-loop system is a sampled-data system, and thus the effect of the sampling rate must be considered. Unlike fixed-gain PID controllers for processes with dead time, the adaptive digital PID controller does not use a Smith predictor.[72-74]

The approach of this paper is nonstandard, focusing on a numerical investigation of the adaptive digital PID controller. Within this numerical investigation, this paper has three main contributions. The first contribution is the simulation-based conjecture (SBC), which states assumptions under which the command-following error is conjectured to be bounded or convergent. The assumptions of SBC include knowledge about the plant parameters as well as properties and knowledge about the sensor, actuator, and feedback nonlinearities. No attempt is made to prove SBC; instead, numerical examples are presented to support its plausibility and motivate future research to prove it.

The second contribution is a demonstration of the effect of the initialization of the recursive-least-squares (RLSs) controller update on the performance of the adaptive digital PID controller. Unlike fixed-gain PID control, where tuning refers to the assignment of feedback parameters, the adaptive digital PID controller is tuned by initializing the RLS matrix P_k, which the adaptive digital PID controller uses to adjust the PID gains. The examples thus provide guidance for determining the effect of this initialization on the transient closed-loop performance. This guidance is not provided by the statement of SBC nor would it be provided by a proof of SBC, were such a proof available.

The third contribution is an investigation of the performance of the adaptive digital PID controller in situations that go beyond the claims of the conjecture. In real-world applications, a PID controller may be subjected to a vast range of conditions that may be unknown and unmodelable. It is therefore essential to assess the ability of the adaptive digital PID controller to operate reliably under conditions that violate the assumptions of SBC.

The contents of this paper are as follows. Section 2 states the sampled-data PID control problem in terms of the basic servo loop with first-order-lag-plus-dead-time dynamics and sensor, actuator, and feedback nonlinearities. The structure of the digital PID controller is presented, including the antiwindup integrator. Section 3 considers stabilizability of the exactly discretized linear dynamics under fixed-gain control. The goal of this section is to show that, under integral control, increased dead time significantly reduces the range of stabilizing gains that the adaptive controller must attain. For the same plant with PID control, Section 4 uses the final value theorem to show that the integrator guarantees asymptotic command following and disturbance rejection for step commands and constant disturbances.

Section 5 presents the adaptive digital PID controller, which is based on RLS. The controller update involves a recursive expression for the 3×3 matrix P_k as well as the controller gain vector θ_k. Section 6 demonstrates how the continuous-time

dynamics are numerically discretized to ensure accuracy of the intersample behavior. Section 7 presents the nominal parameters that are used for all of the examples in this paper.

The remainder of this paper consists of numerical examples illustrating the performance of the adaptive digital PID controller under the assumptions of SBC as well as under conditions that violate the assumptions of SBC. Section 8 presents linear examples (ie, without sensor, actuator, and feedback nonlinearities) that support SBC, whereas Section 9 presents linear examples that demonstrate the effect of violating assumptions of SBC. Sections 10 and 11 present examples that illustrate the effect of sensor, actuator, and feedback nonlinearities, including examples that support SBC as well as examples that violate the assumptions of SBC. In all examples, unless stated otherwise, the sensor noise η is zero. Section 12 goes beyond the focus of this paper by providing a brief investigation of the adaptive digital PID controller for second-order systems. Finally, Section 13 provides an extension of the adaptive digital PID controller that is applicable to a wider class of plants.

2 | ADAPTIVE DIGITAL PID CONTROL PROBLEM

The basic servo loop for a sampled-data Hammerstein-Wiener-Lur'e system with first-order-lag-plus-dead-time dynamics is shown in Figure 1, where r is the command and d is the disturbance. The linear continuous-time dynamics are given by the transfer function

$$G(s) = \frac{Ke^{-\tau_d s}}{\tau_c s + 1}, \tag{1}$$

where $K > 0$ is the DC gain, $\tau_d \geq 0$ is the dead time, and $\tau_c > 0$ is the time constant (also called the lag). The plant is controlled by the adaptive digital PID controller $G_{c,k}$, whose input is the normalized error $\bar{e}_k$ and whose output is the discrete-time requested control u_k. The gains of $G_{c,k}$, and thus the control u_k, are updated at each time step k, with update period $T_s > 0$, by the adaptive control law given in Section 5. The D/A interface for this plant is a zero-order-hold (ZOH) device, whose output is the piecewise-constant continuous-time requested control $u(t)$. In particular, for all $k \geq 0$ and all $t \in [kT_s, (k+1)T_s)$, $u(t)$ is given by

$$u(t) = u_k. \tag{2}$$

The actual control is the continuous-time signal $v = \mathcal{H}(u)$, where the Hammerstein input nonlinearity $\mathcal{H} : \mathbb{R} \to \mathbb{R}$ represents the actuator nonlinearity. The output of G is y_ℓ, where subscript "ℓ" denotes "linear." The sensor output is $y = \mathcal{W}(y_\ell)$, where the Wiener output nonlinearity $\mathcal{W} : \mathbb{R} \to \mathbb{R}$ represents the sensor nonlinearity. The output y_ℓ is fed back to G through the Lur'e feedback nonlinearity $\mathcal{L} : \mathbb{R} \to \mathbb{R}$. In special cases, one or more of the nonlinearities $\mathcal{H}$, $\mathcal{W}$, and $\mathcal{L}$ may be absent. In particular, if $\mathcal{H}$, $\mathcal{W}$, and $\mathcal{L}$ are absent, then they are replaced by the gains 1, 1, and 0, respectively.

In the presence of sensor noise η, the measurement is the noisy sensor output $y_n = y + \eta$. The A/D device samples y_n with sample time T_s to produce the discrete-time measurement $y_{n,k} \triangleq y_n(kT_s)$. In the absence of sensor noise η, $y_{n,k}$ is replaced by $y_k \triangleq y(kT_s)$. The error is given by $e_k = r_k - y_{n,k}$, where r_k is the sampled version of the command r. Note that e_k is a noisy sampled version of the true error $r - y_\ell$.

Error e_k passes through the error-normalization function $g : \mathbb{R} \to \mathbb{R}$ to generate the normalized error $\bar{e}_k$. The error-normalization function g is a sigmoid function that satisfies

$$g'(0) = \nu, \qquad \lim_{e_k \to \infty} g(e_k) = -\lim_{e_k \to -\infty} g(e_k) = \mu, \tag{3}$$

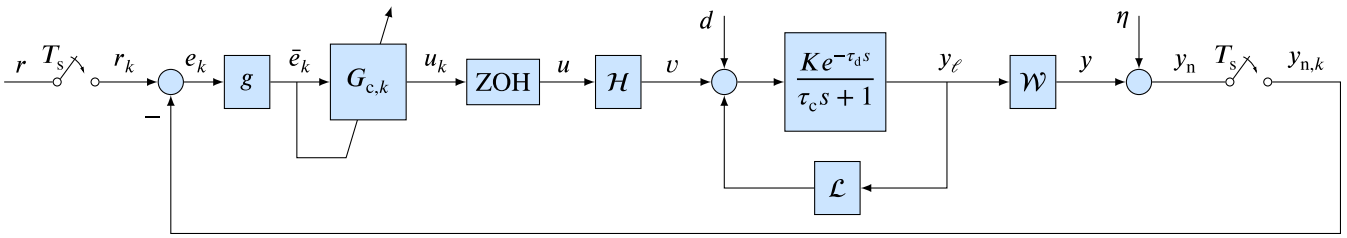

FIGURE 1 Basic servo loop for the sampled-data Hammerstein-Wiener-Lur'e system with first-order-lag-plus-dead-time dynamics, where y_n is the noisy measurement. The error $e_k = r_k - y_{n,k}$ is passed through the error-normalization function g to generate the normalized error $\bar{e}_k$. The normalized error $\bar{e}_k$ is the input to the proportional-integral-derivative controller $G_{c,k}$, whose gains are adaptively updated at each time step. ZOH, zero-order-hold

where $\nu > 0$ and $\mu > 0$. Candidate sigmoid functions that satisfy (3) include the odd, increasing, C^∞ functions

$$g(e_k) = \frac{\mu\nu e_k}{\mu + \nu|e_k|}, \qquad g(e_k) = \frac{2\mu}{\pi}\operatorname{atan}\frac{\pi\nu e_k}{2\mu}, \qquad g(e_k) = \frac{\mu\nu e_k}{\sqrt{\mu^2 + \nu^2 e_k^2}}, \tag{4}$$

$$g(e_k) = \mu\tanh\frac{\nu e_k}{\mu}, \qquad g(e_k) = \frac{2\mu}{\sqrt{\pi}}\int_0^{\sqrt{\pi}\nu e_k/(2\mu)} e^{-x^2}\,\mathrm{d}x. \tag{5}$$

By constraining the magnitude of the input to $G_{c,k}$, these functions ensure robustness to the transients arising from the choice of P_0 required by the adaptive digital PID controller. Note that the units of μ/ν must be equal to the units of e_k. Choosing μ to be dimensionless, it follows that νe_k and $\bar{e}_k = g(e_k)$ are also dimensionless and, thus, the units of ν are the same as the units of $1/e_k$. All five functions are plotted in Figure 2 for $\mu = 1$ and $\nu = 1$.

The discrete-time requested control u_k, which is determined by the adaptive digital PID controller, has the form

$$u_k = \kappa_{p,k}\bar{e}_{k-1} + \kappa_{i,k}\xi_{k-1} + \kappa_{d,k}(\bar{e}_{k-1} - \bar{e}_{k-2}), \tag{6}$$

where $\kappa_{p,k}$, $\kappa_{i,k}$, and $\kappa_{d,k}$ are time-varying PID gains and

$$\xi_k \triangleq \sum_{j=0}^{k}\bar{e}_j. \tag{7}$$

Note that, in (6), the data used by the controller to determine u_k are sampled at steps $k-1$ and $k-2$. This restriction avoids direct feedthrough, which requires instantaneous computation and corresponds to a strictly proper controller. Therefore, (6) is suitable for real-time digital implementation. This digital PID controller structure facilitates the adaptive control algorithm described in Section 5. Alternative digital PID controller structures are considered in related works.[12,75,76]

It turns out that control-magnitude saturation determined by the actuator nonlinearity $\mathcal{H}$ may cause ξ_k to diverge; this is the integrator-windup phenomenon. In order to suppress integrator windup, we replace (7) with

$$\xi_k \triangleq \sum_{j=0}^{k}\bar{e}_j - \begin{cases} \left(\operatorname{sign}\sum_{j=0}^{k}\bar{e}_j\right)(\underline{u} - u_k), & u_k < \underline{u}, \\ 0, & \underline{u} \le u_k \le \bar{u}, \\ \left(\operatorname{sign}\sum_{j=0}^{k}\bar{e}_j\right)(u_k - \bar{u}), & u_k > \bar{u}, \end{cases} \tag{8}$$

where $\underline{u} < \bar{u}$ are the lower and upper antiwindup thresholds; the choice of these thresholds is discussed in Section 5. A related antiwindup technique is given in the work of Åström and Wittenmark.[77,p310-311]

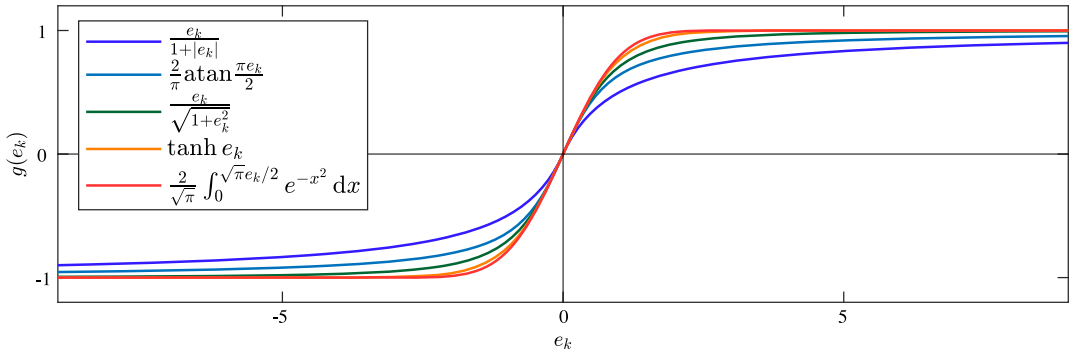

FIGURE 2 Error-normalization functions defined by (4) and (5) with $\mu = 1$ and $\nu = 1$

3 | STABILIZABILITY OF THE EXACTLY DISCRETIZED DYNAMICS UNDER FIXED-GAIN INTEGRAL CONTROL

This section analyzes stabilizability of the sampled-data first-order-lag-plus-dead-time plant in the absence of sensor, actuator, and feedback nonlinearities, with the error-normalization function absent, under the assumption that the integrator gain is constant, and with the proportional and derivatives gains absent. Hence, only integral action is considered.

To exactly discretize (1), we first remove the dead time from G to obtain $\hat{G}(s) \triangleq \frac{K}{\tau_c s+1}$. The zero-order-hold discretization of $\hat{G}$ is given by

$$\hat{G}_d(\mathbf{z}) \triangleq \frac{K(1-\alpha)}{\mathbf{z}-\alpha}, \tag{9}$$

where $\alpha \triangleq e^{-\frac{T_s}{\tau_c}} \in (0,1)$. Assuming that $\tau_d = n_d T_s$, where n_d is a nonnegative integer, it follows that the discrete-time counterpart of the dead time $e^{-\tau_d s} = e^{-n_d T_s s}$ is $\mathbf{z}^{-n_d}$. Using (9), the exact discretization of (1) with sample time T_s is thus given by

$$G_d(\mathbf{z}) \triangleq \frac{K(1-\alpha)}{\mathbf{z}^{n_d}(\mathbf{z}-\alpha)}. \tag{10}$$

Next, let $\kappa_i \in \mathbb{R}$, and consider the discrete-time integral controller

$$G_c(\mathbf{z}) = \frac{\kappa_i}{\mathbf{z}-1}, \tag{11}$$

which yields the loop transfer function

$$L(\mathbf{z}) \triangleq G_d(\mathbf{z})G_c(\mathbf{z}) = \frac{K(1-\alpha)\kappa_i}{\mathbf{z}^{n_d}(\mathbf{z}-\alpha)(\mathbf{z}-1)}. \tag{12}$$

The characteristic polynomial of the closed-loop system is thus given by

$$p(\mathbf{z}) \triangleq \mathbf{z}^{n_d}(\mathbf{z}-1)(\mathbf{z}-\alpha)+\beta, \tag{13}$$

where

$$\beta \triangleq K(1-\alpha)\kappa_i. \tag{14}$$

Proposition 1. *Consider the closed-loop characteristic polynomial p defined by (13), where $\alpha \in (0,1)$, $\beta \in \mathbb{R}$, and n_d is a nonnegative integer. For all nonnegative integers n_d, define*

$$\mathcal{S}(n_d) \triangleq \{(\alpha,\beta) \in (0,1)\times\mathbb{R} : p \text{ is asymptotically stable}\}.$$

Then, the following statements hold.

i) If p is asymptotically stable, then $0<\beta<1$.

ii) Let $n_d = 0$. Then, p is asymptotically stable if and only if $0<\beta<1$ and

$$\beta < 1-\alpha. \tag{15}$$

iii) Let $n_d = 1$. Then, p is asymptotically stable if and only if $0<\beta<1$ and

$$\beta^2+(\alpha+1)\beta < 1-\alpha. \tag{16}$$

iv) Let $n_d = 2$. Then, p is asymptotically stable if and only if $0<\beta<1$ and

$$-\beta^3+(\alpha+1)\beta^2+(\alpha^2+2)\beta < 1-\alpha. \tag{17}$$

v) $\mathcal{S}(2) \subsetneq \mathcal{S}(1) \subsetneq \mathcal{S}(0)$.

vi) There exists $\bar{\beta} > 0$ such that, for all $\beta \in (0,\bar{\beta})$, p is asymptotically stable.

Proof. *i*) to *iv*) follow by applying the Jury test[78,p35] to (13). To show *v*), note that

$$\beta < (\alpha+1)\beta < \beta^2 + (\alpha+1)\beta,$$

which implies $\mathcal{S}(1) \subsetneq \mathcal{S}(0)$. Next, assume that $\beta \in \mathcal{S}(2)$, and it follows that

$$\beta < 2\beta - \beta^3 < -\beta^3 + (\alpha+1)\beta^2 + (\alpha^2+2)\beta < 1-\alpha,$$

which implies

$$\beta^3 < \beta^2 < \beta(1-\alpha).$$

Thus,

$$\begin{aligned}\beta^2 + (\alpha+1)\beta &< \beta^2 + (\alpha+1)\beta + (1-\alpha)\beta - \beta^3 \\ &= \beta^2 + 2\beta - \beta^3 < \beta^2 + (\alpha^2+2)\beta - \beta^3 \\ &< (\alpha+1)\beta^2 + (\alpha^2+2)\beta - \beta^3 \\ &< 1-\alpha.\end{aligned}$$

Hence, $\beta \in \mathcal{S}(1)$. Since, in addition, $\mathcal{S}(2) \neq \mathcal{S}(1)$, it follows that $\mathcal{S}(2) \subsetneq \mathcal{S}(1)$. To prove *vi*), note that the angle of departure for the root $\mathbf{z} = 1$ of (13) as a function of $\beta > 0$ is 180°. It thus follows that there exists $\bar{\beta} > 0$ such that, for all $\beta \in (0, \bar{\beta})$, the roots of (13) lie in the open unit disk and, thus, the corresponding closed-loop system is asymptotically stable. □

It follows from *vi*) of Proposition 1 that, for all nonnegative integers n_d and all $\alpha \in (0,1)$, the discretized plant (10) is stabilizable by an integral controller of form (11). The stability regions for $n_\mathrm{d} \in \{0, 1, \ldots, 15\}$ are illustrated in Figure 3, which shows that these regions are nested. An open conjecture is that these regions are nested for all nonnegative n_d.

4 | ASYMPTOTIC ANALYSIS OF THE EXACTLY DISCRETIZED DYNAMICS UNDER FIXED-GAIN PID CONTROL

This section analyzes the asymptotic response of the sampled-data first-order-lag-plus-dead-time plant in the absence of sensor, actuator, and feedback nonlinearities, with the error-normalization function absent, and under the assumption that the gains of the PID controller (6), (7) are fixed (ie, $\kappa_{\mathrm{p},k} \equiv \kappa_\mathrm{p} \in \mathbb{R}$, $\kappa_{\mathrm{i},k} \equiv \kappa_\mathrm{i} \in \mathbb{R}$, $\kappa_{\mathrm{d},k} \equiv \kappa_\mathrm{d} \in \mathbb{R}$).

The PID controller (6), (7) has the discrete-time linear time-invariant transfer function

$$G_\mathrm{c}(\mathbf{z}) \triangleq \frac{\kappa_\mathrm{p}}{\mathbf{z}} + \frac{\kappa_\mathrm{i}}{\mathbf{z}-1} + \frac{\kappa_\mathrm{d}(\mathbf{z}-1)}{\mathbf{z}^2} = \frac{a_2\mathbf{z}^2 + a_1\mathbf{z} + a_0}{\mathbf{z}^2(\mathbf{z}-1)}, \tag{18}$$

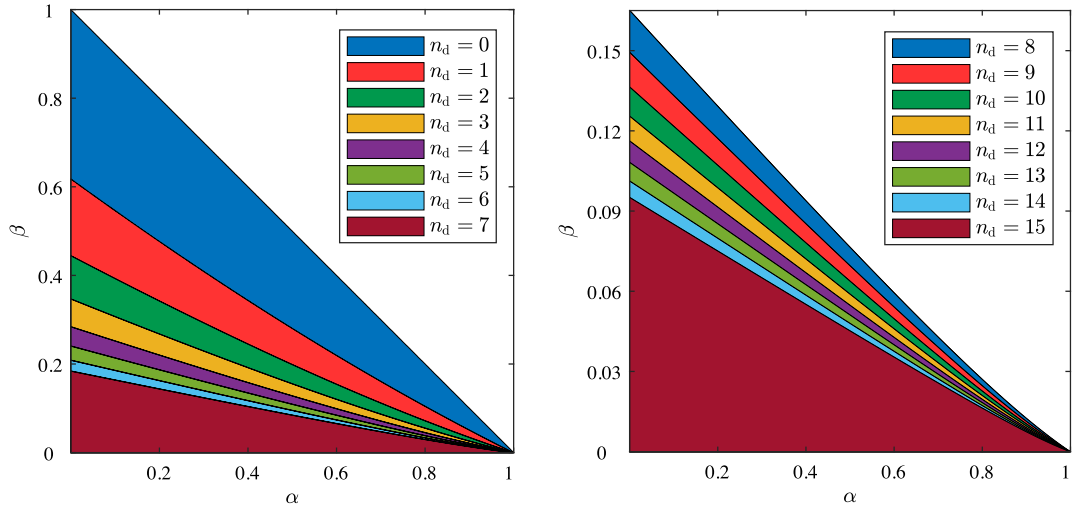

FIGURE 3 Stability regions in terms of (α, β) for $n_\mathrm{d} \in \{0, 1, \ldots, 15\}$. The regions are nested

where

$$a_2 \triangleq \kappa_\mathrm{p} + \kappa_\mathrm{i} + \kappa_\mathrm{d}, \quad a_1 \triangleq -\kappa_\mathrm{p} - 2\kappa_\mathrm{d}, \quad a_0 \triangleq \kappa_\mathrm{d}. \tag{19}$$

Note that the order of G_c is three or less, depending on its zeros. In particular, if $\kappa_\mathrm{i} = 0$, then $a_2 + a_1 + a_0 = 0$, and thus, the numerator of G_c has a root at $\mathbf{z} = 1$, which cancels the pole at $\mathbf{z} = 1$. In this case, (18) becomes

$$G_\mathrm{c}(\mathbf{z}) = \frac{(\kappa_\mathrm{p} + \kappa_\mathrm{d})\mathbf{z} - \kappa_\mathrm{d}}{\mathbf{z}^2}. \tag{20}$$

However, if $\kappa_\mathrm{i} \neq 0$, then $a_2 + a_1 + a_0 = \kappa_\mathrm{i} \neq 0$, and thus, $\mathbf{z} = 1$ is not a zero of G_c. The DC gain of G_c is thus given by

$$|G_\mathrm{c}(1)| = \begin{cases} \kappa_\mathrm{p}, & \kappa_\mathrm{i} = 0, \\ \infty, & \kappa_\mathrm{i} \neq 0. \end{cases} \tag{21}$$

Combining plant (10) with controller (18) implies that the closed-loop transfer function $\tilde{G}_{er}$ from the command r to the error e is given by

$$\begin{aligned} \tilde{G}_{er}(\mathbf{z}) &\triangleq \frac{1}{1 + G_\mathrm{d}(\mathbf{z})G_\mathrm{c}(\mathbf{z})} \\ &= \frac{\mathbf{z}^{n_\mathrm{d}+2}(\mathbf{z} - \alpha)(\mathbf{z} - 1)}{\mathbf{z}^{n_\mathrm{d}+2}(\mathbf{z} - \alpha)(\mathbf{z} - 1) + K(1 - \alpha)(a_2\mathbf{z}^2 + a_1\mathbf{z} + a_0)}. \end{aligned} \tag{22}$$

Assuming that the closed-loop transfer function $\tilde{G}_{er}$ is asymptotically stable, the asymptotic response of $\tilde{G}_{er}$ to a unit step command with $d = 0$ and $\eta = 0$ is given by the discrete-time final-value theorem[79, p139]

$$\begin{aligned} \lim_{k\to\infty} e_k &= \lim_{\mathbf{z}\to 1}(\mathbf{z} - 1)\tilde{G}_{er}(\mathbf{z})\frac{\mathbf{z}}{\mathbf{z} - 1} \\ &= \lim_{\mathbf{z}\to 1} \frac{\mathbf{z}^{n_\mathrm{d}+3}(\mathbf{z} - \alpha)(\mathbf{z} - 1)}{\mathbf{z}^{n_\mathrm{d}+2}(\mathbf{z} - \alpha)(\mathbf{z} - 1) + K(1 - \alpha)(a_2\mathbf{z}^2 + a_1\mathbf{z} + a_0)} \\ &= \begin{cases} \frac{1}{1+K\kappa_\mathrm{p}}, & \kappa_\mathrm{i} = 0, \\ 0, & \kappa_i \neq 0. \end{cases} \end{aligned} \tag{23}$$

Likewise, the closed-loop transfer function $\tilde{G}_{ed}$ from the disturbance d to the error e is given by

$$\begin{aligned} \tilde{G}_{ed}(\mathbf{z}) &\triangleq \frac{G_\mathrm{d}(\mathbf{z})}{1 + G_\mathrm{d}(\mathbf{z})G_\mathrm{c}(\mathbf{z})} \\ &= \frac{K(1 - \alpha)\mathbf{z}^2(\mathbf{z} - 1)}{\mathbf{z}^{n_\mathrm{d}+2}(\mathbf{z} - \alpha)(\mathbf{z} - 1) + K(1 - \alpha)(a_2\mathbf{z}^2 + a_1\mathbf{z} + a_0)}. \end{aligned} \tag{24}$$

Assuming that the closed-loop transfer function $\tilde{G}_{ed}$ is asymptotically stable, the asymptotic response of $\tilde{G}_{ed}$ to a unit step disturbance with $r = 0$ and $\eta = 0$ is given by

$$\begin{aligned} \lim_{k\to\infty} e_k &= \lim_{\mathbf{z}\to 1}(\mathbf{z} - 1)\tilde{G}_{ed}(\mathbf{z})\frac{\mathbf{z}}{\mathbf{z} - 1} \\ &= \lim_{\mathbf{z}\to 1} \frac{K(1 - \alpha)\mathbf{z}^3(\mathbf{z} - 1)}{\mathbf{z}^{n_{\mathrm{d}+2}}(\mathbf{z} - \alpha)(\mathbf{z} - 1) + K(1 - \alpha)(a_2\mathbf{z}^2 + a_1\mathbf{z} + a_0)} \\ &= \begin{cases} \frac{K}{1+K\kappa_\mathrm{p}}, & \kappa_\mathrm{i} = 0, \\ 0, & \kappa_i \neq 0. \end{cases} \end{aligned} \tag{25}$$

Therefore, if the closed-loop transfer functions $\tilde{G}_{er}$ and $\tilde{G}_{ed}$ are asymptotically stable and $\kappa_\mathrm{i} \neq 0$, then, for all step commands and step disturbances, the asymptotic command-following error is zero for arbitrary values of κ_p, κ_d, n_d, K, and α.

5 | ADAPTIVE DIGITAL PID CONTROLLER AND THE SBC

Control (6) can be expressed as

$$u_k = \phi_k \theta_k, \tag{26}$$

where

$$\phi_k \triangleq \begin{bmatrix} \bar{e}_{k-1} & \xi_{k-1} & \bar{e}_{k-1} - \bar{e}_{k-2} \end{bmatrix} \in \mathbb{R}^{1\times 3}, \quad \theta_k \triangleq \begin{bmatrix} \kappa_{\mathrm{p},k} \\ \kappa_{\mathrm{i},k} \\ \kappa_{\mathrm{d},k} \end{bmatrix} \in \mathbb{R}^3. \tag{27}$$

Note that regressor ϕ_k is constructed from the past values of e_k and ξ_k; and the controller coefficient vector θ_k contains the time-dependent proportional, integral, and derivative gains $\kappa_{\mathrm{p},k}$, $\kappa_{\mathrm{i},k}$, and $\kappa_{\mathrm{d},k}$.

To determine the adaptive law for updating θ_k, let $\theta \in \mathbb{R}^3$, and consider the *retrospective performance variable* defined by

$$\hat{z}_k(\theta) \triangleq \bar{e}_k - \sigma(u_{k-1} - \phi_{k-1}\theta), \tag{28}$$

where σ is either 1 or -1. Furthermore, define the *retrospective cost function* $J_k : \mathbb{R}^3 \to [0, \infty)$ by

$$J_k(\theta) \triangleq \sum_{i=0}^{k} \hat{z}_i^2(\theta) + (\theta - \theta_0)^{\mathrm{T}} P_0^{-1} (\theta - \theta_0), \tag{29}$$

where $\theta_0 \in \mathbb{R}^3$ is the initial vector of PID gains and $P_0 \in \mathbb{R}^{3\times 3}$ is a positive-definite matrix that provides regularization. Applying recursive least squares minimization,[80,81,p20] to (29) implies that, for all $k \geq 0$,

$$\theta_{k+1} = \theta_k + (\sigma \bar{e}_k - u_{k-1} + \phi_{k-1}\theta_k) P_{k+1} \phi_{k-1}^{\mathrm{T}}, \tag{30}$$

where

$$P_{k+1} = P_k - \frac{1}{1 + \phi_{k-1} P_k \phi_{k-1}^{\mathrm{T}}} P_k \phi_{k-1}^{\mathrm{T}} \phi_{k-1} P_k, \tag{31}$$

and where $\bar{e}_{-3} = \bar{e}_{-2} = \bar{e}_{-1} \triangleq 0$, $\xi_{-1} \triangleq 0$, and $u_{-1} \triangleq 0$ are the initial conditions. The adaptive digital PID controller is thus given by (8), (26), (27), (30), and (31). Note that this choice of initial conditions implies that $\phi_{-1} = 0$. It thus follows that $P_1 = P_0$ and $\theta_1 = \theta_0$. Consequently, if $\theta_0 = 0$, then the first possibly nonzero control input is u_2. A timing diagram showing the implementation of the adaptive digital PID controller is given in Figure 4. Note that the adaptive digital PID control can be specialized to adaptive digital PI, PD, ID, P, I, and D control by omitting the corresponding components of ϕ_k and θ_k.

The following result describes properties of (26)-(31). A proof is given in theorem 1 in the work of Islam and Bernstein.[80]

Proposition 2. *Consider (26)-(31), where $\theta_0 \in \mathbb{R}^3$ and $P_0 \in \mathbb{R}^{3\times 3}$ is positive definite. Then, for all $k \geq 0$, θ_{k+1} is the unique global minimizer of J_k.*

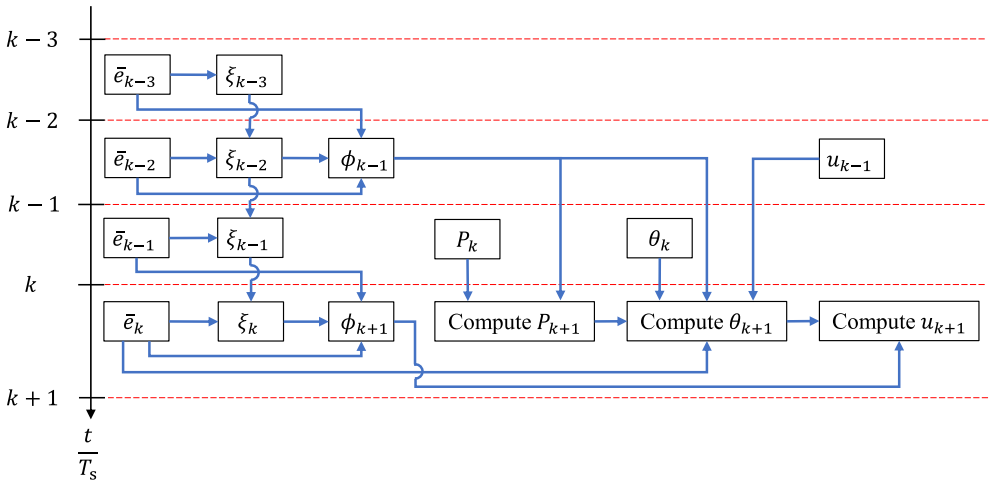

FIGURE 4 Timing diagram for the adaptive digital proportional-integral-derivative controller. The controller coefficient vector θ_{k+1} and the control $u_{k+1} = \phi_{k+1}\theta_{k+1}$ are computed between steps k and $k+1$ for implementation at step $k+1$

Next, we present the SBC, which specifies assumptions under which the signals in the basic servo loop are bounded or convergent. The following definitions are used in SBC. Let $f : \mathbb{R} \to \mathbb{R}$. Then, f is nondecreasing (respectively, nonincreasing) if, for all $x, y \in \mathbb{R}$ such that $x \le y$, it follows that $f(x) \le f(y)$ (respectively, $f(x) \ge f(y)$). Furthermore, f is increasing (respectively, decreasing) if, for all $x, y \in \mathbb{R}$ such that $x < y$, it follows that $f(x) < f(y)$ (respectively, $f(x) > f(y)$). If $\mathcal{H}$ is nondecreasing, then trend $\mathcal{H} = 1$; if $\mathcal{H}$ is nonincreasing, then trend $\mathcal{H} = -1$. The same terminology applies to $\mathcal{W}$.

For SBC, the lower and upper antiwindup thresholds needed for (8) determine the range of feasible commands r, where command r is *feasible* if there exists a constant control input u that can produce output $y = r$. Feasibility is addressed by (A12). For SBC, the existence of a limit implies that the limit is finite.

Simulation-based conjecture (SBC). Consider the basic servo loop shown in Figure 1, where the adaptive digital PID controller $G_{c,k}$ is given by (8), (26), (27), (31), and (30). Furthermore, consider the following assumptions.

(A1) K is constant and nonzero, and sign K is known, but K is otherwise unknown.
(A2) τ_c is constant and positive, but τ_c is otherwise unknown.
(A3) τ_d is constant and nonnegative, but τ_d is otherwise unknown.
(A4) r is constant but is otherwise unknown.
(A5) d is constant but is otherwise unknown.
(A6) $\mathcal{H}$ is either nondecreasing or nonincreasing and trend $\mathcal{H}$ is known, but $\mathcal{H}$ is otherwise unknown.
(A7) $\mathcal{W}$ is either nondecreasing or nonincreasing and trend $\mathcal{W}$ is known, but $\mathcal{W}$ is otherwise unknown.
(A8) $\mathcal{L}$ is either nondecreasing or nonincreasing, but $\mathcal{L}$ is otherwise unknown.
(A9) $\sigma \triangleq (\text{trend } \mathcal{H})(\text{trend } \mathcal{W})\text{sign } K$.
(A10) η is bounded but is otherwise unknown.
(A11) $\eta = 0$, that is, $y_n = y$.
(A12) $\mathcal{F}(r, d) \triangleq \{(u, y_\ell) \in [\underline{u}, \bar{u}] \times \mathbb{R} : K(\mathcal{L}(y_\ell) + \mathcal{H}(u) + d) = y_\ell \text{ and } \mathcal{W}(y_\ell) = r\}$ is nonempty.
(A13) $\mathcal{W}$ is either increasing or decreasing.
(A14) $\mathcal{W}(r) = r$.

Then, for all $\nu > 0$ and all positive-definite P_0, the following statements hold.

i. Assume that (A1) to (A10) are satisfied. Then, for all initial conditions of the plant and integrator state, u_k, ξ_k, y_k, $\kappa_{p,k}$, $\kappa_{i,k}$, and $\kappa_{d,k}$ are bounded.
ii. Assume that (A1) to (A12) are satisfied. Then, for all initial conditions of the plant and integrator state, $\lim_{k\to\infty} u_k$, $\lim_{k\to\infty} \xi_k$, $\lim_{k\to\infty} y_k$, $\lim_{k\to\infty} \kappa_{p,k}$, $\lim_{k\to\infty} \kappa_{i,k}$, and $\lim_{k\to\infty} \kappa_{d,k}$ exist, and $\lim_{t\to\infty} y(t) = r$.
iii. Assume that (A1) to (A14) are satisfied. Then, for all initial conditions of the plant and integrator state, $\lim_{t\to\infty} y_\ell(t) = r$.

Although the setpoint command r is usually known in practice, (A4) allows for the possibility that only error e_k is known. This situation occurs in applications where the error is measured directly as the offset from the command, but the commanded setpoint r is not separately measured. A measurement of r is useful in the case where command feedforward is used; however, only feedback control using e_k is considered in this paper.

For a given command r and a disturbance d, set $\mathcal{F}(r, d)$ defined in (A12) is the *feasibility set*. This set consists of the constant values of the input u and output y for which the output of the sensor nonlinearity $\mathcal{W}$ is equal to command r in the presence of the disturbance d. If $\mathcal{F}(r, d)$ is not empty, then there exist a constant input u and a constant output y_ℓ under which output y of $\mathcal{W}$ is equal to command r in the presence of disturbance d. In this case, the command r is *feasible*; otherwise, r is *infeasible*. Note that the feasibility of r depends on d as well as gain K and nonlinearities $\mathcal{H}$, $\mathcal{W}$, and $\mathcal{L}$. Finally, note that, in the case where $\mathcal{H}$ and $\mathcal{W}$ are absent, $\mathcal{F}(r, d)$ is given by

$$\mathcal{F}(r, d) \triangleq \left\{u \in [\underline{u}, \bar{u}] : K(\mathcal{L}(r) + u + d) = r\right\}, \tag{32}$$

which is nonempty since $u = r/K - \mathcal{L}(r) - d \in \mathcal{F}(r, d)$.

Note that, because d, K, $\mathcal{H}$, $\mathcal{W}$, and $\mathcal{L}$ are assumed to be unknown, it is not possible to verify (A12) to determine whether or not a given setpoint command r is feasible. Furthermore, for a given setpoint command r that is known to be feasible, it is not possible to determine *a priori* the control input u needed to ensure that $\lim_{t\to\infty} y(t) = r$. However, it follows from SBC that the adaptive digital PID controller yields the required asymptotic control input. Note that (A13) and (A14) are sufficient conditions under which output y_ℓ of G converges to r.

In order to maximize the range of feasible commands r, it is desirable to choose $\bar{u} - \underline{u}$ to be as large as possible. On the other hand, choosing $\bar{u} - \underline{u}$ to be as small as possible tends to reduce the effect of windup as reflected by the magnitude of ξ_k. This tradeoff must thus be considered in selecting $\bar{u}$ and $\underline{u}$. If $\lim_{u\to-\infty}\mathcal{H}(u) = -\infty$, then we set $\underline{u} = -\infty$, which implies that the first case in (8) is absent. Likewise, if $\lim_{u\to\infty}\mathcal{H}(u) = \infty$, then we set $\bar{u} = \infty$, which implies that the third case in (8) is absent. However, since all real actuators are subject to magnitude saturation, these cases do not occur in practice. For example, the standard saturation function is

$$\mathcal{H}(u) = \begin{cases} u, & |u| \le 1, \\ \operatorname{sign} u, & |u| > 1. \end{cases} \tag{33}$$

In this case, it is desirable to choose $\underline{u} = -1$ and $\bar{u} = 1$ to minimize the impact of integrator windup. As will be shown, choosing $\underline{u} << -1$ and $\bar{u} >> 1$ may exacerbate windup; however, these choices do not contradict SBC. Choosing suitable values of $\underline{u}$ and $\bar{u}$ may require some knowledge of $\mathcal{H}$; however, this knowledge is not assumed in SBC.

Note that (A6) to (A8) do not require $\mathcal{H}$, $\mathcal{W}$, and $\mathcal{L}$ to be continuous; however, since these functions are either nonincreasing or nondecreasing, they can have only jump discontinuities. For example, $\mathcal{W}$ may represent sensor quantization. To avoid cases that are not amenable to simulation, these functions are chosen to have at most a finite number of jumps in every finite interval. Finally, $\mathcal{H}$, $\mathcal{W}$, and $\mathcal{L}$ may be piecewise C^1 with slope discontinuities.

6 | NUMERICAL SIMULATION OF THE INTERSAMPLE BEHAVIOR

This section describes the numerical integration method used to simulate the intersample behavior of the continuous-time dynamics of G combined with the adaptive digital PID controller. The adaptive digital controller $G_{c,k}$ shown in Figure 1 operates on the measured noisy error e_k available at the time step k to provide the requested control u_{k+1} at the next time step $k + 1$. However, the continuous-time dynamics evolve between sample times. In order to assess the effect of the adaptive digital PID controller on the intersample behavior, the state trajectory is numerically integrated between sample instants using the Matlab ODE45 function. In particular, for all examples, ODE45 is called 1000 times during each sample interval of length T_s. ODE45 uses the default tolerance 10^{-8} to determine the required variable step lengths during each integration interval of length $T_s/1000$. The choice of integration interval of length $T_s/1000$ is used to relate the variance of the discrete-time process and sensor noise to the intensities of the corresponding continuous-time noise signals.

In the case where the dead time τ_d is an integer multiple n_d of the sample time T_s, the effect of the dead time τ_d at the sample times is exactly represented by z^{-n_d}. Since the continuous-time dynamics without dead time can be exactly integrated with a zero-order-hold input, it follows that, in this case, the plant with dead time can be exactly propagated at the sample times. This ability can be used to assess the accuracy of the fixed-step numerical integration. In particular, for each example, where τ_d is an integer multiple n_d of T_s, the sampled values are propagated using exact discretization of the continuous-time dynamics. These values are superimposed on the fixed-step numerical integration of the continuous-time dynamics from the initial condition. This technique is illustrated in Figure 5 for plant (1), with $K = 1$, $\tau_c = 1$ s, and $\tau_d = 5$ s; and where $d = 0$, $\eta = 0$, and $u = 1$. Letting $T_s = 1$ s/sample implies that $n_d = \tau_d/T_s = 5$ samples, and, thus, the state at the sample times can be obtained using the exactly discretized dynamics as well as fixed-step numerical integration. Figure 5 shows the step response of the plant. This procedure is used to validate the accuracy of the numerical integration for all examples for which exact discretization is possible.

7 | NOMINAL PARAMETERS FOR ALL EXAMPLES IN THIS PAPER

For all of the examples in this paper, θ_k is initialized as $\theta_0 = 0$ to reflect the absence of additional prior modeling information. However, the digital PID gains can be initialized arbitrarily in practice based on prior knowledge. In addition, for all of the examples, g is chosen to be the first function in (4), and, unless stated otherwise, $\mu = 1$, $\nu = 0.02$, and $P_0 = p_0 I_3$, where $p_0 = 1$ and I_3 is the 3×3 identity matrix.

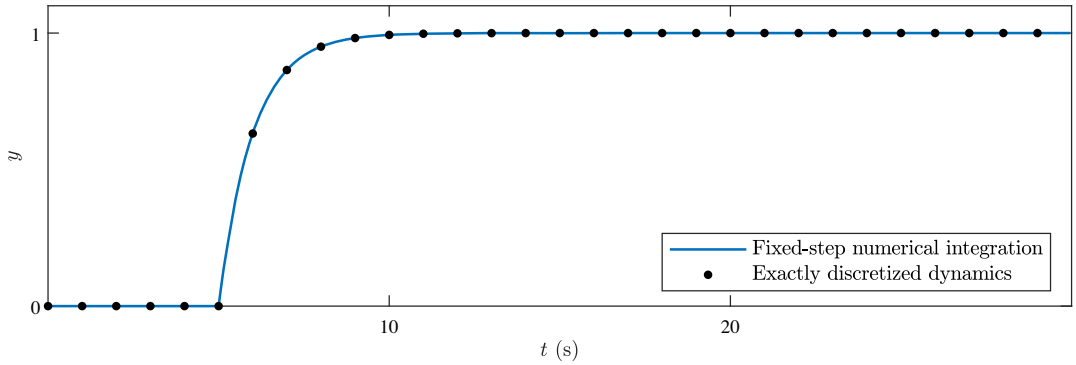

FIGURE 5 Fixed-step numerical integration based on ODE45 (blue line) is used to integrate (1) with $K = 1$, $\tau_c = 1$ s, and $\tau_d = 5$ s, where $d = 0$, $\eta = 0$, and $u = 1$. The black dots represent the response of the exactly discretized plant (1) with $T_s = 1$ s/sample. This procedure is used to validate the accuracy of the numerical integration for all examples for which exact discretization is possible (ie, τ_d is an integer multiple of T_s)

For all of the examples, unless stated otherwise, the nominal plant parameters are $K = 1$, $\tau_c = 1$ s, $\tau_d = 1$ s, and $T_s = 0.1$ s/sample. With these nominal values, it follows that $n_d = 10$ samples. Unless stated otherwise, for all examples in this paper, command r and disturbance d are abruptly changing and are given by

$$r(t) = \begin{cases} 8, & 0 \le t < 0.2t_f, \\ -9, & 0.2t_f \le t < 0.6t_f, \\ 4, & 0.6t_f \le t \le t_f, \end{cases} \qquad d(t) = \begin{cases} -5, & 0 \le t < 0.4t_f, \\ 8, & 0.4t_f \le t \le t_f, \end{cases} \tag{34}$$

where the duration t_f of the simulation for each example is given by the final time on the horizontal axis of the associated time-history figures. Since r and d are not constant, these choices of the command and disturbance are not consistent with SBC. However, after each change in r and d, which are piecewise constant, the asymptotic error can be assessed, where "asymptotic" refers to the response just before the next change in r or d. Unless stated otherwise, for all examples in this paper, the sensor noise η is zero. Finally, for all examples in this paper, unless stated otherwise, the antiwindup thresholds are chosen to be $\bar{u} = -\underline{u} = 50$. Except in cases where r is infeasible and windup can occur, these values are inconsequential.

8 | LINEAR EXAMPLES SUPPORTING SBC

The examples in this section consider the performance of the adaptive digital PID controller for the basic servo loop shown in Figure 1, where $v = \mathcal{H}(u) = u$, $y = \mathcal{W}(y_\ell) = y_\ell$, and $\mathcal{L}(y_\ell) = 0$. In order to investigate the effect of plant parameters and controller weightings on closed-loop performance, the nominal plant parameters and controller weightings are modified in each example by perturbing them both above and below their nominal values. In particular, the examples in this section consider the effect of variations in K, τ_c, τ_d, and T_s, where both fast and slow sampling are considered, and where "fast" refers to a sample interval that is shorter than the dead time and "slow" refers to a sample interval that is longer than the dead time. The values considered are shown in Table 1.

TABLE 1 Summary of adaptive digital PID control for linear examples supporting SBC

Example	Investigated Effect	Remarks
1	RLS initialization $P_0 = p_0 I_3$	$p_0 = 0.1, 1, 10$
2	Slope $\nu = g'(0)$	$\nu = 0.01, 0.02, 0.04$
3	Gain K	$K = 0.5, 1, 2$
4	Time constant τ_c	$\tau_c = 0.2, 1, 5$ s
5	Dead time τ_d	$\tau_d = 0.49, 3, 5.01$ s
6	Fast sampling with $T_s < \tau_d$	$T_s = 0.047, 0.1, 0.23$ s/sample
7	Slow sampling with $T_s > \tau_d$	$T_s = 1.9, 5, 11.7$ s/sample
8	Sensor noise η	Uniform white noise with $\mu_\eta = 1, 2, 3$

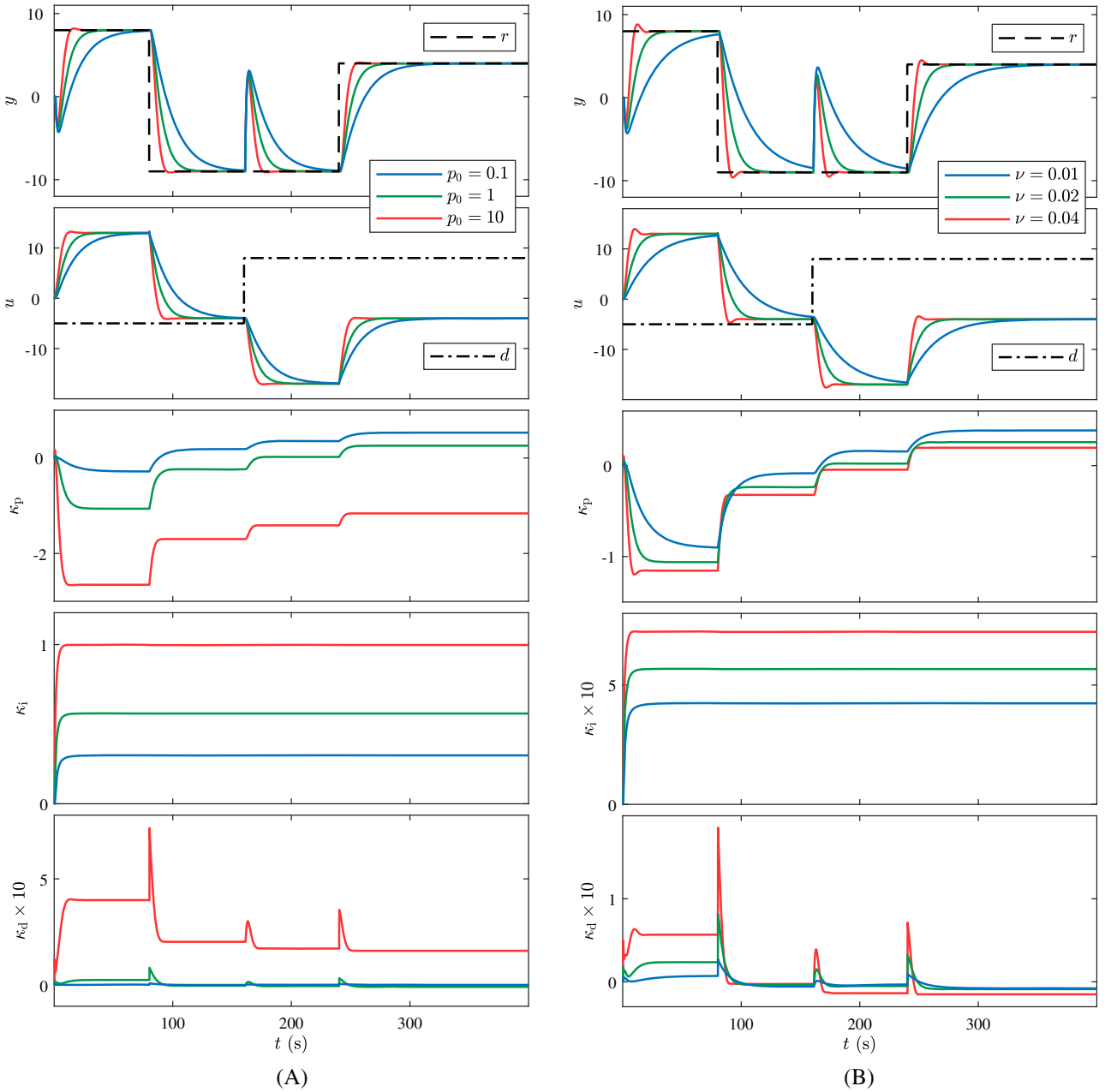

FIGURE 6 A, Example 1. Command following and disturbance rejection are achieved with $p_0 = 0.1, 1, 10$; B, Example 2. Command following and disturbance rejection are achieved with $\nu = 0.01, 0.02, 0.04$

Example 1. *RLS initialization* $P_0 = p_0 I_3$. Figure 6A shows asymptotic command following and disturbance rejection for $p_0 = 0.1, 1, 10$. Note that larger values of p_0 yield more aggressive response leading to faster rise time and larger overshoot.

Example 2. *Slope* $\nu = g'(0)$. Figure 6B shows asymptotic command following and disturbance rejection for $\nu = 0.01, 0.02, 0.04$. Note that larger values of ν yield more aggressive response leading to faster rise time and larger overshoot.

Example 3. *Gain K.* Figure 7A shows asymptotic command following and disturbance rejection for $K = 0.5, 1, 2$. It can be seen that the overshoot increases as K increases. For a unit step command and zero disturbance, Figure 7B

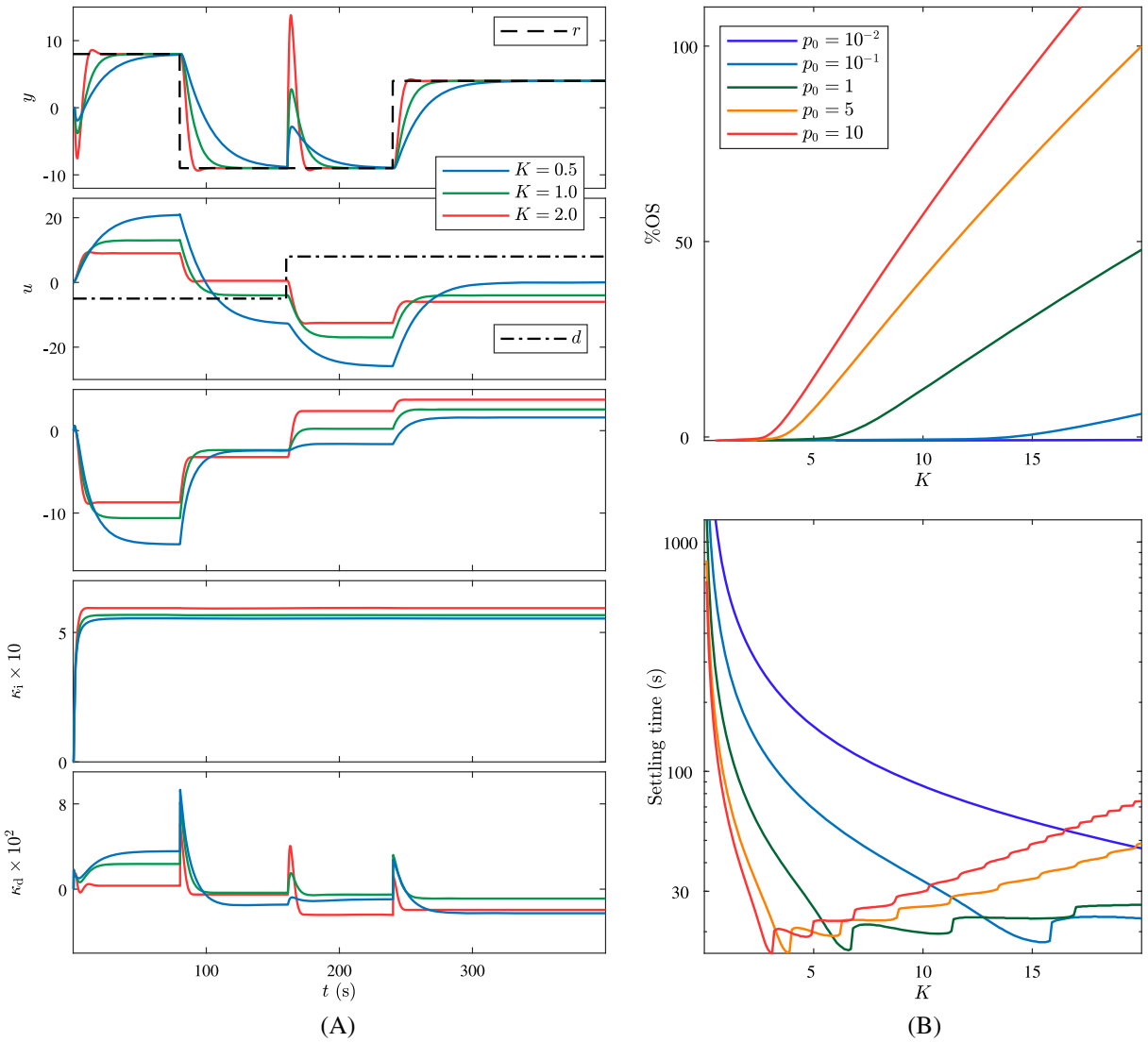

FIGURE 7 A, Example 3: Command following and disturbance rejection for various values of K. The overshoot is larger for larger K; B, Example 3: Percent overshoot (%OS) and settling time as a function of K for several values of p_0 with $r = 1$ and $d = 0$

shows the percent overshoot and settling time as a function of K for several values of p_0. Reducing p_0 reduces the overshoot and tends to increase the settling time for small values of K, but can decrease the settling time for large values of K.

Example 4. *Time constant* τ_c. Figure 8A shows asymptotic command following and disturbance rejection for $\tau_c = 0.2, 1, 5$ s. It can be seen that the overshoot increases as τ_c increases, which corresponds to slower plant dynamics. For a unit step command and zero disturbance, Figure 8B shows the percent overshoot and settling time as a function of τ_c for various values of p_0. Reducing p_0 reduces the overshoot and tends to increase the settling time for small values of τ_c, but can decrease the settling time for large values of τ_c.

Example 5. *Dead time* τ_d. Figure 9A shows asymptotic command following and disturbance rejection for $\tau_d = 0.49, 3, 5.01$ s. Note that τ_d/T_s need not be an integer. It can be seen that the overshoot increases as τ_d increases. For a unit step command and zero disturbance, Figure 9B shows the percent overshoot and settling time as a function of τ_d for several values of p_0. Reducing p_0 reduces the overshoot and tends to increase the settling time for small values of τ_d, but can decrease the settling time for large values of τ_d.

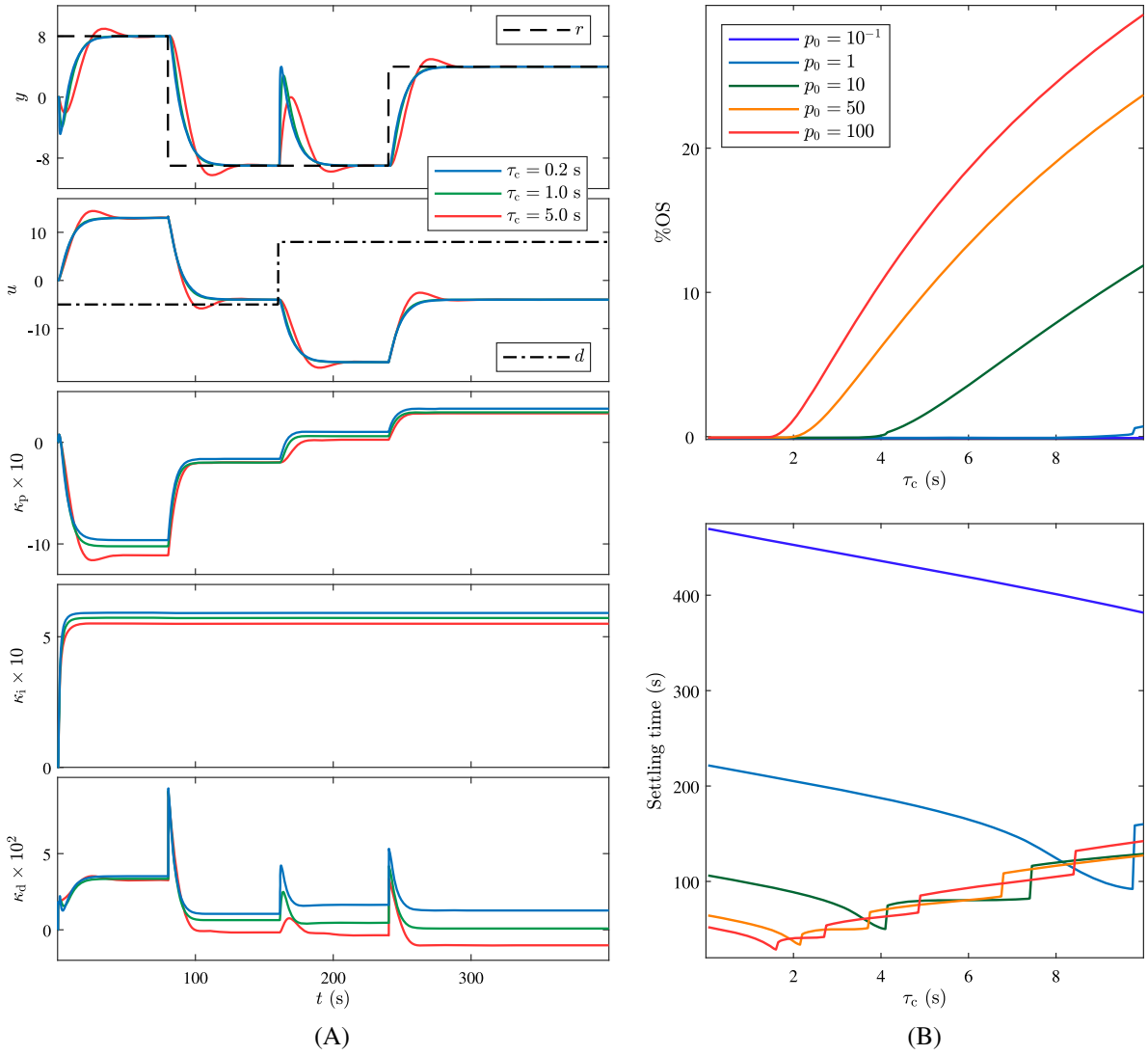

FIGURE 8 A, Example 4: Command following and disturbance rejection for various values of τ_c. The overshoot is larger for larger τ_c; B, Example 4: Percent overshoot (%OS) and settling time as a function of τ_c for various values of p_0 with $r = 1$ and $d = 0$

Example 6. *Fast sampling with* $T_s < \tau_d$. Figure 10A shows asymptotic command following and disturbance rejection for $T_s = 0.047, 0.1, 0.23$ s/sample. Fast sampling, that is, $T_s < \tau_d$, increases overshoot and decreases settling time. For a unit step command and zero disturbance, Figure 10B shows the percent overshoot and settling time as a function of T_s for several values of p_0. Reducing p_0 reduces the overshoot and increases the settling time.

Example 7. *Slow sampling with* $T_s > \tau_d$. Figure 11A shows asymptotic command following and disturbance rejection for $T_s = 1.9, 5, 11.7$ s/sample. Slow sampling, that is, $T_s > \tau_d$, tend to reduce or eliminate overshoot and increases settling time.

Example 8. *Sensor noise* η. Assume that η is white noise that is uniformly distributed in $[0, 2\mu_\eta]$, where $\mu_\eta = 1, 2, 3$ is the mean. Figure 11B shows that the noisy measurement y_n and response y approximately follow command r. However, response y has an offset with r, which is due to the nonzero-mean uniformly distributed white sensor noise.

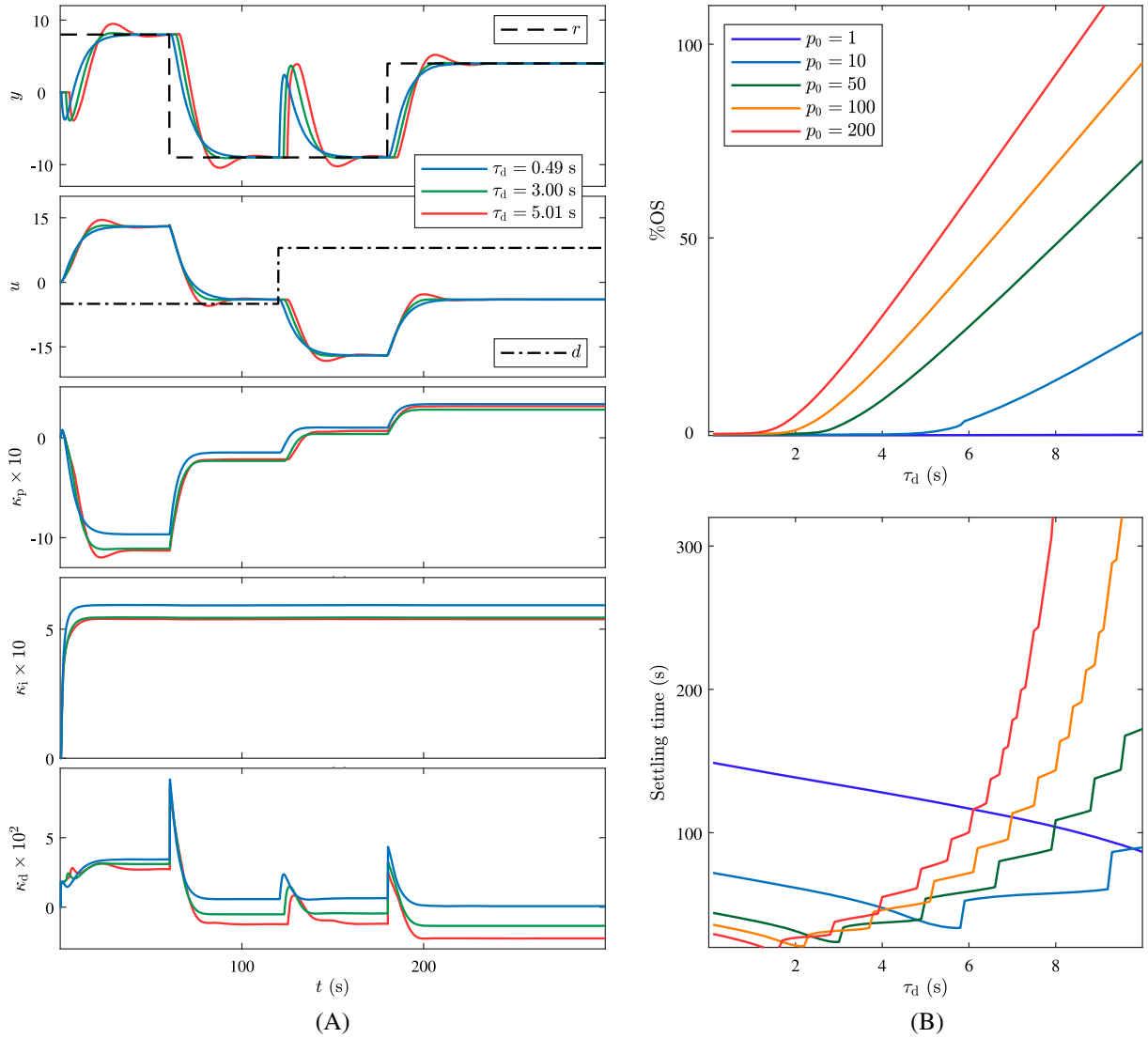

FIGURE 9 A, Example 5: Command following and disturbance rejection for various values of τ_d. The overshoot is larger for larger τ_d; B, Example 5: Percent overshoot (%OS) and settling time as a function of τ_d for various values of p_0 with $r = 1$ and $d = 0$

9 | LINEAR EXAMPLES VIOLATING THE ASSUMPTIONS OF SBC

The examples in this section consider the performance of the adaptive digital PID controller for the basic servo loop shown in Figure 1 in the case where one or more of (A1) to (A9) are violated. For all of the examples in this section, the sampled-data system is linear; that is, $v = \mathcal{H}(u) = u$, $y = \mathcal{W}(y_\ell) = y_\ell$, and $\mathcal{L}(y_\ell) = 0$. In order to investigate the effect of violating the assumptions of SBC, we consider examples with conditions that may be encountered in practice and that violate these assumptions. In particular, the examples in this section consider incorrect sign K, nonstep commands r, nonstep disturbances d, sensor noise η, actuator dynamics, slowly varying K, τ_c, τ_d, abruptly varying K, τ_c, τ_d, and three kinds of sampling jitter. The values considered are summarized in Table 2.

Example 9. *Incorrect* sign K. Since $\mathcal{H}(u) = u$ and $\mathcal{W}(y_\ell) = y_\ell$, (A9) implies that σ must be chosen such that $\sigma = \text{sign } K$. Figure 12A shows asymptotic command following and disturbance rejection for the cases where $(K, \sigma) = (1, 1), (-1, -1)$, that is, σ is chosen such that $\sigma = \text{sign } K$. Figure 12A also shows the cases where $(K, \sigma) = (-1, 1), (1, -1)$, that is, the choice of σ does not satisfy $\sigma = \text{sign } K$. In this case, control u and response y do not converge.

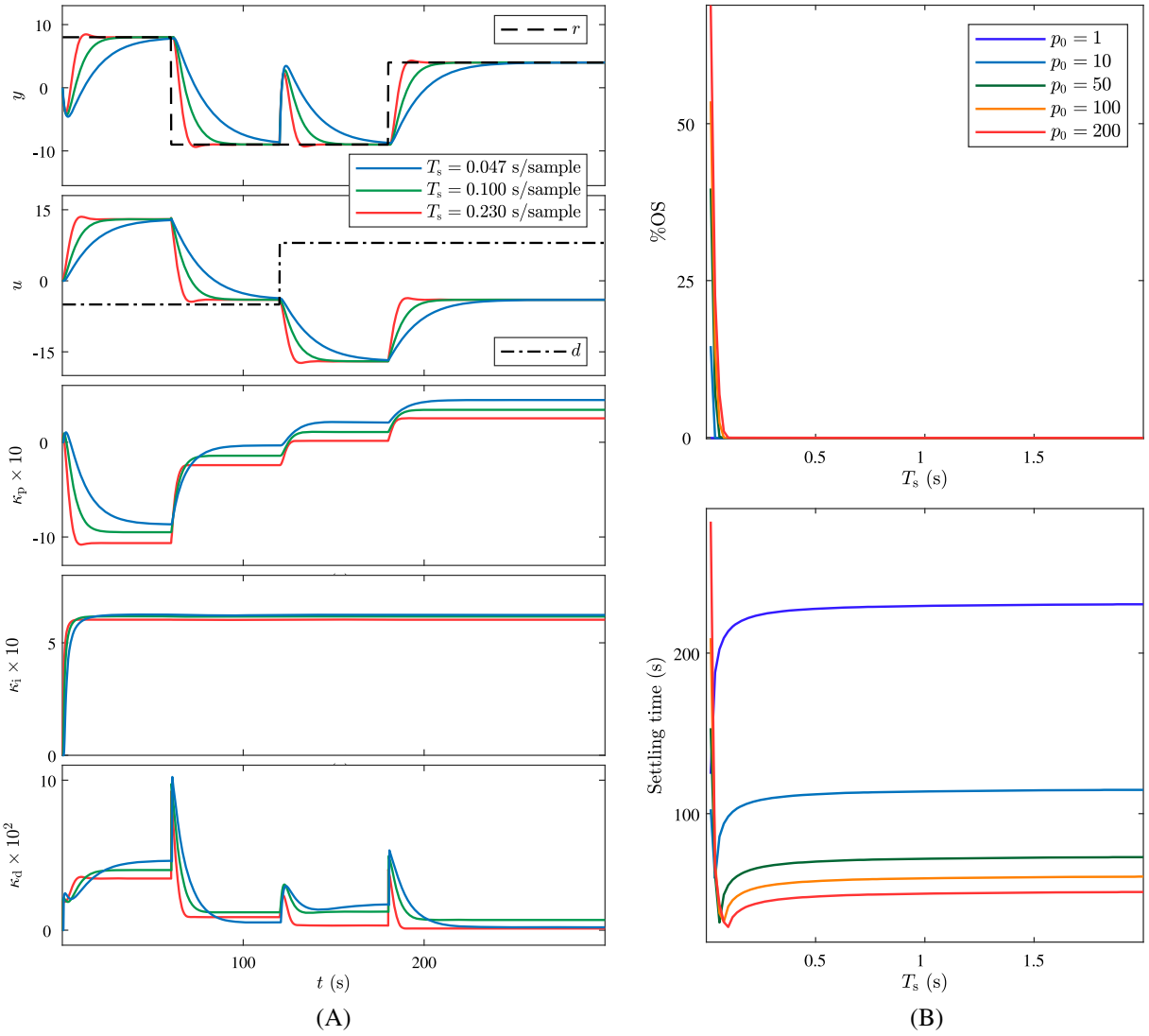

FIGURE 10 A, Example 6: Command following and disturbance rejection with fast sampling, that is, $T_s < \tau_d$. The overshoot is larger for larger sample times; B, Example 6: Percent overshoot (%OS) and settling time as a function of T_s for various values of p_0 with $r = 1$ and $d = 0$

Example 10. *Sigmoidal command r.* Consider the case where the command r is not piecewise-constant; specifically, consider the sigmoidal command

$$r(t) = \begin{cases} \frac{17}{1+e^{0.01(t-120)}} - 9, & 0 \le t < 200\,\text{s}, \\ \frac{13}{1+e^{0.01(260-t)}} - 9, & t \ge 200\,\text{s}. \end{cases} \tag{35}$$

Figure 12B shows asymptotic command following and disturbance rejection for $p_0 = 10^{-8}, 10^{-7}, 10^{-6}$. Note that the overshoot increases as p_0 increases.

Example 11. *Harmonic and broadband disturbance d.* Consider the case where the disturbance d is not constant; specifically, consider

$$d(t) = 15 + 2\sin 0.5t + \bar{d}(t), \tag{36}$$

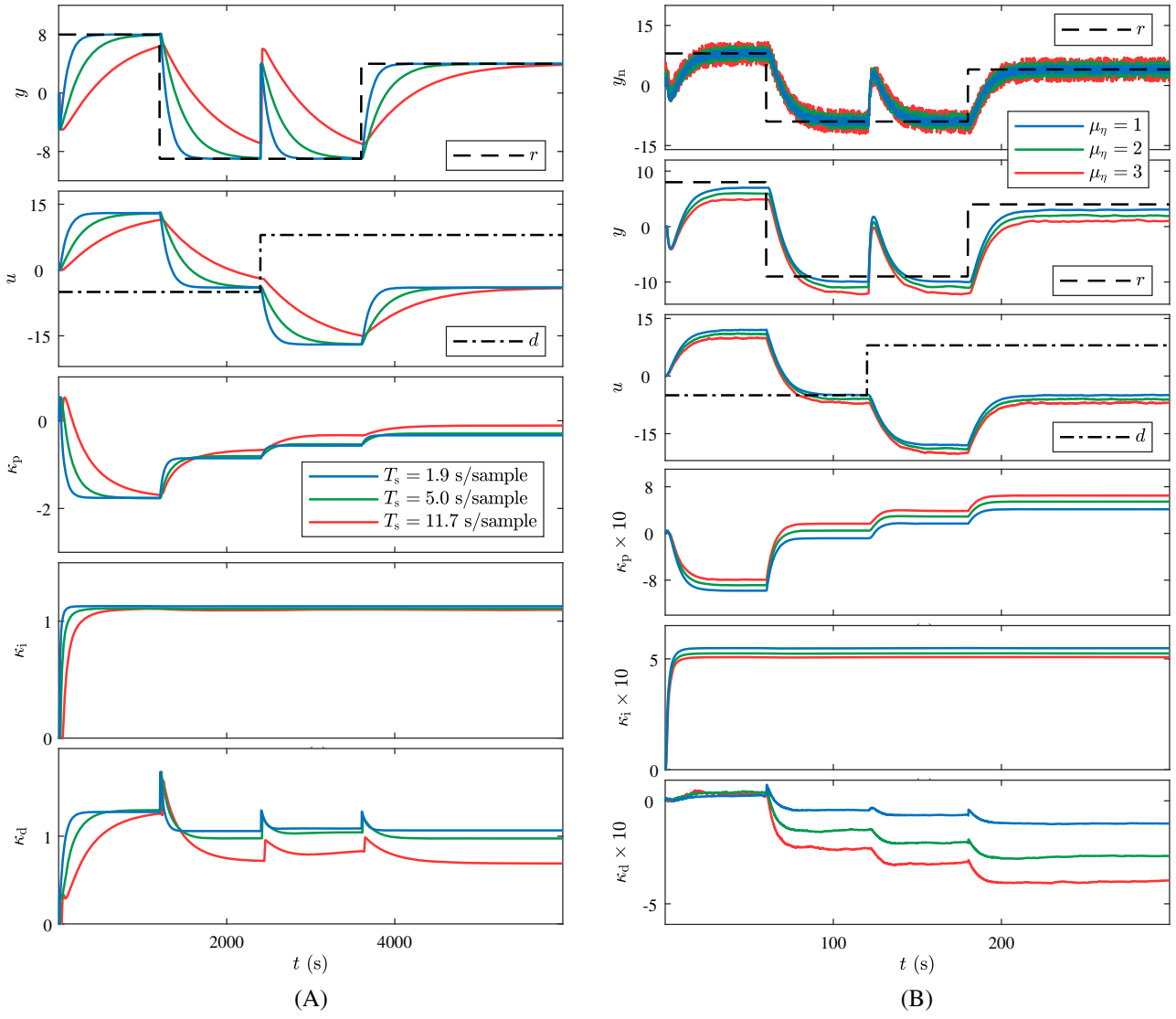

FIGURE 11 A, Example 7: Command following and disturbance rejection with slow sampling, that is, $T_s > \tau_d$. Slow sampling tend to reduce or eliminate overshoot and increases settling time; B, Example 8: Command following and disturbance rejection with nonzero-mean uniformly distributed white sensor noise. The noisy measurement y_n follows the command r; however, y has an offset with r

TABLE 2 Summary of adaptive digital proportional-integral-derivative control for linear examples violating the assumptions of simulation-based conjecture. The notation in the third column is defined within the respective example

Example	Investigated effect	Remarks
9	Incorrect sign K	$K = \pm 1$, $\sigma = \pm 1$
10	Sigmoidal command r	$p_0 = 10^{-8}, 10^{-7}, 10^{-6}$
11	Harmonic and broadband disturbance d	$d(t) = 15 + 2\sin 0.5t + \bar{d}(t)$
14	Sensor noise η	Gaussian white noise with $\sigma_\eta = 0.5, 1, 2$
13	Actuator dynamics	$f_a = 0.05, 0.1, 0.2$ Hz
14	Slowly varying K	$K_{max} = 3, 5$
15	Slowly varying τ_c	$\tau_{c,max} = 5, 10$
16	Slowly varying τ_d	$\tau_{d,max} = 3, 6$
17	Abruptly varying K	$K = 1$ changes to $\bar{K} = 4, 7$
18	Abruptly varying τ_c	$\tau_c = 1$ changes to $\bar{\tau}_c = 0.1, 10$
19	Abruptly varying τ_d	$\tau_d = 1$ changes to $\bar{\tau}_d = 4, 8$
20	Absolute clock jitter with asynchronous A/D and D/A devices	$T_{s,k} = 1 + s_k - s_{k-1}$, $T_{h,k} = 1 + h_k - h_{k-1}$
21	Relative clock jitter with synchronous A/D and D/A devices	$T_{s,k} = T_{h,k} = 1 + s_k$
22	Relative clock jitter with asynchronous A/D and D/A devices	$T_{s,k} = 1 + s_k$, $T_{h,k} = 1 + h_k$

Abbreviations: A/D, analog-to-digital; D/A, digital-to-analog.

where $\bar{d}$ is zero-mean, Gaussian continuous-time white noise with approximate intensity[82-84] $1000\sigma_d^2/T_s = 1000/T_s$, where $\sigma_d = 1$ is the standard deviation of the discrete-time Gaussian random variable at each time step, and the intensity is the variance (ie, the square of the standard deviation) divided by the numerical integration step size $T_s/1000$. Figure 13A shows that the controller cannot eliminate the effect of disturbance on response y; however, response y approximately follows command r with oscillations.

Example 12. *Sensor noise η.* Assume that η is Gaussian white noise with mean 2 and intensity $1000\sigma_\eta^2/T_s$, where $\sigma_\eta = 0.5, 1, 2$. Figure 13B shows that the noisy measurement y_n and response y approximately follow command r. However, response y has an offset with r, which is due to the nonzero-mean Gaussian white sensor noise.

Example 13. *Actuator dynamics.* Assume that the actuator has dynamics given by

$$G_a(s) = \frac{\omega_a^2}{s^2 + \sqrt{2}\omega_a s + \omega_a^2}, \tag{37}$$

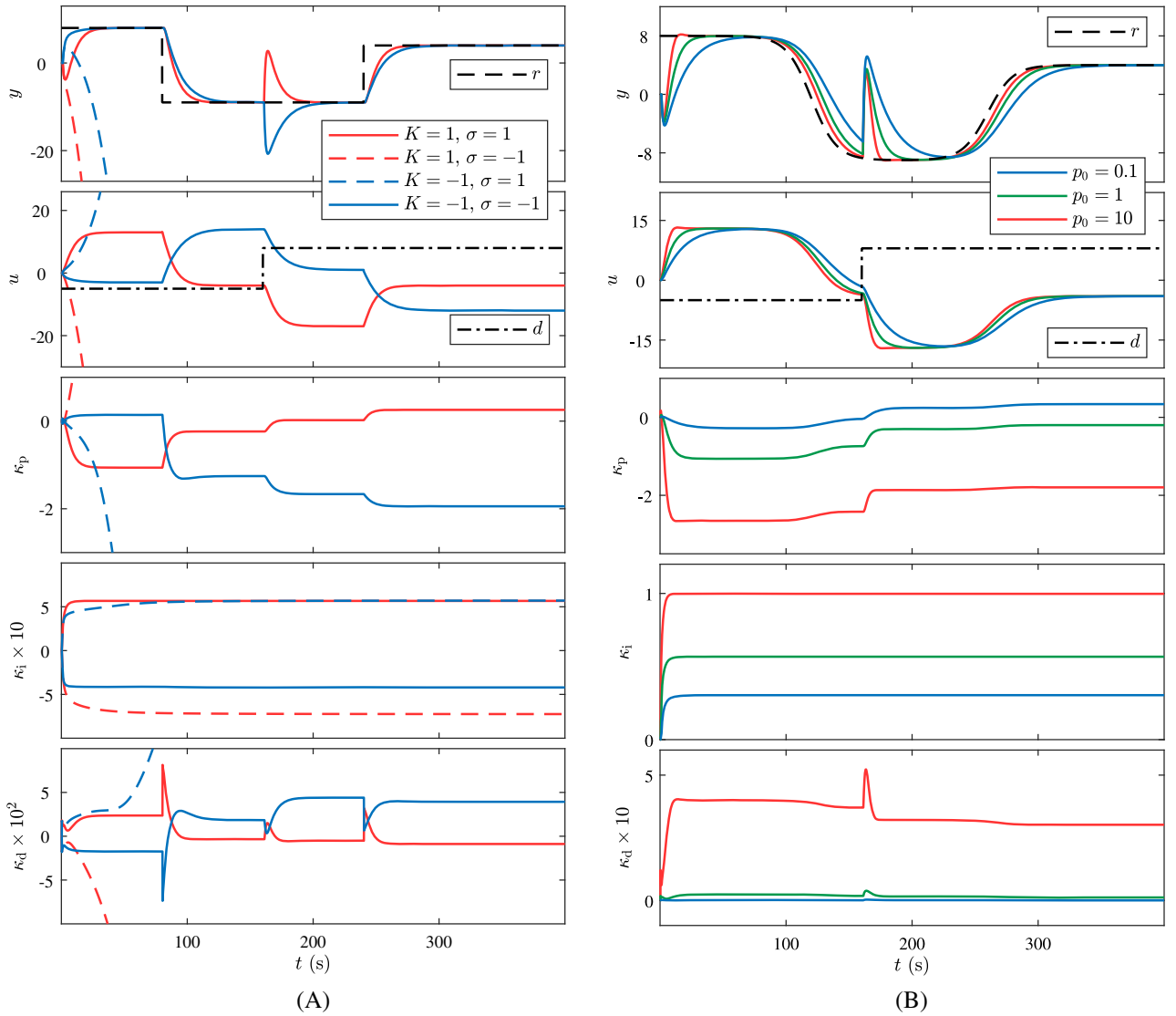

FIGURE 12 A, Example 9: Command following and disturbance rejection for various choices of K and σ. Asymptotic command following and disturbance rejection is only achieved in the case $\sigma = \text{sign } K$; B, Example 10: Command following and disturbance rejection with a sigmoidal command, where the measurement y tends to follow the nonconstant command r closely

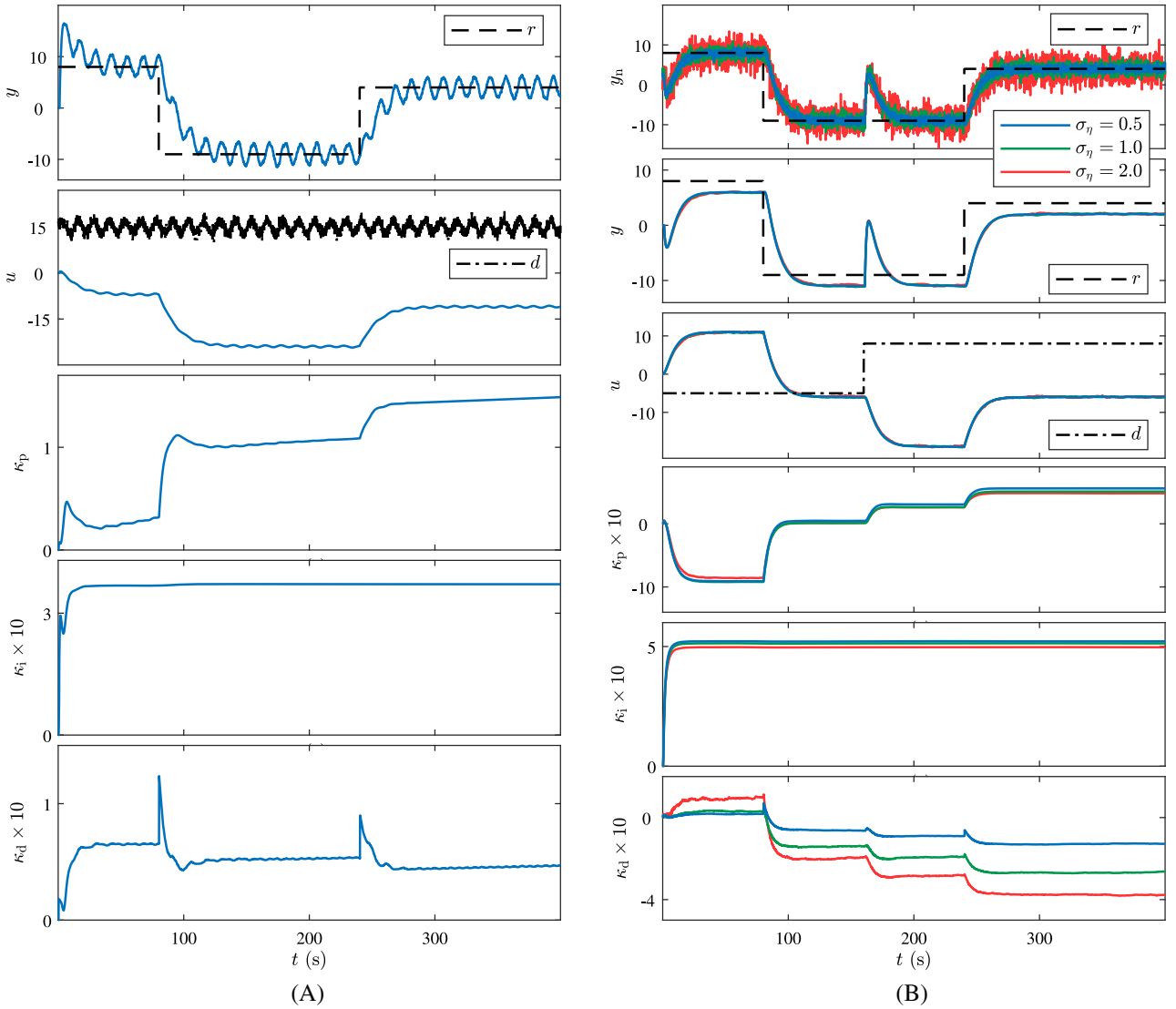

FIGURE 13 A, Example 11: Command following and disturbance rejection with nonzero-mean Gaussian-plus-harmonic disturbance. The controller is unable to follow the command asymptotically. The response y oscillates about the command r; B, Example 12: Command following and disturbance rejection with nonzero-mean Gaussian white sensor noise. The noisy measurement y_n follows the command r; however, y has an offset with r due to the nonzero-mean Gaussian white sensor noise

where $\omega_a \triangleq 2\pi f_a$, and f_a is the actuator cutoff frequency. Figure 14A shows asymptotic command following and disturbance rejection for $f_a = 0.05, 0.1, 0.2$. The overshoot decreases as f_a is increased. Note that, since $\tau_c = 1$, the actuator dynamics are slower than the plant dynamics.

Example 14. *Slowly varying K.* Assume that K increases linearly from 1 to K_{max} from $t = 0$ s to $t = 150$ s and then decreases linearly from K_{max} to 1 from $t = 150$ s to $t = 300$ s. Figure 14B shows asymptotic command following and disturbance rejection for $K_{max} = 3, 5$. Numerical simulations suggest that, if the rate of change of K is sufficiently small, then asymptotic command following and disturbance rejection can be achieved.

Example 15. *Slowly varying* τ_c. Assume that τ_c increases linearly from 1 s to $\tau_{c,max}$ from $t = 0$ s to $t = 150$ s and then decreases linearly from $\tau_{c,max}$ to 1 s from $t = 150$ s to $t = 300$ s. Figure 15A shows asymptotic command following and disturbance rejection for $\tau_{c,max} = 3, 5$. Numerical simulations suggest that, if the rate of change of τ_c is sufficiently small, then asymptotic command following and disturbance rejection can be achieved.

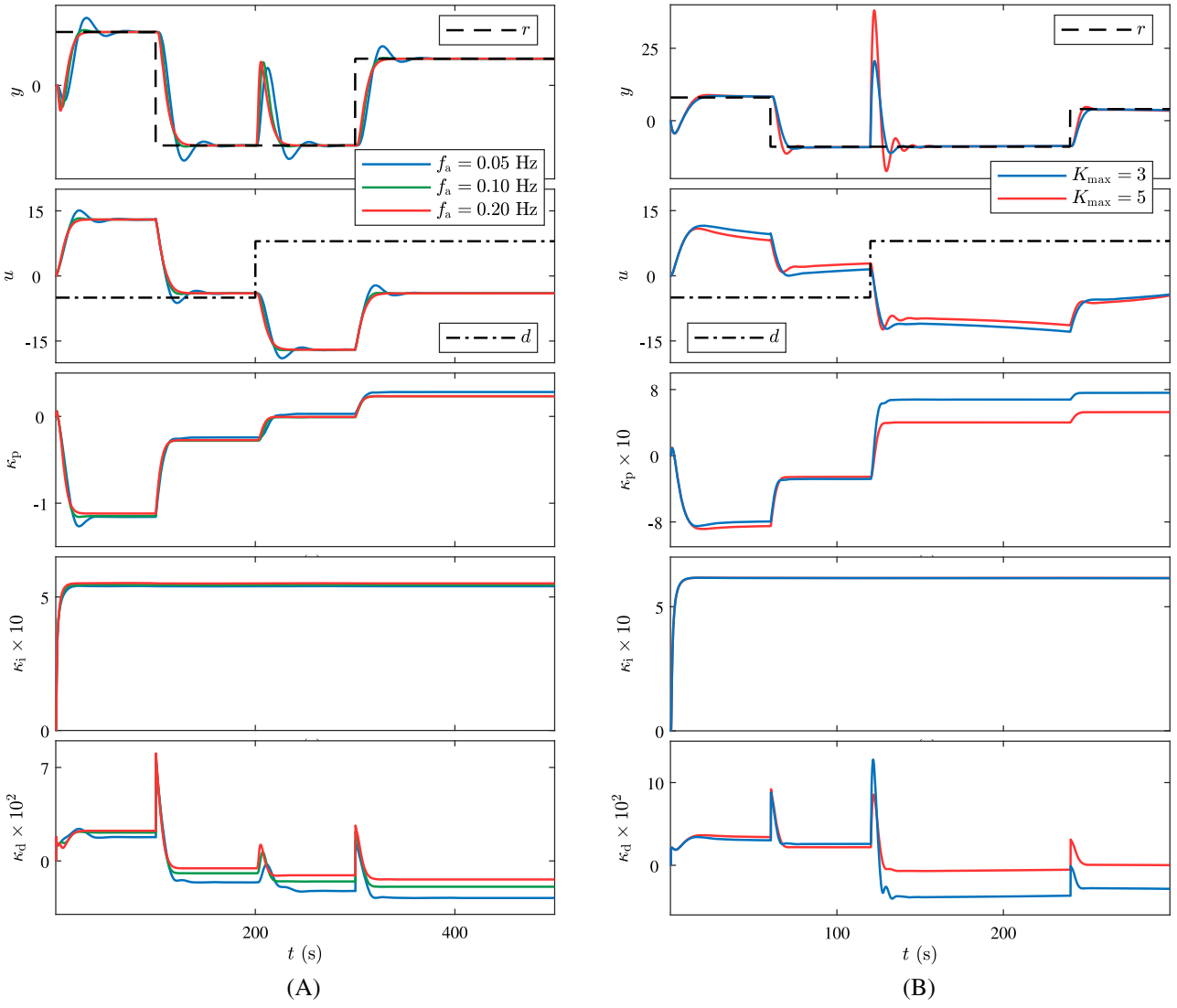

FIGURE 14 A, Example 13: Command following and disturbance rejection with an actuator whose second-order dynamics are slower than the plant dynamics; B, Example 14: Command following and disturbance rejection can be achieved with slowly varying gain K

Example 16. *Slowly varying* τ_d. Assume that τ_d increases linearly from 1 s to $\tau_{d,max}$ from $t = 0$ s to $t = 150$ s and then decreases linearly from $\tau_{d,max}$ to 1 s from $t = 150$ s to $t = 300$ s. Figure 15B shows asymptotic command following and disturbance rejection for $\tau_{d,max} = 3, 6$. Numerical simulations suggest that, if the rate of change of τ_d is sufficiently small, then asymptotic command following and disturbance rejection can be achieved.

Example 17. *Abruptly varying* K. Assume that K increases abruptly from 1 to $\bar{K}$ at $t = 90$ s. Figure 16A shows asymptotic command following and disturbance rejection for $\bar{K} = 4, 7$. In the case where $\bar{K} = 7$, the closed-loop system becomes unstable immediately after the abrupt change but stability is recovered. Figure 16B shows the error-normalization g and the points computed during the simulation.

Example 18. *Abruptly varying* τ_c. Assume that τ_c increases abruptly from 1 s to $\bar{\tau}_c$ at $t = 180$ s. Figure 17A shows asymptotic command following and disturbance rejection for $\bar{\tau}_c = 0.1, 10$. In this case, the closed-loop system remains stable after the abrupt change in τ_c.

Example 19. *Abruptly varying* τ_d. Assume that τ_d increases abruptly from 1 s to $\bar{\tau}_d$ at $t = 270$ s. Figure 17B shows asymptotic command following and disturbance rejection for $\bar{\tau}_d = 4, 8$. In the case where $\bar{\tau}_d = 8$, the closed-loop

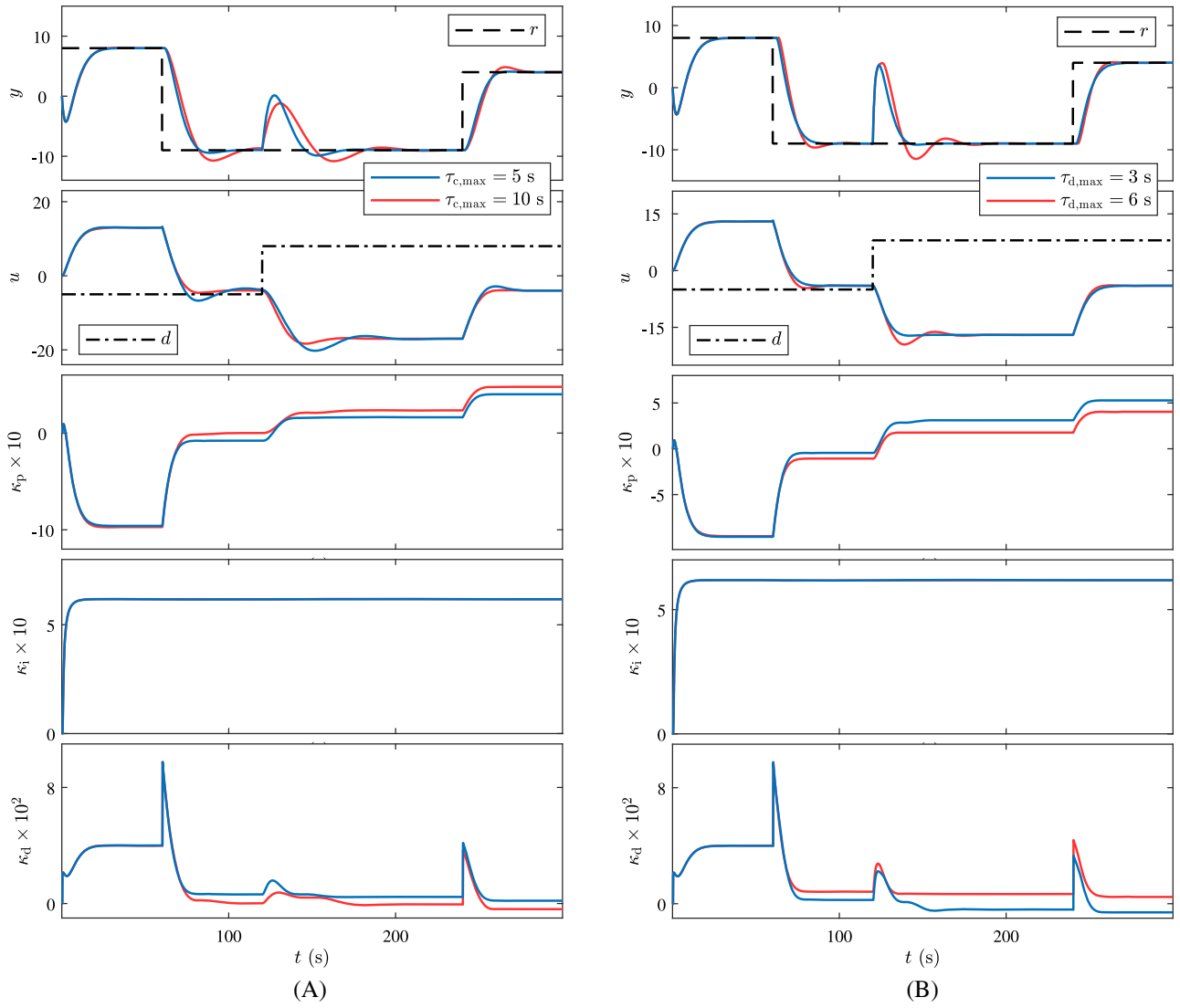

FIGURE 15 A, Example 15: Command following and disturbance rejection can be achieved with slowly varying time constant τ_c; B, Example 16: Command following and disturbance rejection can be achieved with slowly varying dead time τ_d

system becomes unstable immediately after the abrupt change but the adaptive digital PID control restabilizes the closed-loop system.

Example 20. *Absolute clock jitter with asynchronous A/D and D/A devices.* Assume that the A/D and D/A devices operate asynchronously, and thus the sample interval $T_{s,k}$ and the hold interval $T_{h,k}$ vary at each time step k due to timing jitter as shown in Figure 18A. Let $T_{s,k}$ and $T_{h,k}$ be given by

$$T_{s,k} = 1 + s_k - s_{k-1}, \quad T_{h,k} = 1 + h_k - h_{k-1}, \tag{38}$$

where s_k and h_k are uniformly distributed random variables in $[0, j]$, where $j \in \{0.2, 0.4, 0.8\}$. Figure 18B shows that, as in the case of slowly varying dead time shown in Example 16, the jitter has no discernible effect on the closed-loop performance.

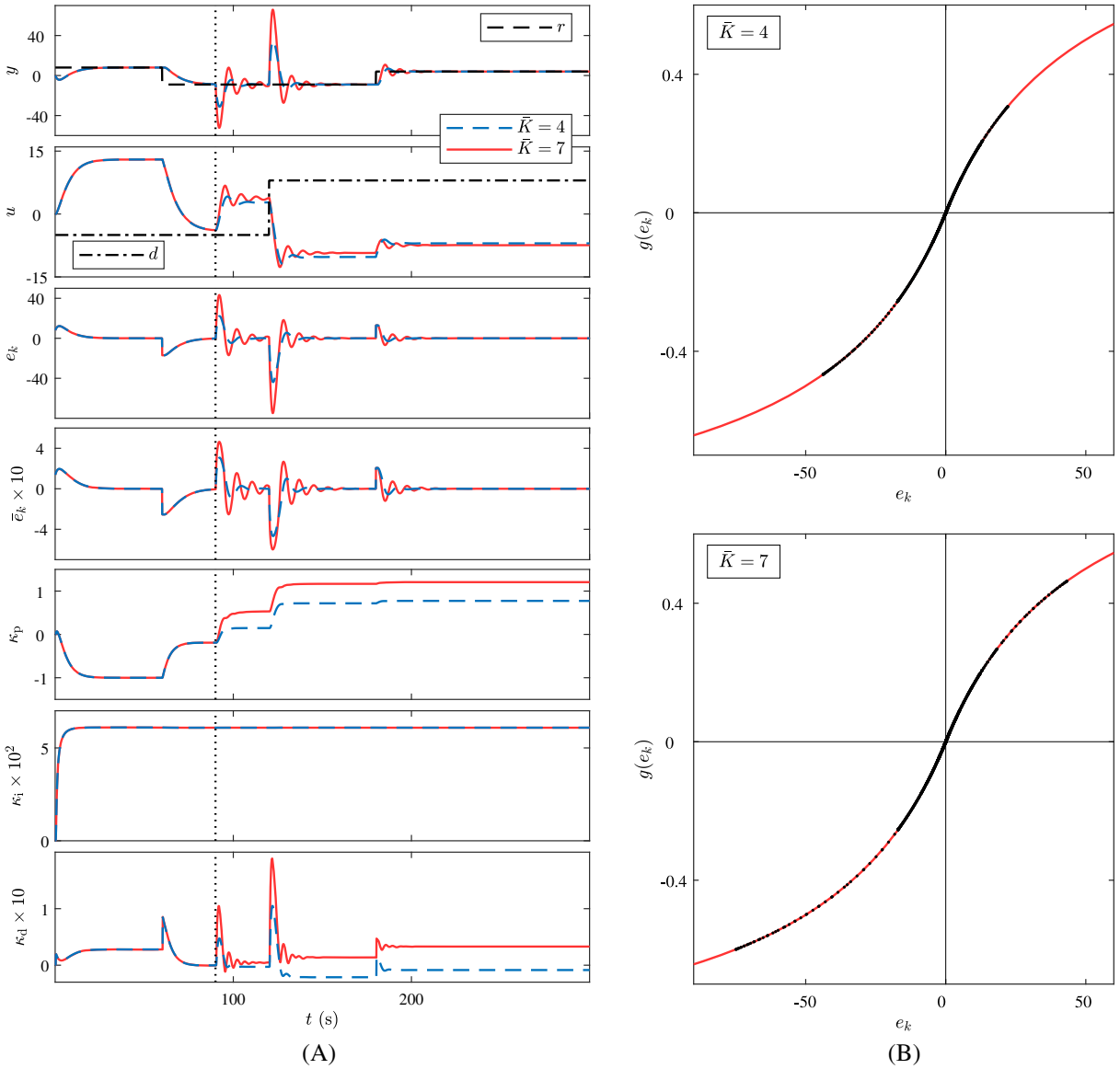

FIGURE 16 A, Example 17: Command following and disturbance rejection with abruptly varying gain K. The controller adapts to the abrupt changes in the gain K and achieves asymptotic command following and disturbance rejection. For $\bar{K} = 7$ the closed-loop system is unstable for some time after the abrupt change in K and the adaptive controller recovers closed-loop stability; B, Example 17: Error-normalization g as a function of e_k. Each black dot denotes a point $(e_k, g(e_k))$ computed during the simulation

Example 21. *Relative clock jitter with synchronous A/D and D/A.* Assume that the A/D and D/A devices operate synchronously, that is, $T_{s,k} = T_{h,k}$, but the sample interval $T_{s,k}$ varies at each time step k due to timing jitter, as shown in Figure 19A. Let j be a positive integer, and let $T_{s,k}$ be given by

$$T_{s,k} = 1 + s_k, \tag{39}$$

where s_k is a uniformly distributed random variable in $[0, j]$. Let $j \in \{0.2, 0.4, 0.8\}$. Figure 19B shows that, as in the case of slowly varying dead time shown in Example 16, the jitter has no discernible effect on the closed-loop performance.

Example 22. *Relative clock jitter with asynchronous A/D and D/A devices.* Assume that the A/D and D/A devices operate asynchronously, and thus the sample interval $T_{s,k}$ and the hold interval $T_{h,k}$ vary at each time step k due to

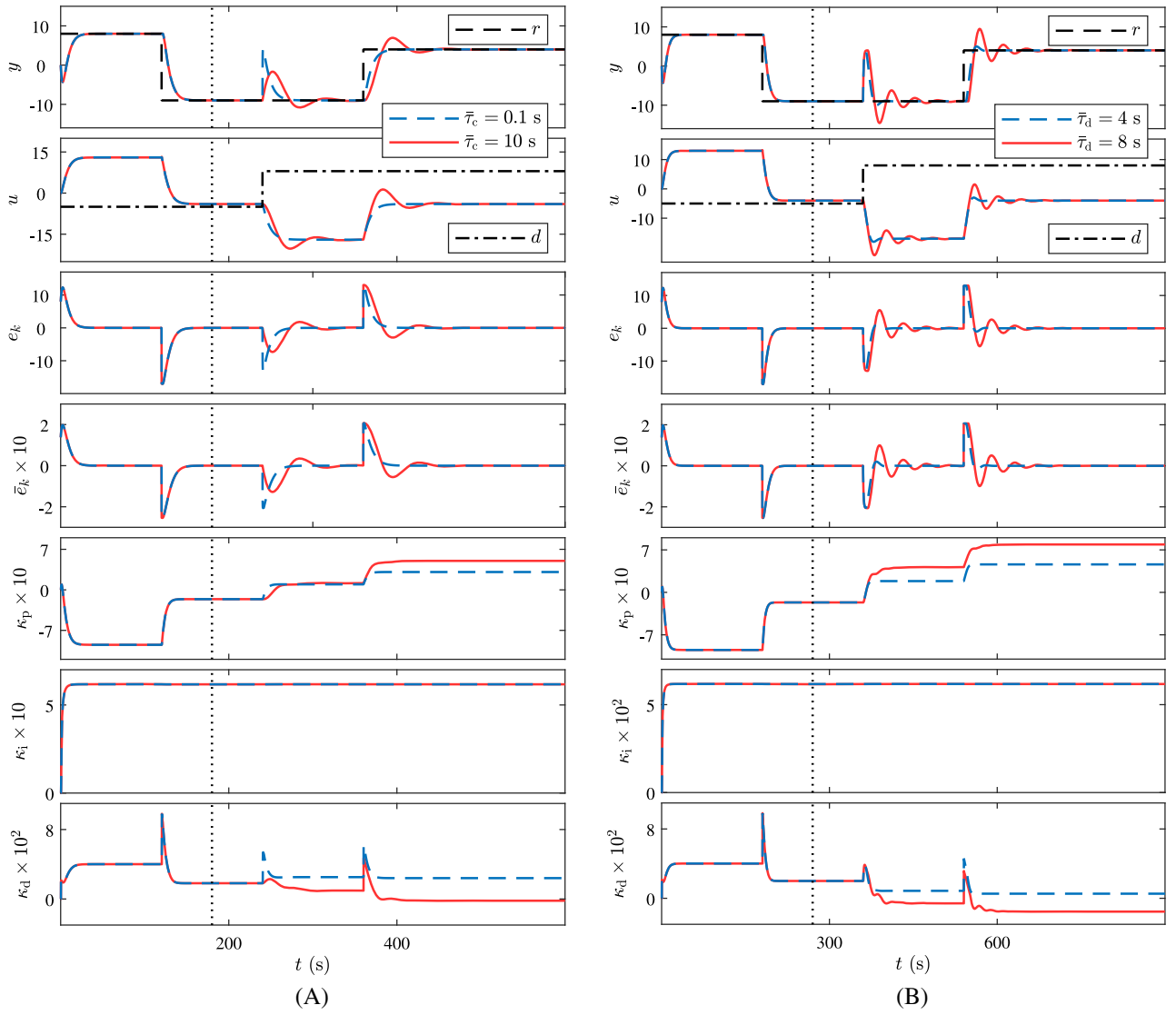

FIGURE 17 A, Example 18: Command following and disturbance rejection with abruptly changing time constant τ_c. The controller adapts to the abrupt changes in the time constant τ_c and achieves asymptotic command following and disturbance rejection; B, Example 19: Command following and disturbance rejection with abruptly changing dead time τ_d. The controller adapts to the abrupt changes in the dead time τ_d and achieves asymptotic command following and disturbance rejection. For $\bar{\tau}_d = 8$ the closed-loop is unstable for some time after the abrupt change in τ_d and the adaptive controller recovers closed-loop stability

timing jitter, as shown in Figure 20A. Let $T_{s,k}$ and $T_{h,k}$ be given by

$$T_{s,k} = 1 + s_k, \quad T_{h,k} = 1 + h_k, \tag{40}$$

where s_k and h_k are uniformly distributed random variables in $[0, j]$, where $j \in \{0.2, 0.4, 0.8\}$. Figure 20B shows that, as in the case of slowly varying dead time shown in Example 16, the jitter has no discernible effect on the closed-loop performance.

10 | NONLINEAR EXAMPLES SUPPORTING SBC

The examples in this section consider the performance of the adaptive digital PID controller for the basic servo loop shown in Figure 1 in the case where either $\mathcal{H}$, $\mathcal{W}$, or $\mathcal{L}$ is a nonlinear map. All of these examples satisfy the assumptions of SBC. In order to investigate the effect of $\mathcal{H}$, $\mathcal{W}$, and $\mathcal{L}$ on the closed-loop performance, various choices of these functions are

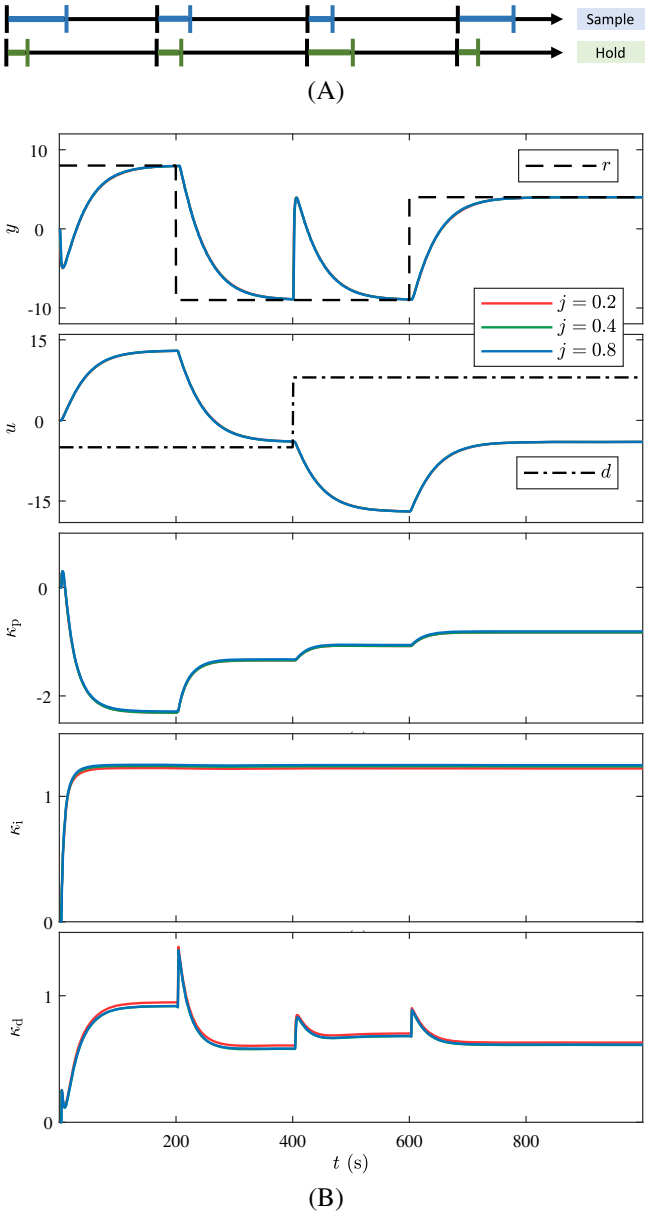

FIGURE 18 A, Example 20: Timing diagram for absolute clock jitter with asynchronous analog-to-digital and digital-to-analog devices. The black vertical bars indicate the nominal absolute clock intervals; B, Example 20: Command following and disturbance rejection with absolute clock jitter with asynchronous analog-to-digital and digital-to-analog devices. No discernible effect on the closed-loop performance is observed

considered. In particular, the examples in this section consider the effect of control-magnitude saturation and deadzone as well as sensor-magnitude saturation and deadzone. The properties considered are summarized in Table 3. Note that Example 23 supports (A1) to (A9) but does not satisfy the additional assumption (A12).

Example 23. *Infeasible r.* Assume that $\mathcal{H}$ and $\mathcal{L}$ are absent, and let $\mathcal{W}$ be given by the magnitude-saturation nonlinearity

$$\mathcal{W}(y_\ell) = \begin{cases} -3, & y_\ell \leq -3, \\ y_\ell, & -3 < y_\ell < 3, \\ 3, & y_\ell \geq 3. \end{cases} \tag{41}$$

Figure 21A shows asymptotic command following and disturbance rejection, where either $\overline{u} = -\underline{u} = 1$ (blue trace) or $\overline{u} = -\underline{u} = 5$ (red trace). Figure 21B shows $\mathcal{W}$ and the points computed during the simulation. Since, for all $t > 0$, $|r(t)| \geq 4$, (41) implies that (A12) is not satisfied, that is, r is infeasible. Note that, although command following is not achieved in this case, u_k, ξ_k, y_k, $\kappa_{\mathrm{p},k}$, $\kappa_{\mathrm{i},k}$, and $\kappa_{\mathrm{d},k}$ remain bounded. The boundedness of these signals is due to the antiwindup technique (8).

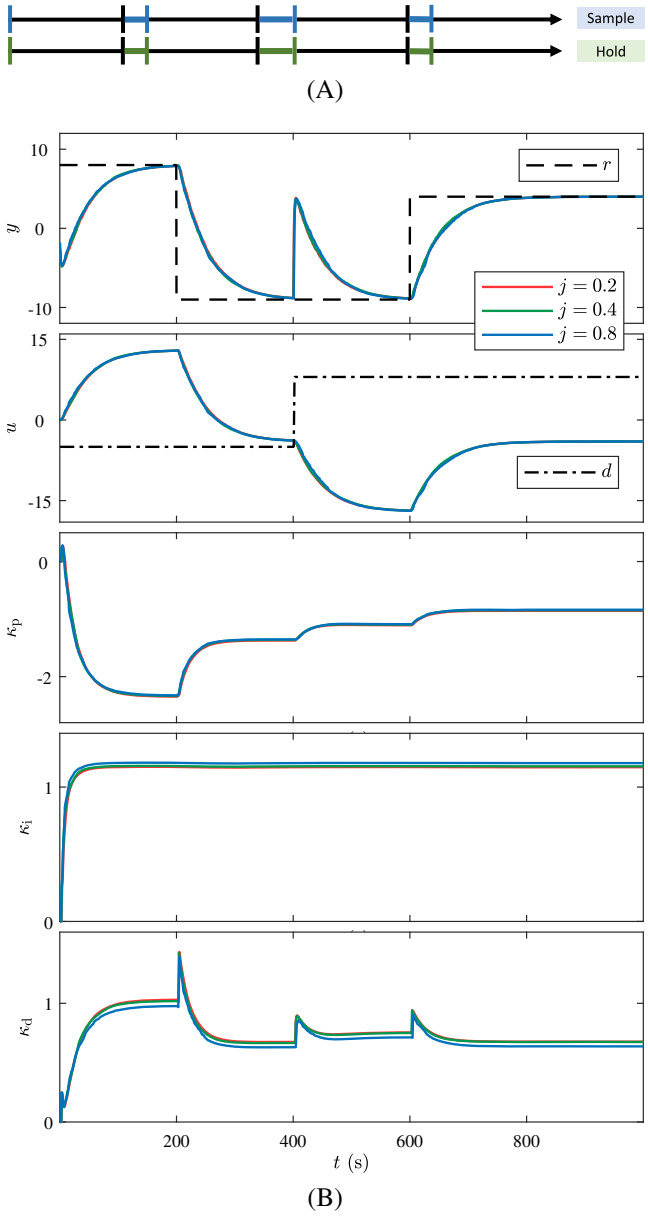

FIGURE 19 A, Example 21: Timing diagram for relative clock jitter with synchronous analog-to-digital and digital-to-analog devices. The interval between the blue and green vertical bars and the black vertical bars indicates the nominal relative clock intervals; B, Example 21: Command following and disturbance rejection with relative clock jitter with synchromous analog-to-digital and digital-to-analog devices. No discernible effect on the closed-loop performance is observed

Example 24. *Increasing $\mathcal{W}$ with $r = \mathcal{W}(r)$.* Let $\mathcal{W}$ be given by

$$\mathcal{W}(y_\ell) = \frac{1}{79}\left((y_\ell - 1)^3 + 289\right). \tag{42}$$

Note that $\mathcal{W}$ is increasing and, for all $t > 0$, $\mathcal{W}(r(t)) = r(t)$, that is, $\mathcal{W}(8) = 8$, $\mathcal{W}(-9) = -9$, and $\mathcal{W}(4) = 4$. Figure 22A shows asymptotic command following and disturbance rejection. Figure 22B shows $\mathcal{W}$ and the points computed during the simulation. In this case, note that (A13) and (A14) are satisfied, and command following is achieved by both y_ℓ and y, as stated by SBC.

Example 25. *Control-magnitude saturation $\mathcal{H}$.* Assume that $\mathcal{W}$ and $\mathcal{L}$ are absent, and let $\mathcal{H}$ be given by the asymmetric magnitude-saturation nonlinearity

$$\mathcal{H}(u) = \begin{cases} -18, & u \le -18, \\ u, & -18 < u < 15, \\ 15, & u \ge 15. \end{cases} \tag{43}$$

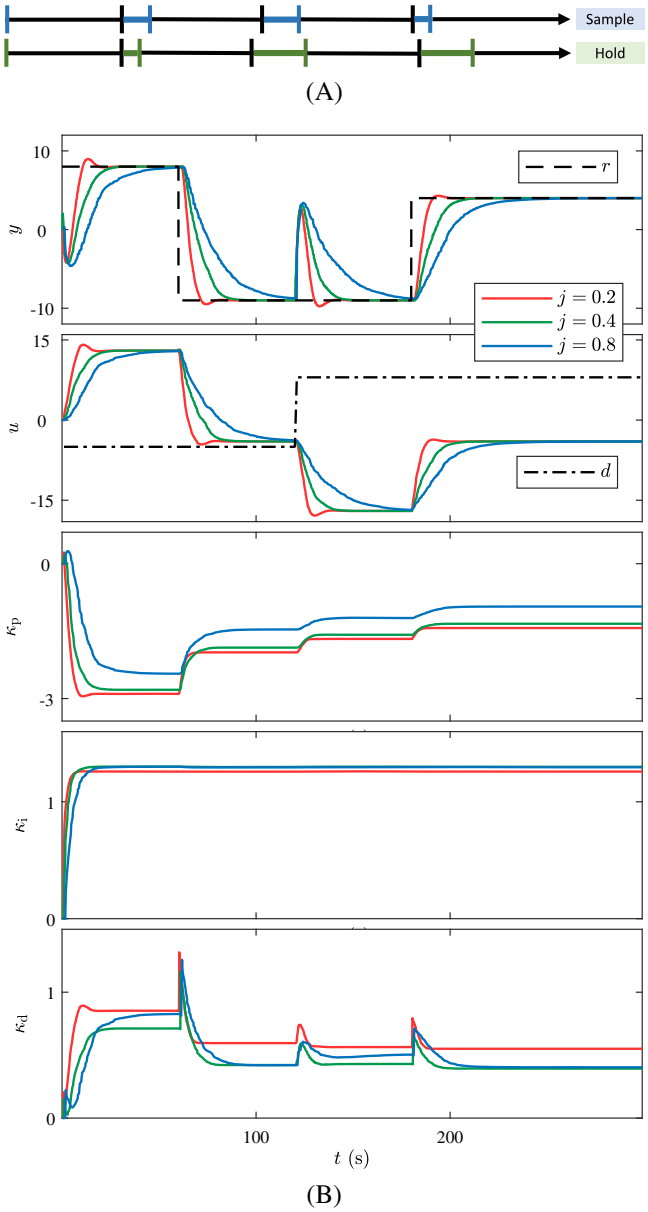

FIGURE 20 A, Example 22: Timing diagram for relative clock jitter with asynchronous analog-to-digital and digital-to-analog devices. The interval between the blue and green vertical bars and the black vertical bars indicates the nominal relative clock intervals; B, Example 22: Command following and disturbance rejection with relative clock jitter with asynchromous analog-to-digital and digital-to-analog devices. No discernible effect on the closed-loop performance is observed

TABLE 3 Summary of adaptive digital proportional-integral-derivative control for nonlinear examples supporting simulation-based conjecture

Example	Investigated effect	Remarks
23	Infeasible r	(A12) is not satisfied
24	Increasing $\mathcal{W}$ with $r = \mathcal{W}(r)$	(A12) is satisfied
25	Control-magnitude saturation $\mathcal{H}$	Asymmetric
26	Control-magnitude deadzone $\mathcal{H}$	Asymmetric
27	Sensor-magnitude saturation $\mathcal{W}$	Asymmetric
28	Sensor-magnitude deadzone $\mathcal{W}$	Asymmetric
29	Continuous $\mathcal{H}$ and $\mathcal{W}$	Nondecreasing $\mathcal{H}$ and $\mathcal{W}$
30	Continuous $\mathcal{H}$ and $\mathcal{W}$	Nonincreasing $\mathcal{H}$, nondecreasing $\mathcal{W}$
31	Discontinuous $\mathcal{H}$	Nondecreasing $\mathcal{H}$
32	Discontinuous $\mathcal{W}$	Nondecreasing $\mathcal{W}$
33	Continuous $\mathcal{L}$	Nondecreasing $\mathcal{L}$, consider $\mathcal{L}$ and $-\mathcal{L}$
34	Discontinuous $\mathcal{L}$	Nondecreasing $\mathcal{L}$, consider $\mathcal{L}$ and $-\mathcal{L}$

Let $\tau_c = 10$ s and $\overline{u} = -\underline{u} = 20$. Figure 23A shows that asymptotic command following and disturbance rejection are achieved in the presence of control-magnitude saturation.

Example 26. *Control-magnitude deadzone $\mathcal{H}$.* Assume that $\mathcal{W}$ and $\mathcal{L}$ are absent, and let $\mathcal{H}$ be given by

$$\mathcal{H}(u) = \begin{cases} u + 8, & u < -8, \\ 0, & -8 \le u \le 12, \\ u - 12, & u > 12. \end{cases} \tag{44}$$

Let $\overline{u} = -\underline{u} = 30$. Figure 23B shows that asymptotic command following and disturbance rejection are achieved in the presence of control-magnitude deadzone.

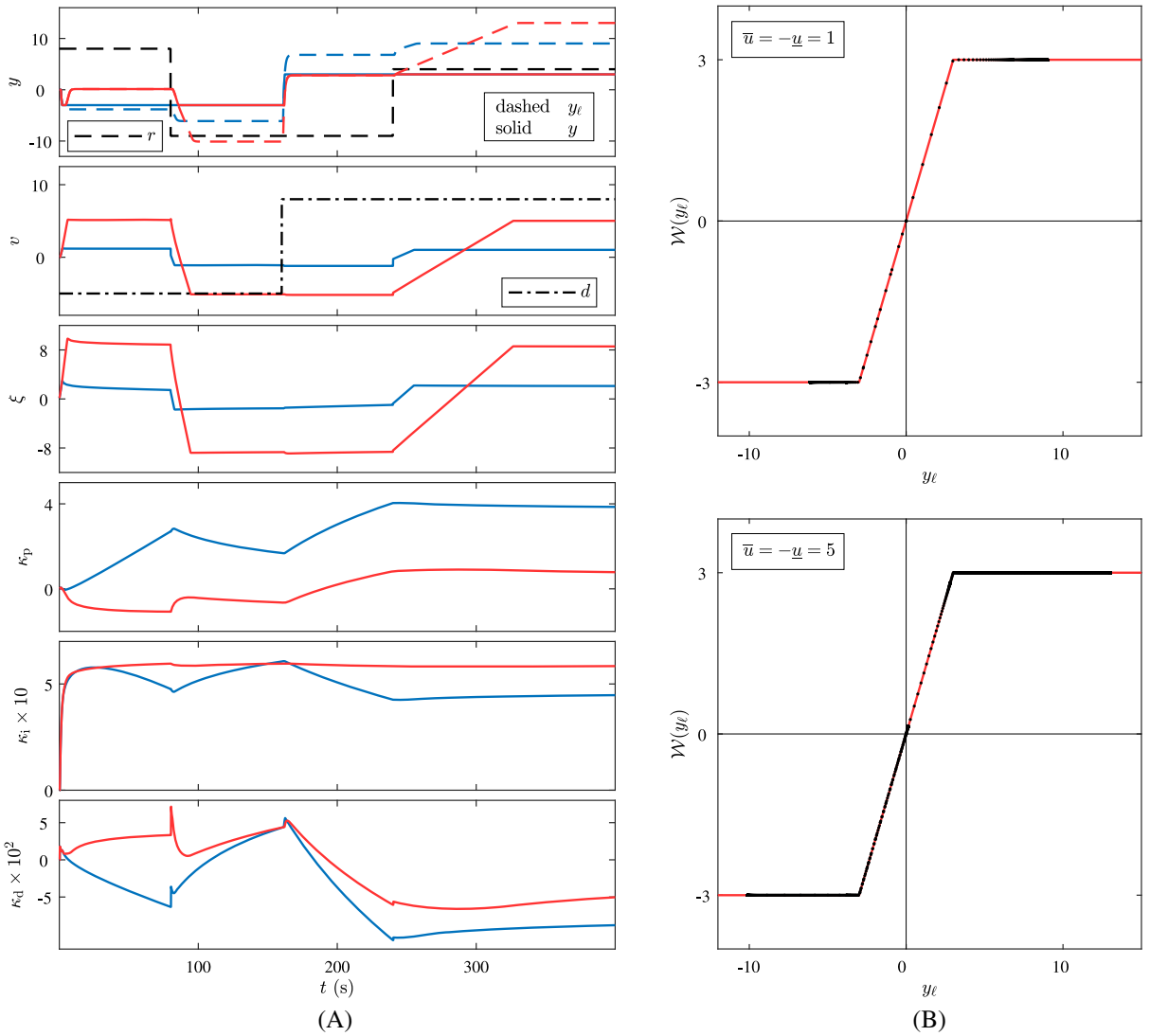

FIGURE 21 A, Example 23: Command following and disturbance rejection with infeasible command r. Command following is not achieved but all signals remain bounded; B, Example 23: $\mathcal{W}$ as a function of y_ℓ. Each black dot denotes a point $(y_\ell(t), \mathcal{W}(y_\ell(t)))$ computed during the simulation

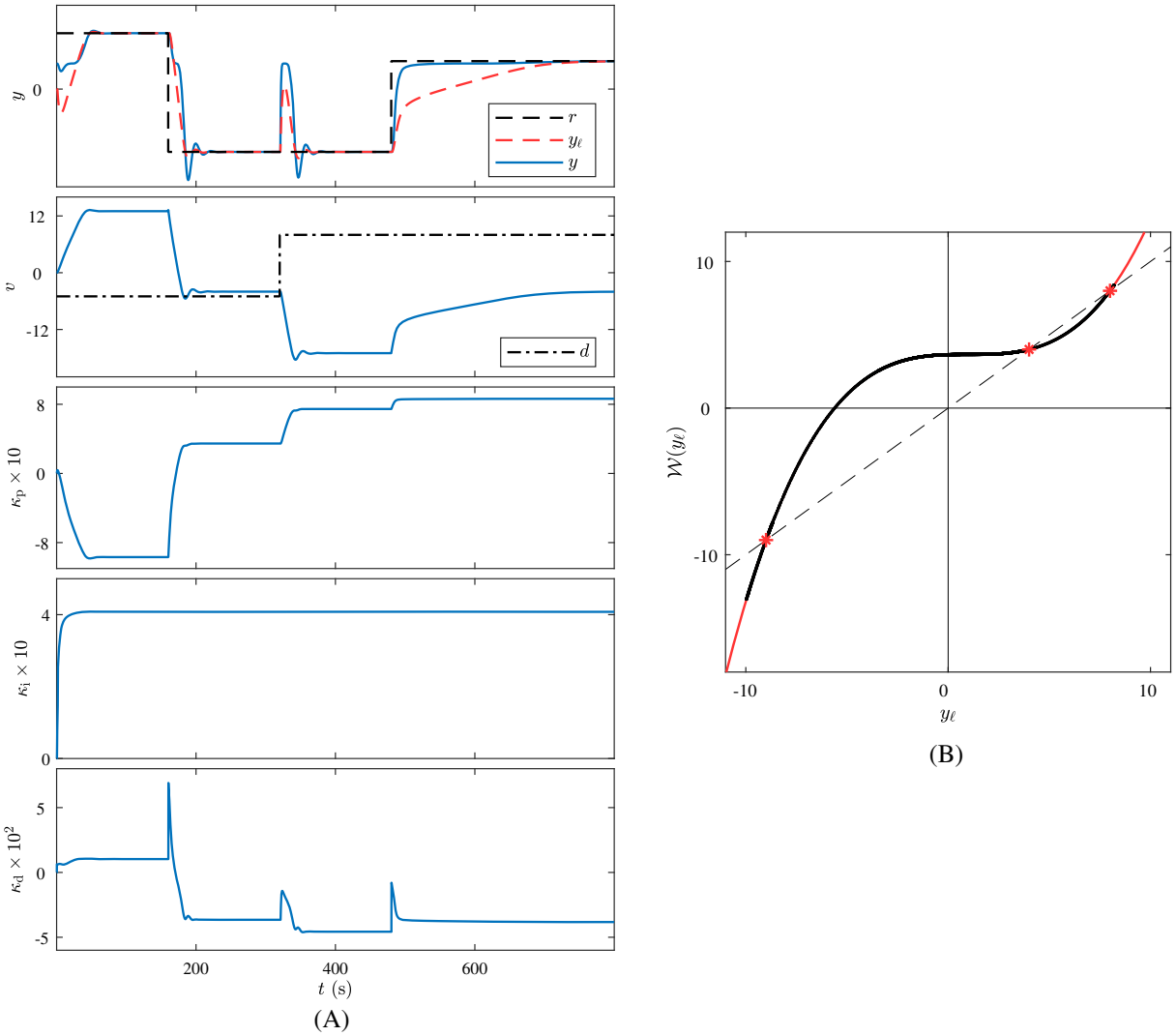

FIGURE 22 A, Example 24: Command following and disturbance rejection with increasing $\mathcal{W}$ and $r = \mathcal{W}(r)$. Both y_ℓ and y follow the command r asymptotically; B, Example 24: $\mathcal{W}$ as a function of y_ℓ. Each black dot denotes a point $(y_\ell(t), \mathcal{W}(y_\ell(t)))$ computed during the simulation. The red stars indicate the points $(y_\ell, \mathcal{W}(y_\ell)) = (r, r)$. The dashed line is the locus of $(\bar{y}, \mathcal{W}(\bar{y}))$ that satisfy $\bar{y} = \mathcal{W}(\bar{y})$

Example 27. *Sensor-magnitude saturation* $\mathcal{W}$. Assume that $\mathcal{H}$ and $\mathcal{L}$ are absent, and let $\mathcal{W}$ be given by

$$\mathcal{W}(y_\ell) = \begin{cases} -10, & y_\ell \le -10, \\ y_\ell, & -10 < y_\ell < 9, \\ 9, & y_\ell \ge 9. \end{cases} \tag{45}$$

Let $K = 3$ and $\overline{u} = -\underline{u} = 30$. Figure 24A shows that asymptotic command following and disturbance rejection are achieved in the presence of sensor-magnitude saturation.

Example 28. *Sensor-magnitude deadzone* $\mathcal{W}$. Assume that $\mathcal{H}$ and $\mathcal{L}$ are absent, and let $\mathcal{W}$ be given by

$$\mathcal{W}(y_\ell) = \begin{cases} y_\ell + 8, & y_\ell < -8, \\ 0, & -8 \le y_\ell \le 12, \\ y_\ell - 12, & y_\ell > 12. \end{cases} \tag{46}$$

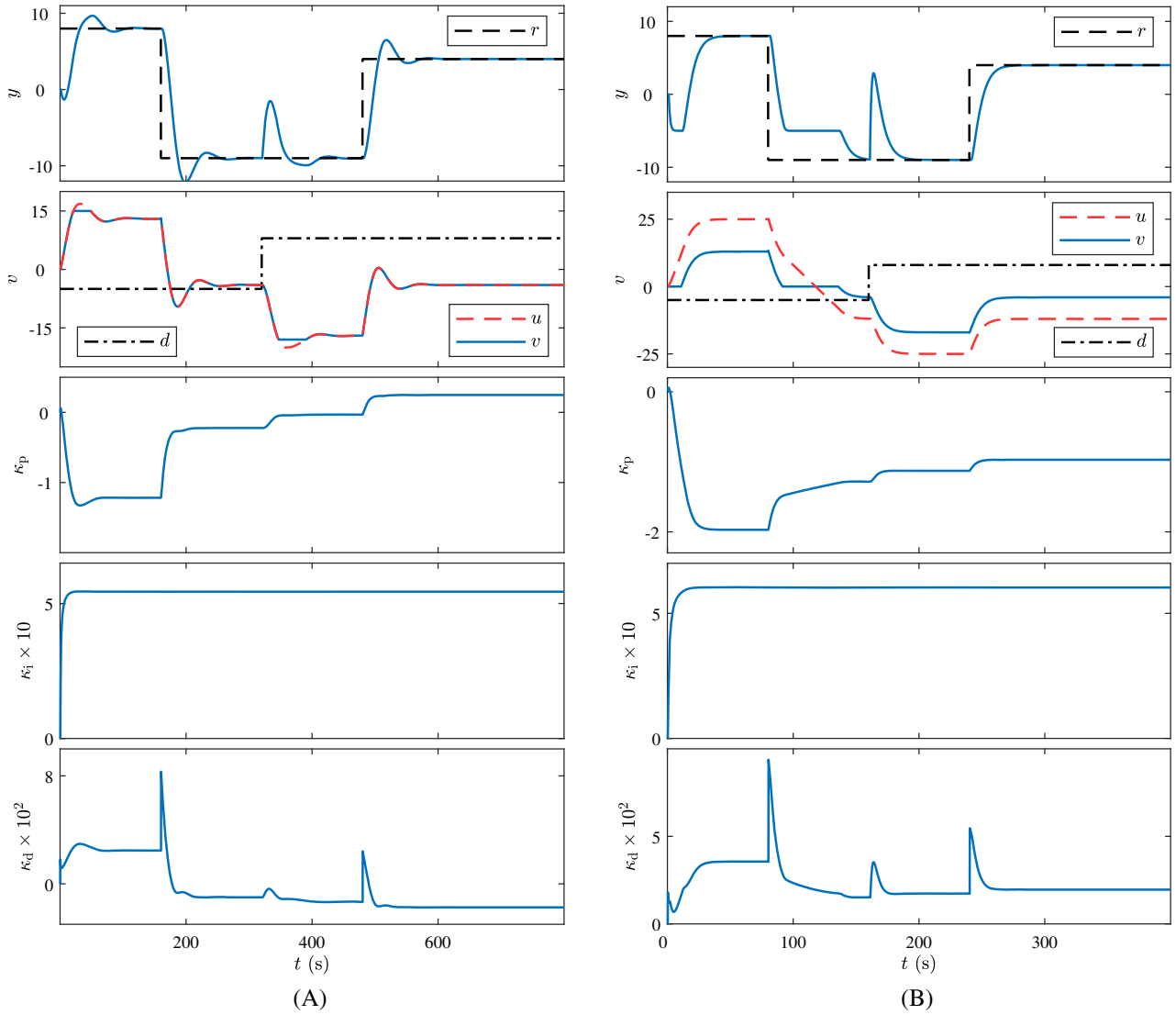

FIGURE 23 A, Example 25: Command following and disturbance rejection with control-magnitude saturation; B, Example 26: Command following and disturbance rejection with control-magnitude deadzone

Let $\overline{u} = -\underline{u} = 30$. Figure 24B shows that asymptotic command following and disturbance rejection are achieved in the presence of sensor-magnitude deadzone.

Example 29. *Continuous $\mathcal{H}$ and $\mathcal{W}$.* Consider the case where $\mathcal{H}$ and $\mathcal{W}$ are present and given by

$$\mathcal{W}(y_\ell) = \frac{40(1 - e^{-y_\ell})}{1 + e^{-y_\ell}} - 26, \quad \mathcal{H}(u) = u + 5\tanh u + 5. \tag{47}$$

Figure 25A shows asymptotic command following and disturbance rejection. Figure 25B shows $\mathcal{H}$ and $\mathcal{W}$ as well as the points computed during the simulation. Since $\mathcal{H}$ and $\mathcal{W}$ are increasing, and $K = 1$, (A9) implies that σ must be chosen to be 1.

Example 30. *Continuous $\mathcal{H}$ and $\mathcal{W}$ with negative trends.* Reconsider Example 29 with $\mathcal{H}$ multiplied by -1. Figure 26A shows asymptotic command following and disturbance rejection. Figure 26B shows $\mathcal{H}$ and $\mathcal{W}$ as well as the points computed during the simulation. Since $\mathcal{H}$ is decreasing, $\mathcal{W}$ is increasing, and $K = 1$, (A9) implies that σ must be chosen to be -1.

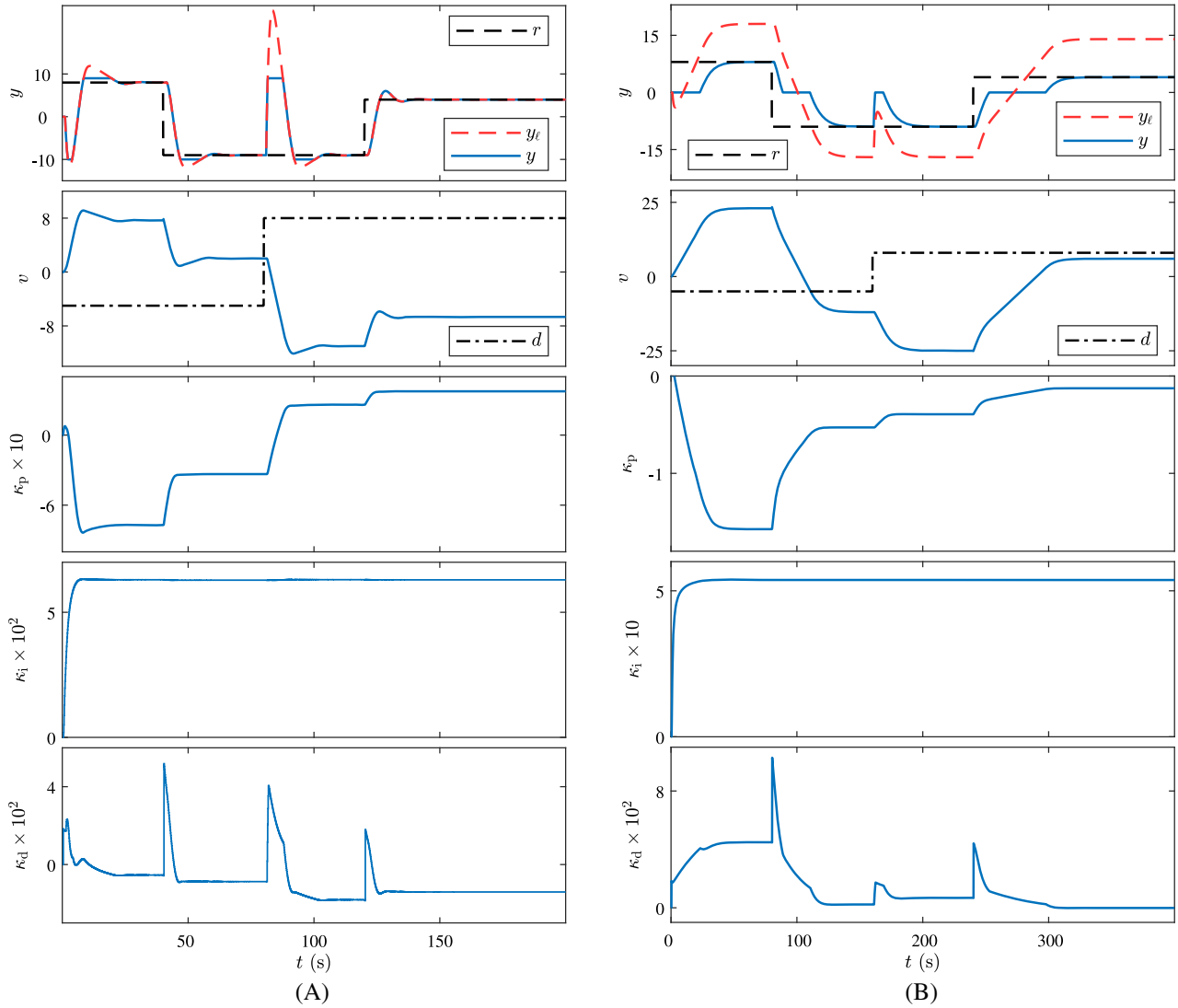

FIGURE 24 A, Example 27: Command following and disturbance rejection with sensor-magnitude saturation; B, Example 28: Command following and disturbance rejection with sensor-magnitude deadzone

Example 31. *Discontinuous* $\mathcal{H}$. Assume that $\mathcal{W}$ and $\mathcal{L}$ are absent and let $\mathcal{H}$ be the discontinuous actuator nonlinearity

$$\mathcal{H}(u) = u + 4\left\lceil \frac{u-3}{4} \right\rceil - 3. \tag{48}$$

Figure 27A shows asymptotic command following and disturbance rejection. Figure 27B shows $\mathcal{H}$ and the points computed during the simulation. Note that SBC does not impose any assumption on the continuity of $\mathcal{H}$.

Example 32. *Discontinuous* $\mathcal{W}$. Assume that $\mathcal{H}$ and $\mathcal{L}$ are absent and let $\mathcal{W}$ be the discontinuous output nonlinearity

$$\mathcal{W}(y_\ell) = y_\ell + 4\left\lfloor \frac{y_\ell + 3}{4} \right\rfloor + 3. \tag{49}$$

Figure 28A shows asymptotic command following and disturbance rejection. Figure 28B shows $\mathcal{W}$ and the points computed during the simulation. Note that SBC does not impose any assumption on the continuity of $\mathcal{W}$.

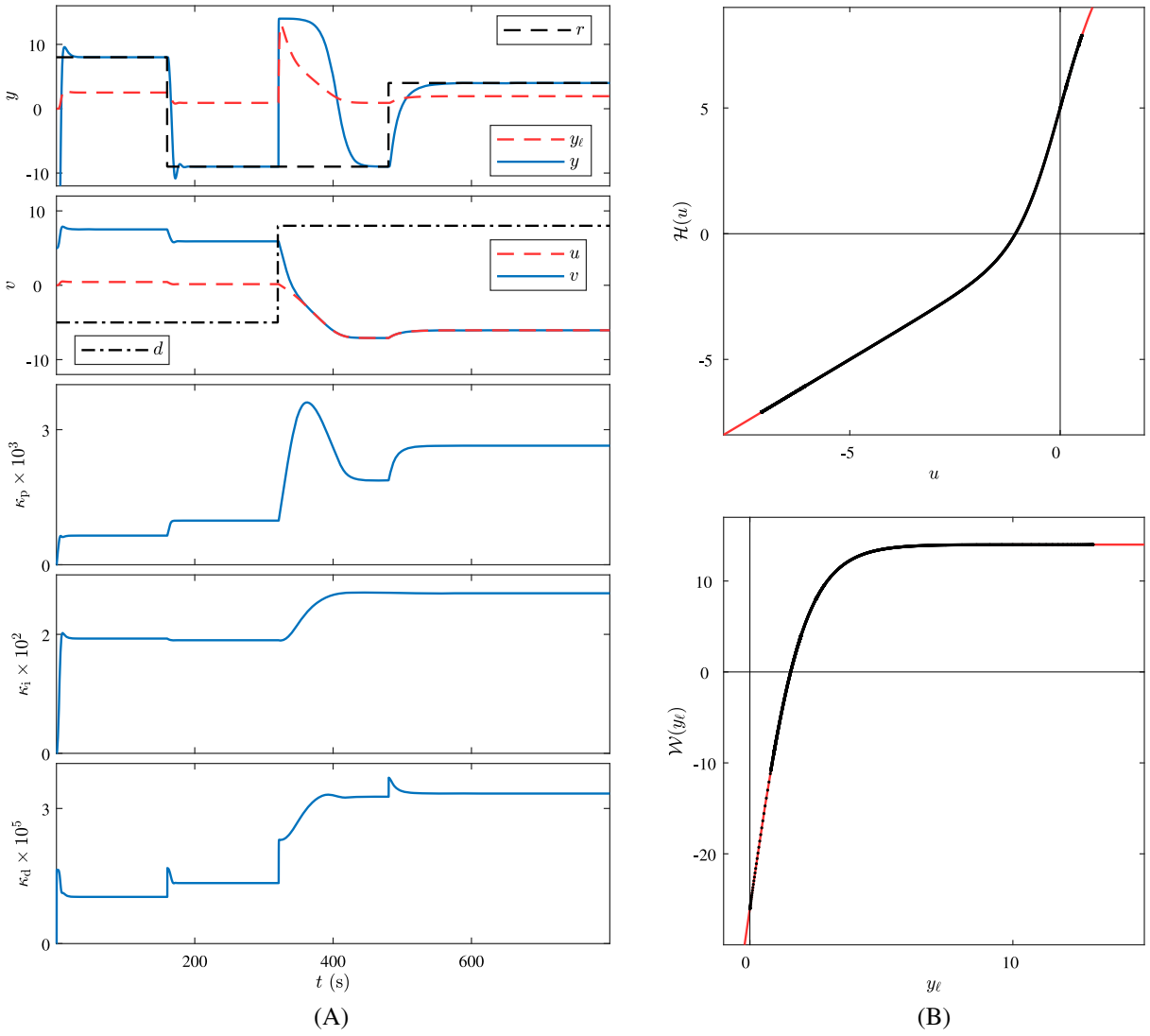

FIGURE 25 A, Example 29: Command following and disturbance rejection with nondecreasing $\mathcal{H}$ and $\mathcal{W}$; B, Example 29: $\mathcal{H}$ as a function of u and $\mathcal{W}$ as a function of y_ℓ. Each black dot denotes a point $(u(t), \mathcal{H}(u(t)))$ and $(y_\ell(t), \mathcal{W}(y_\ell(t)))$ computed during the simulation

Example 33. *Continuous* $\mathcal{L}$. Assume that $\mathcal{H}$ and $\mathcal{W}$ are absent, and let $\mathcal{L}$ be the continuous, increasing feedback nonlinearity

$$\mathcal{L}(y_\ell) = 1 + \begin{cases} \sqrt{y_\ell}, & y_\ell \geq 0, \\ -\sqrt{-y_\ell}, & y_\ell < 0. \end{cases} \tag{50}$$

Since SBC does not assume that trend $\mathcal{L}$ is known, the system is simulated with both $\mathcal{L}$ and $\mathcal{L}$ replaced with $-\mathcal{L}$. In both cases, Figure 29A shows asymptotic command following and disturbance rejection.

Example 34. *Discontinuous* $\mathcal{L}$. Assume that $\mathcal{H}$ and $\mathcal{W}$ are absent and let $\mathcal{L}$ be the discontinuous, nondecreasing feedback nonlinearity

$$\mathcal{L}(y_\ell) = 1 + \left\lceil \frac{y_\ell}{2} \right\rceil. \tag{51}$$

Since SBC does not assume that trend $\mathcal{L}$ is known, the system is simulated with both $\mathcal{L}$ and $\mathcal{L}$ replaced with $-\mathcal{L}$. In both cases, Figure 29B shows asymptotic command following and disturbance rejection. Note that SBC does not impose any assumption on the continuity of $\mathcal{L}$.

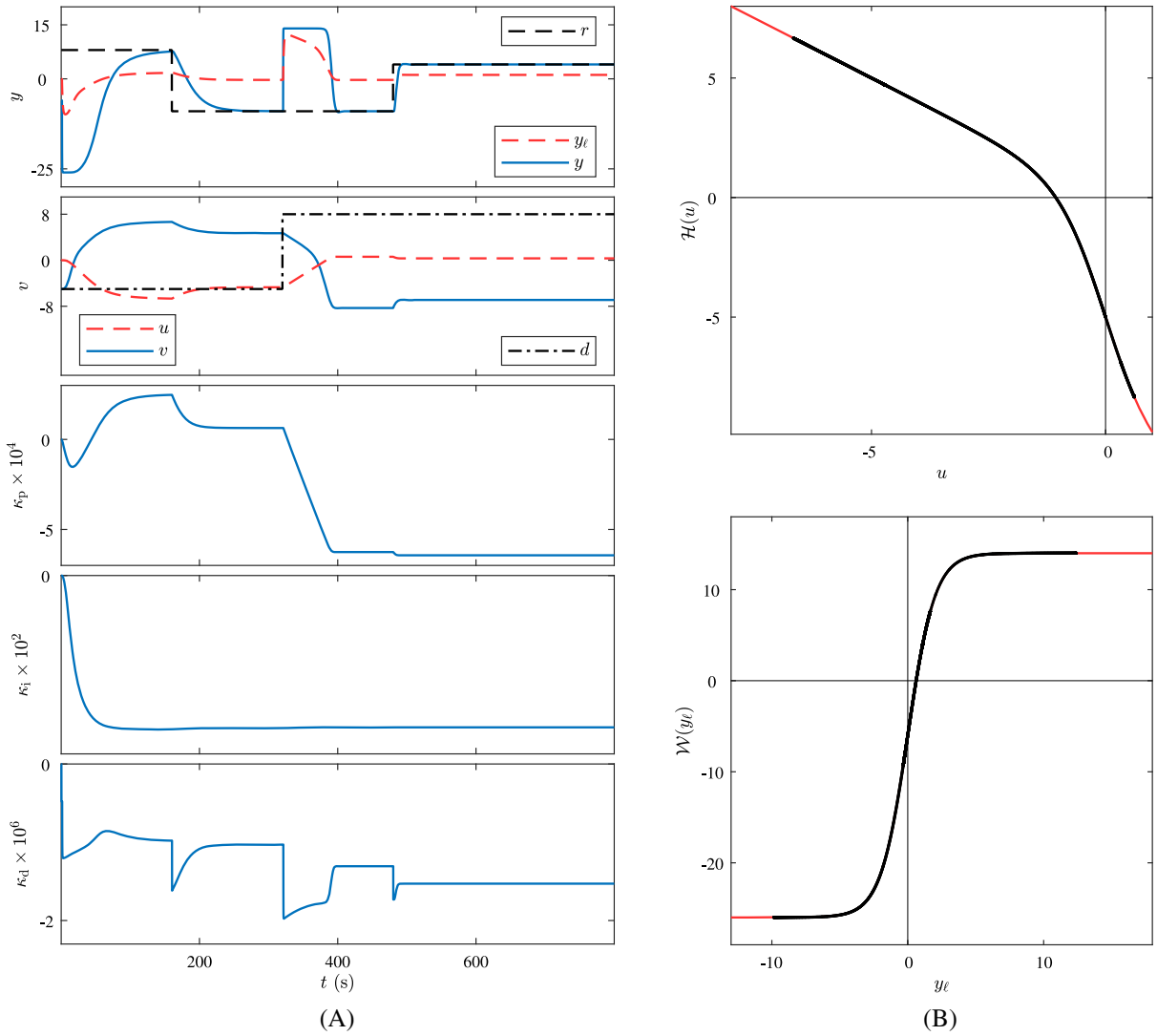

FIGURE 26 A, Example 30: Command following and disturbance rejection with nonincreasing $\mathcal{H}$ and nondecreasing $\mathcal{W}$; B, Example 30: $\mathcal{H}$ as a function of u and $\mathcal{W}$ as a function of y_ℓ. Each black dot denotes a point $(u(t), \mathcal{H}(u(t)))$ and $(y_\ell(t), \mathcal{W}(y_\ell(t)))$ computed during the simulation

11 | NONLINEAR EXAMPLES VIOLATING THE ASSUMPTIONS OF SBC

The examples in this section consider the performance of the adaptive digital PID controller for the basic servo loop shown in Figure 1 in the case where one or more of (A1) to (A9) are violated. For all of these examples, either $\mathcal{H}$ or $\mathcal{W}$ is a nonlinear function. In order to investigate the effect of violating the assumptions of SBC with nonlinear $\mathcal{W}, \mathcal{H}$, we consider examples with conditions that may be encountered in practical applications and that violate SBC. In particular, the examples in this section consider the effect of control and measurement-rate saturation, infeasible r due to control and magnitude saturation, infeasible r due to discontinuous $\mathcal{H}$ and $\mathcal{W}$, and nonmonotonic $\mathcal{H}$, $\mathcal{W}$, and $\mathcal{L}$. The properties and values considered are summarized in Table 4.

Example 35. *Control-rate saturation.* Let $\bar{\delta}_u > 0$ and $\underline{\delta}_u < 0$ be the positive and negative control-rate-saturation levels, respectively. In terms of samples, the maximum allowable increase and decrease in the control input over each sampling period are thus $\bar{\delta}_u T_s$ and $\underline{\delta}_u T_s$, respectively. Let $(\underline{\delta}_u, \bar{\delta}_u) = (-1, 0.5), (-2, 1), (-3, 2)$. Figure 30A shows asymptotic command following and disturbance rejection. These simulations suggest that asymptotic command following and disturbance rejection are achieved with arbitrarily small control-rate-saturation levels.

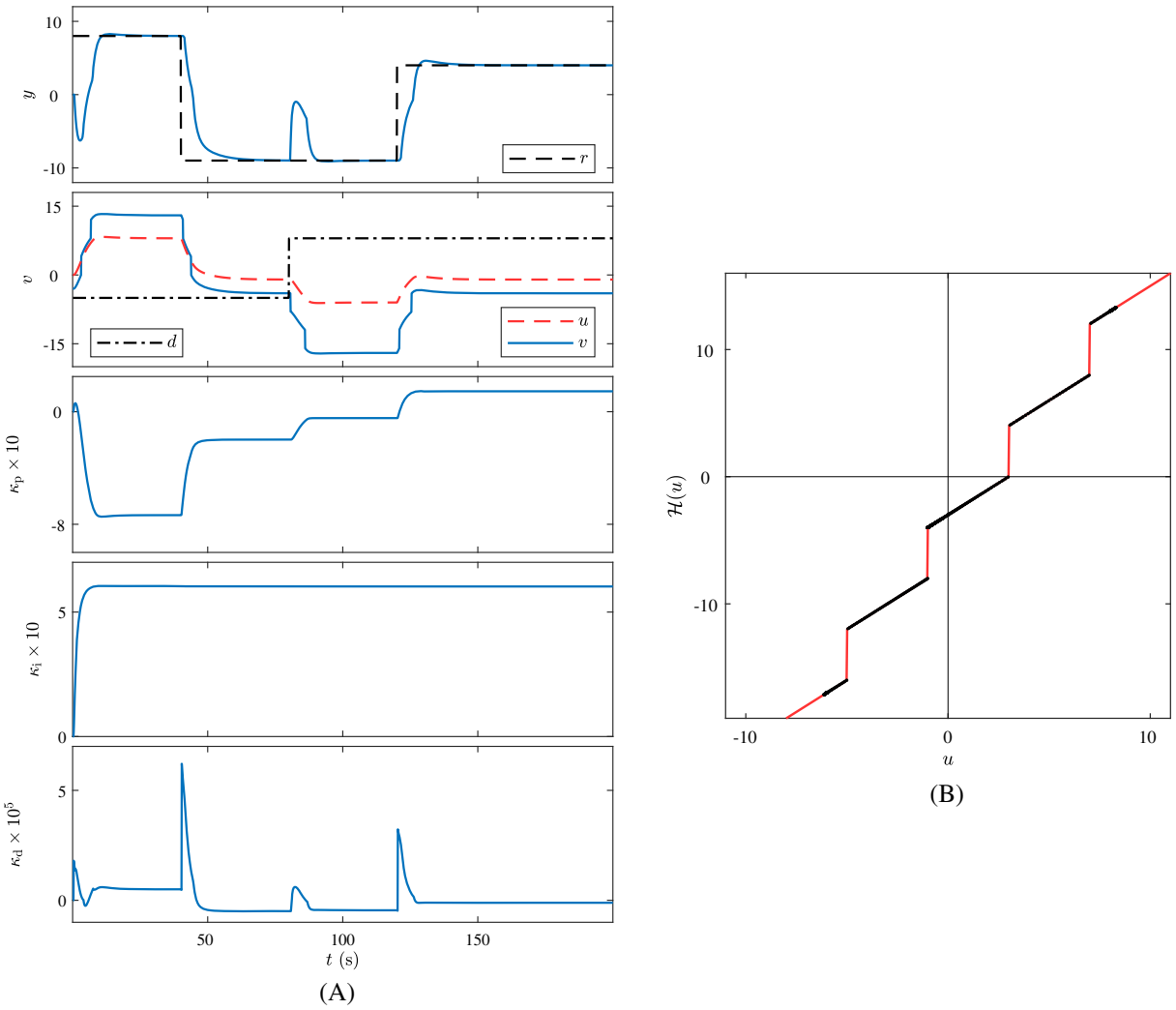

FIGURE 27 A, Example 31: Command following and disturbance rejection with discontinuous $\mathcal{H}$. Note that simulation-based conjecture does not impose a continuity assumption on $\mathcal{H}$; B, Example 31: $\mathcal{H}$ as a function of u. Each black dot denotes a point $(u(t), \mathcal{H}(u(t)))$ computed during the simulation

Example	Investigated effect	Remarks
35	Control-rate saturation	$(\underline{\delta}_u, \overline{\delta}_u) = (-2, 1), (-3, 2), (-4, 3)$
36	Measurement-rate saturation	$(\underline{\delta}_y, \overline{\delta}_y) = (-2, 1), (-3, 2), (-4, 3)$
37	Infeasible r due to control-magnitude saturation $\mathcal{H}$	Asymmetric
38	Infeasible r due to sensor-magnitude saturation $\mathcal{W}$	Increasing sensor saturation
39	Infeasible r due to discontinuous $\mathcal{H}$	Quantization
40	Infeasible r due to discontinuous $\mathcal{W}$	Quantization
41	Nonmonotonic $\mathcal{H}$, $\mathcal{W}$, and $\mathcal{L}$	(A6)-(A8) are not satisfied
42	Nonmonotonic $\mathcal{H}$, $\mathcal{W}$, and $\mathcal{L}$	(A6)-(A8) are not satisfied

TABLE 4 Summary of adaptive digital proportional-integral-derivative control for nonlinear examples violating the assumptions of simulation-based conjecture

Example 36. *Measurement-rate saturation.* Let $\overline{\delta}_y > 0$ and $\underline{\delta}_y < 0$ be the positive and negative measurement-rate-saturation levels, respectively. In terms of samples, the maximum allowable increase and decrease in the sensor measurement over each sampling period are thus $\overline{\delta}_y T_s$ and $\underline{\delta}_y T_s$, respectively. Let $(\underline{\delta}_y, \overline{\delta}_y) = (-0.5, 0.3), (-0.7, 0.5), (-0.9, 1)$. Figure 30B shows asymptotic command following and disturbance rejection. These simulations suggest that asymptotic command following and disturbance rejection are achieved with arbitrarily small measurement-rate-saturation levels.

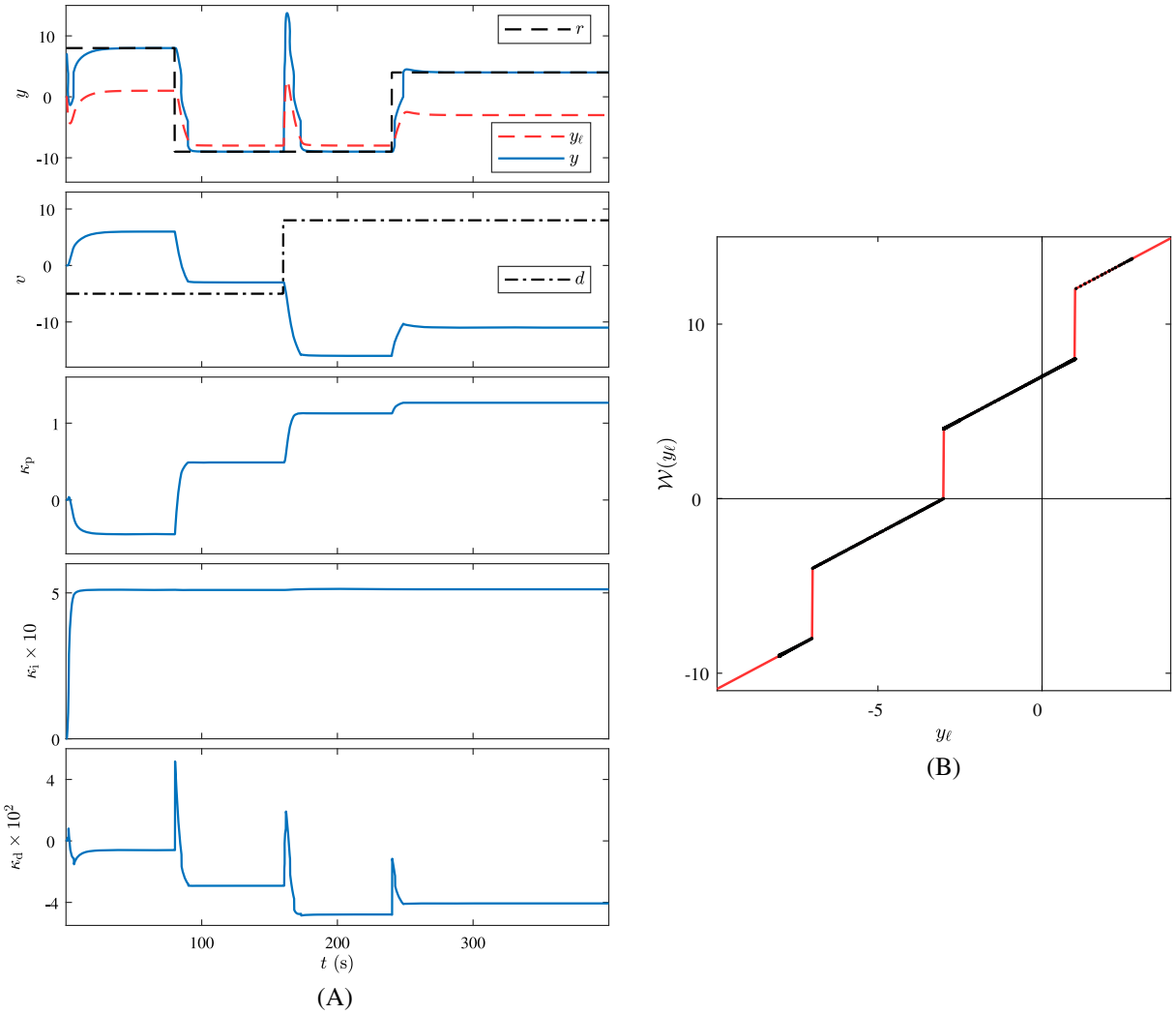

FIGURE 28 A, Example 32: Command following and disturbance rejection with discontinuous $\mathcal{W}$. Note that simulation-based conjecture does not impose a continuity assumption on $\mathcal{W}$; B, Example 32: $\mathcal{W}$ as a function of y_ℓ. Each black dot denotes a point $(y_\ell(t), \mathcal{W}(y_\ell(t)))$ computed during the simulation

Example 37. *Infeasible r due to control-magnitude saturation $\mathcal{H}$.* Assume that $\mathcal{W}$ and $\mathcal{L}$ are absent and $\mathcal{H}$ is the control-magnitude saturation given by

$$\mathcal{H}(u) = 2 + \begin{cases} \frac{u}{2}, & |u| < 20, \\ 10 \operatorname{sign} u, & |u| \geq 20. \end{cases} \tag{52}$$

Let $\bar{u} = -\underline{u} = 10$ and $\tau = 10$. Figure 31A shows asymptotic command following and disturbance rejection. Figure 31B shows $\mathcal{H}$ as well as the points computed during the simulation. Note that, due to control-magnitude saturation $\mathcal{H}$, r is infeasible during some time intervals (eg, for $t < 20$ s); therefore, integrator windup can occur. However, since the antiwindup thresholds $\bar{u}$ and $\underline{u}$ are chosen to be sufficiently small, the antiwindup technique (8) prevents integrator windup, and thus all signals remain bounded.

Example 38. *Infeasible r due to sensor-magnitude saturation $\mathcal{W}$.* Assume that $\mathcal{H}$ and $\mathcal{L}$ are absent, and let $\mathcal{W}$ be the sensor-magnitude saturation nonlinearity

$$\mathcal{W}(y_\ell) = 4\operatorname{atan}(y_\ell - 2). \tag{53}$$

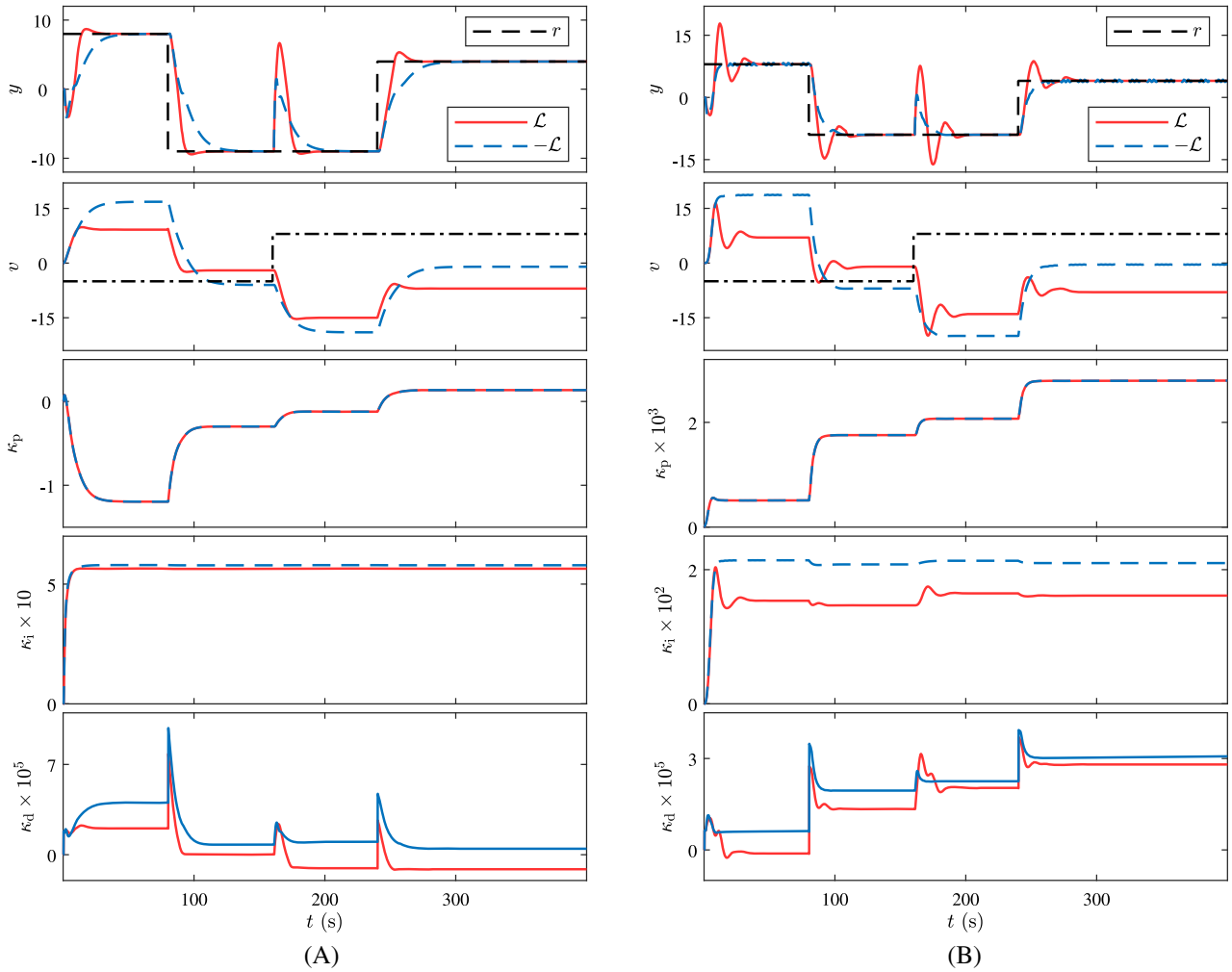

FIGURE 29 A, Example 33: Command following and disturbance rejection with continuous $\mathcal{L}$ and $-\mathcal{L}$. Note that simulation-based conjecture does not impose any assumption on trend $\mathcal{L}$; B, Example 34: Command following and disturbance rejection with discontinuous $\mathcal{L}$ and $-\mathcal{L}$. Note that simulation-based conjecture does not impose any assumptions on trend $\mathcal{L}$ or continuity of $\mathcal{L}$

Let $\bar{u} = -\underline{u} = 15$. Figure 32A shows asymptotic command following and disturbance rejection. Figure 32B shows $\mathcal{W}$ and the points computed during the simulation. Note that, due to the sensor-magnitude saturation $\mathcal{W}$, r is infeasible until $t = 240$ s, and thus windup is possible. However, since the antiwindup thresholds $\bar{u}$ and $\underline{u}$ are chosen to be sufficiently small, the antiwindup technique (8) prevents windup, and thus all signals remain bounded.

Example 39. *Infeasible r due to discontinuous $\mathcal{H}$.* Assume that $\mathcal{W}$ and $\mathcal{L}$ are absent, and consider the discontinuous actuator nonlinearity

$$\mathcal{H}(u) = 2\lceil u \rceil + 2.63, \tag{54}$$

which implies that the control input v is quantized. In this case, r is infeasible. Figure 33A shows that asymptotic command following and disturbance rejection are approximately achieved. In fact, the controller makes u_k chatter between two control values that yield the smallest and second smallest possible command following errors.

Example 40. *Infeasible r due to discontinuous $\mathcal{W}$.* Assume that $\mathcal{H}$ and $\mathcal{L}$ are absent, and consider the discontinuous sensor nonlinearity

$$\mathcal{W}(y_\ell) = 2\lceil y_\ell \rceil + 2.63, \tag{55}$$

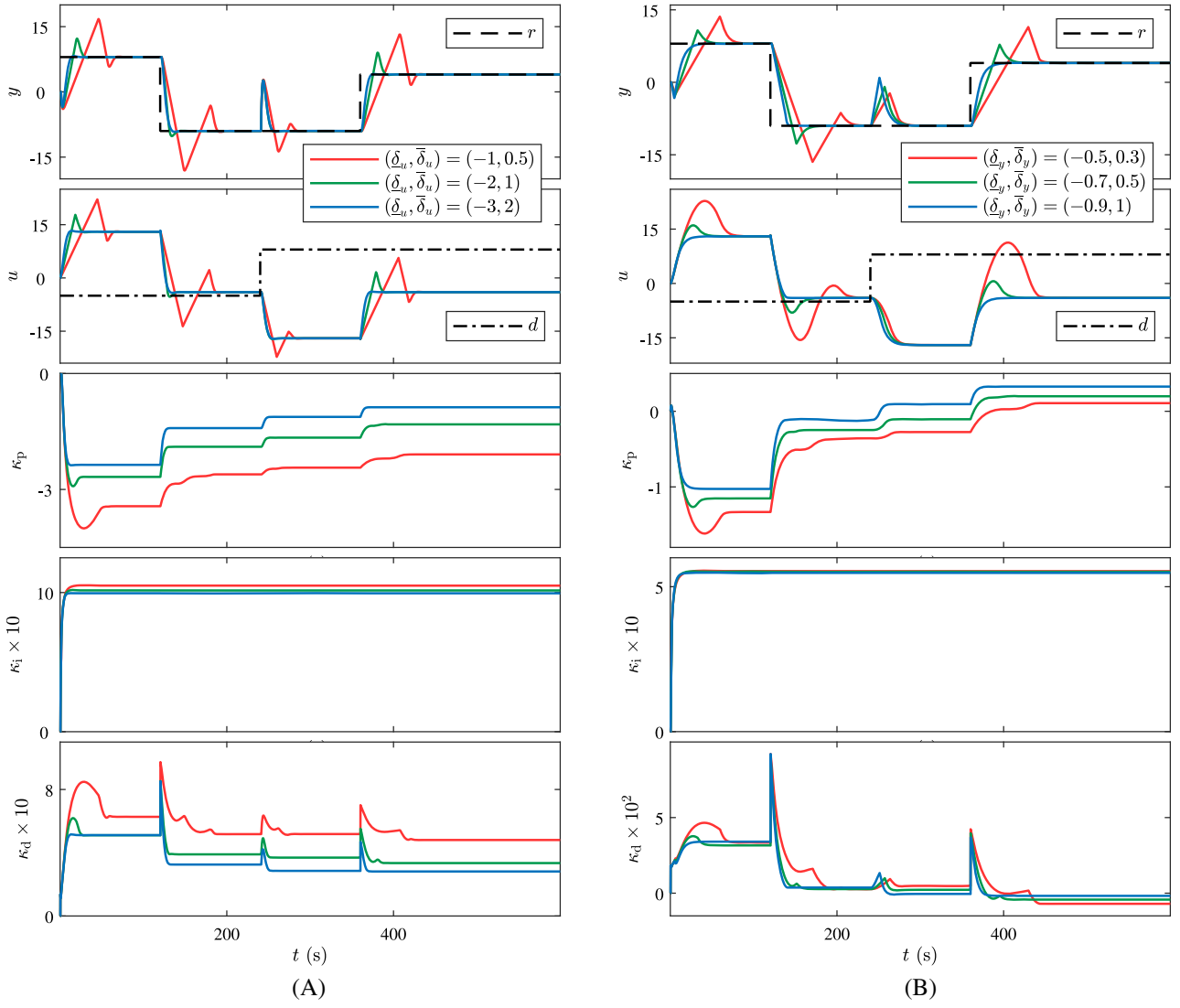

FIGURE 30 A, Example 35: Command following and disturbance rejection with control-rate saturation; B, Example 36: Command following and disturbance rejection with measurement-rate saturation

which implies that the measurement y is quantized. Figure 33B shows that asymptotic command following and disturbance rejection are approximately achieved. In fact, the controller makes u_k chatter between two control values that yield the smallest and second smallest possible command following errors.

Example 41. *Nonmonotonic $\mathcal{H}$, $\mathcal{W}$, and $\mathcal{L}$.* Consider the nonmonotonic sensor, actuator, and feedback nonlinearities

$$\mathcal{H}(u) = u + 2\sin u + 5, \qquad \mathcal{W}(y_\ell) = |y_\ell - 5| - 20, \qquad \mathcal{L}(y_\ell) = \frac{y_\ell}{1 + y_\ell^2} + 1, \tag{56}$$

which do not satisfy (A6) to (A8). Figure 34A shows that asymptotic command following and disturbance rejection are achieved despite the fact that all three nonlinearities are nonmonotonic. Figure 34B shows $\mathcal{H}$, $\mathcal{W}$, and $\mathcal{L}$ and the points computed during the simulation.

Example 42. *Nonmonotonic $\mathcal{H}$, $\mathcal{W}$, and $\mathcal{L}$.* Assume that $\mathcal{W}$ and $\mathcal{L}$ are absent, and consider the nonmonotonic actuator nonlinearity $\mathcal{H}(u) = 15\sin u$, which does not satisfy (A6). Figure 35A shows that command following and disturbance rejection are not achieved. Next, assume that $\mathcal{H}$ and $\mathcal{L}$ are absent, and consider the nonmonotonic sensor nonlinearity $\mathcal{W}(y_\ell) = 15\cos(2y_\ell^2)$, which does not satisfy (A7). Figure 35B shows that command following and disturbance

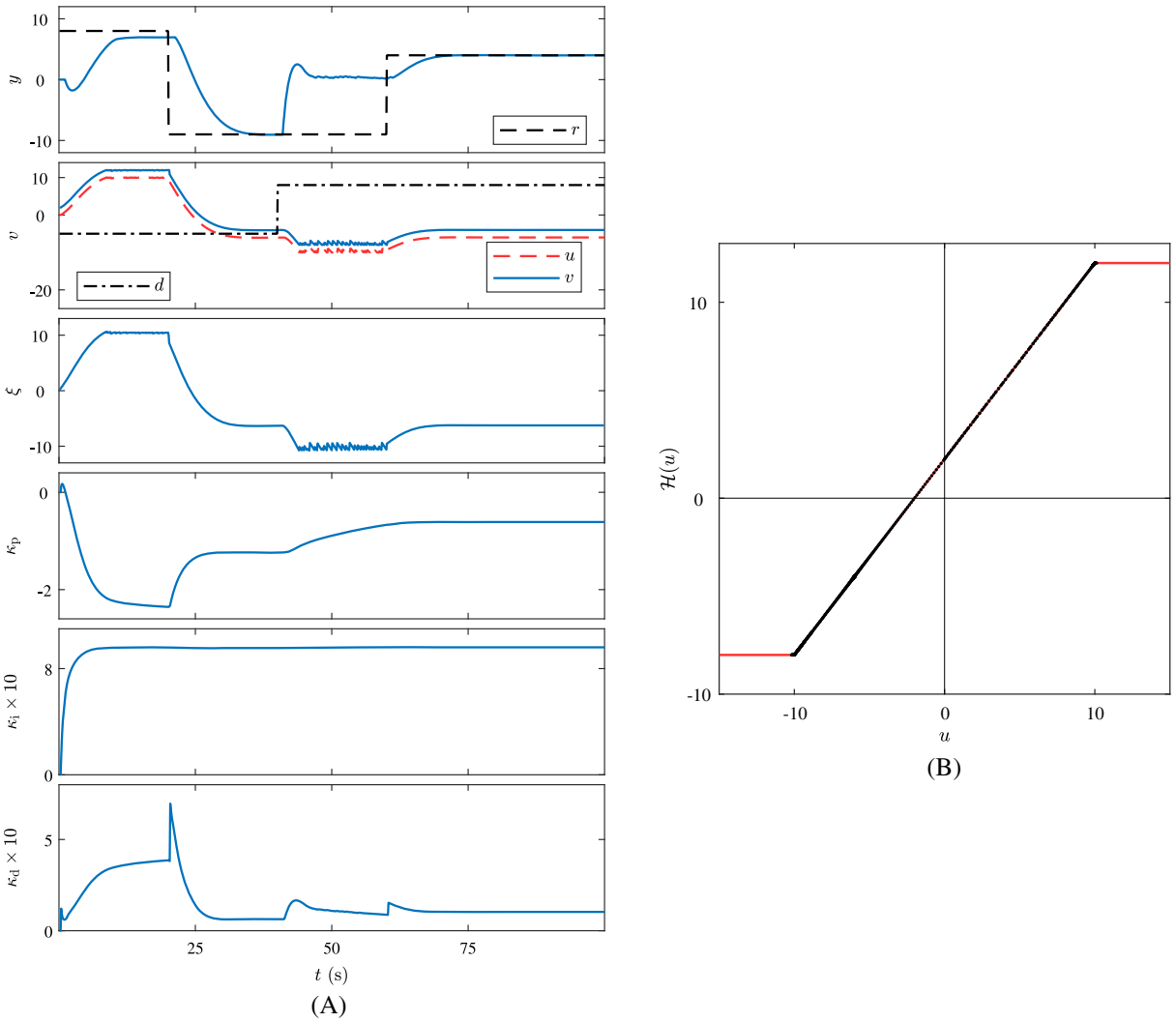

FIGURE 31 A, Example 37: Command following and disturbance rejection with infeasible command due to control-magnitude saturation. The antiwindup technique (8) prevents windup and all signals remain bounded; B, Example 37: $\mathcal{H}$ as a function of u. Each black dot denotes a point $(u(t), \mathcal{H}(u(t)))$ computed during the simulation

rejection are not achieved. Next, assume that $\mathcal{H}$ and $\mathcal{W}$ are absent, and consider the nonmonotonic sensor nonlinearity $\mathcal{L}(y_\ell) = 0.1y_\ell^2$, which does not satisfy (A8). Figure 35C shows that command following and disturbance rejection are not achieved. Figures 35D, 35E, and 35F show $\mathcal{H}$, $\mathcal{W}$, and $\mathcal{L}$ for each case. Unlike Example 41, violating (A6) to (A8) prevents asymptotic command following and disturbance rejection.

12 | ADAPTIVE DIGITAL PID CONTROL OF SECOND-ORDER SYSTEMS

This section applies the adaptive digital PID controller to second-order plants. No attempt is made to state and demonstrate a conjecture as in the case of SBC for first-order-lag-plus-dead-time dynamics. Rather, the goal is to demonstrate the feasibility of the adaptive digital PID controller for these plants while providing insight into tuning and closed-loop performance.

Consider the continuous-time, second-order plant with dead time given by

$$G(s) = \frac{e^{-\tau_d s}}{(s+a)(s+b)}, \tag{57}$$

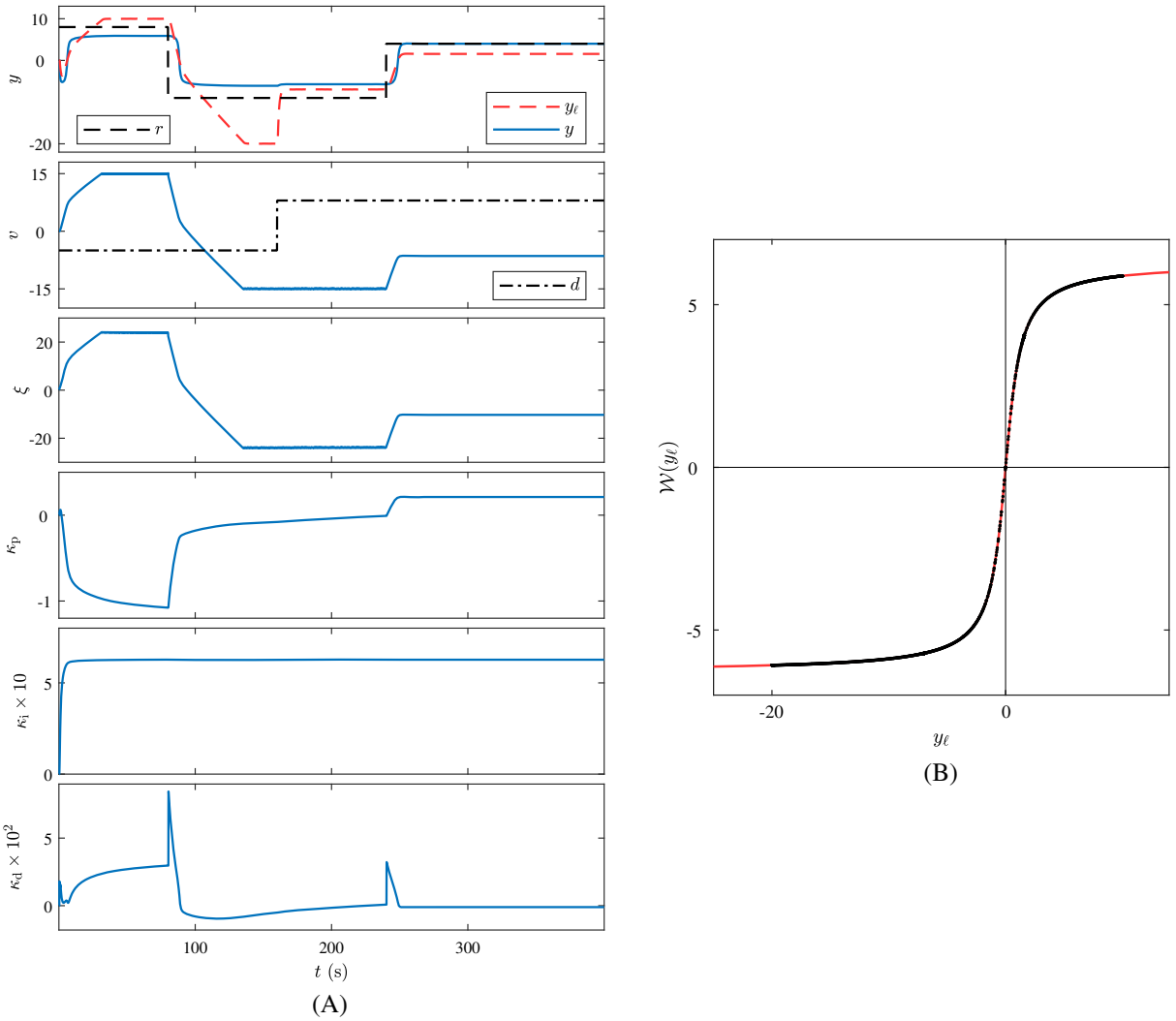

FIGURE 32 A, Example 38: Command following and disturbance rejection with infeasible command due to sensor-magnitude saturation. The antiwindup technique (8) prevents windup and all signals remain bounded; B, Example 38: $\mathcal{W}$ as a function of y_ℓ. Each black dot denotes a point $(y_\ell(t), \mathcal{W}(y_\ell(t)))$ computed during the simulation

where $\tau_d \geq 0$ is the dead time and a and b are either real numbers or complex conjugates. Assuming that $n_d = \tau_d/T_s$ is an integer, it follows that the exactly discretized dynamics are given by

$$G_d(\mathbf{z}) = \begin{cases} \frac{[ae^{aT_s}(e^{bT_s}-1)-be^{bT_s}(e^{aT_s}-1)]\mathbf{z}+a(e^{bT_s}-1)-b(e^{aT_s}-1)}{ab(a-b)(\mathbf{z}e^{aT_s}-1)(\mathbf{z}e^{bT_s}-1)\mathbf{z}^{n_d}}, & a \neq b, a \neq 0, b \neq 0, \\ \frac{[e^{bT_s}(bT_s-1)+1]\mathbf{z}+e^{bT_s}-bT_s-1}{b^2(\mathbf{z}-1)(\mathbf{z}e^{bT_s}-1)\mathbf{z}^{n_d}}, & a = 0, b \neq 0, \\ \frac{[e^{2bT_s}-(bT_s+1)e^{bT_s}]\mathbf{z}+bT_se^{bT_s}-e^{bT_s}+1}{b^2(\mathbf{z}e^{bT_s}-1)^2\mathbf{z}^{n_d}}, & a = b \neq 0, \\ \frac{T_s^2(\mathbf{z}+1)}{2(\mathbf{z}-1)^2\mathbf{z}^{n_d}}, & a = b = 0. \end{cases} \tag{58}$$

These expressions show that the relative degree of the exactly discretized dynamics is $n_d + 1$. Note that poles of the continuous-time dynamics $G(s)$, which are $s = -a$ and $s = -b$, are mapped to $\mathbf{z} = e^{-aT_s}$ and $\mathbf{z} = e^{-bT_s}$, respectively, to form poles of the discrete-time dynamics $G_d(\mathbf{z})$. However, depending on the values of a and b, the sampling zero of the discrete-time dynamics $G_d(\mathbf{z})$ may lie anywhere between -1 and 0 on the real axis. In addition, in the case where a and b are not both zero, it can be shown that the sampling zero of $G_d(\mathbf{z})$ converges to zero as $T_s \to \infty$ and converges to -1 as $T_s \to 0$.

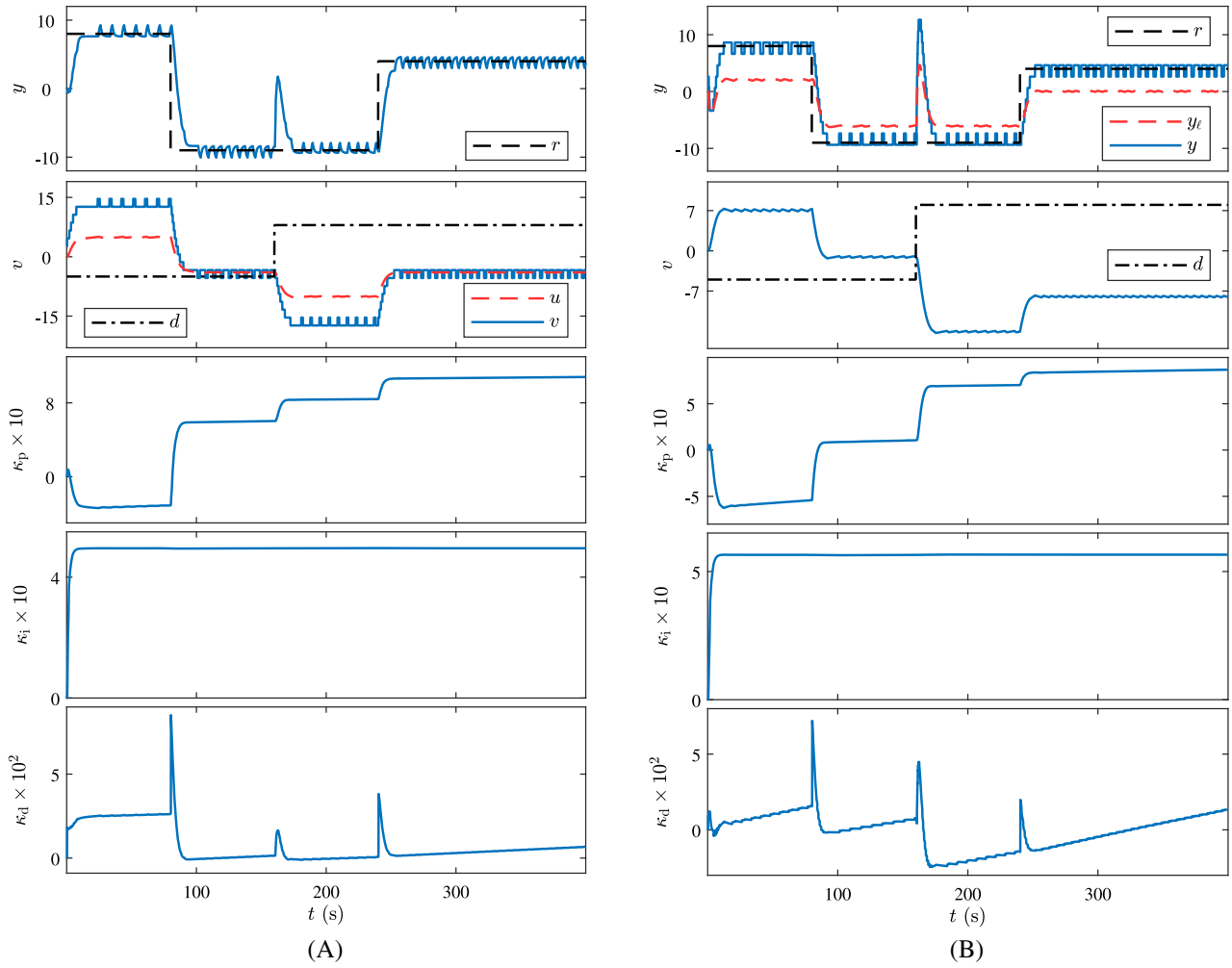

FIGURE 33 A, Example 39: Command following and disturbance rejection with infeasible command due to quantized actuation. The signals y_k and u_k chatter; B, Example 40: Command following and disturbance rejection with infeasible command due to quantized measurements. The signals y_k, u_k chatter

Example	Plant	Remarks
43	Damped oscillator with dead time	$\tau_d = 1, 5, 10$ s
44	Undamped oscillator with dead time	$\tau_d = 1, 1.5, 2$ s
45	Damped rigid body with dead time	$\tau_d = 0.5, 1$ s
46	Undamped rigid body	$\tau_d = 0$

TABLE 5 Summary of adaptive digital proportional-integral-derivative control of second-order plants

To demonstrate the performance of adaptive digital PID controller, we consider examples with dynamics given by the second-order plant (57). The properties and values considered are summarized in Table 5. For the last two examples, which are more challenging, the extended adaptive digital PID control described in the next section is used.

Example 43. *Damped oscillator with dead time.* Consider the plant

$$G(s) = \frac{e^{-\tau_d s}}{2s^2 + 5s + 10}, \tag{59}$$

which represents the dynamics of a damped oscillator with dead time. Let $\tau_d = n_d T_s$, where n_d is a positive integer. It follows from (58) that the discrete-time counterpart of $G(s)$ with sample time $T_s = 0.1$ s is

$$G_d(\mathbf{z}) = \frac{0.0023\mathbf{z} + 0.0021}{(\mathbf{z}^2 - 1.735\mathbf{z} + 0.7788)\mathbf{z}^{n_d}}. \tag{60}$$

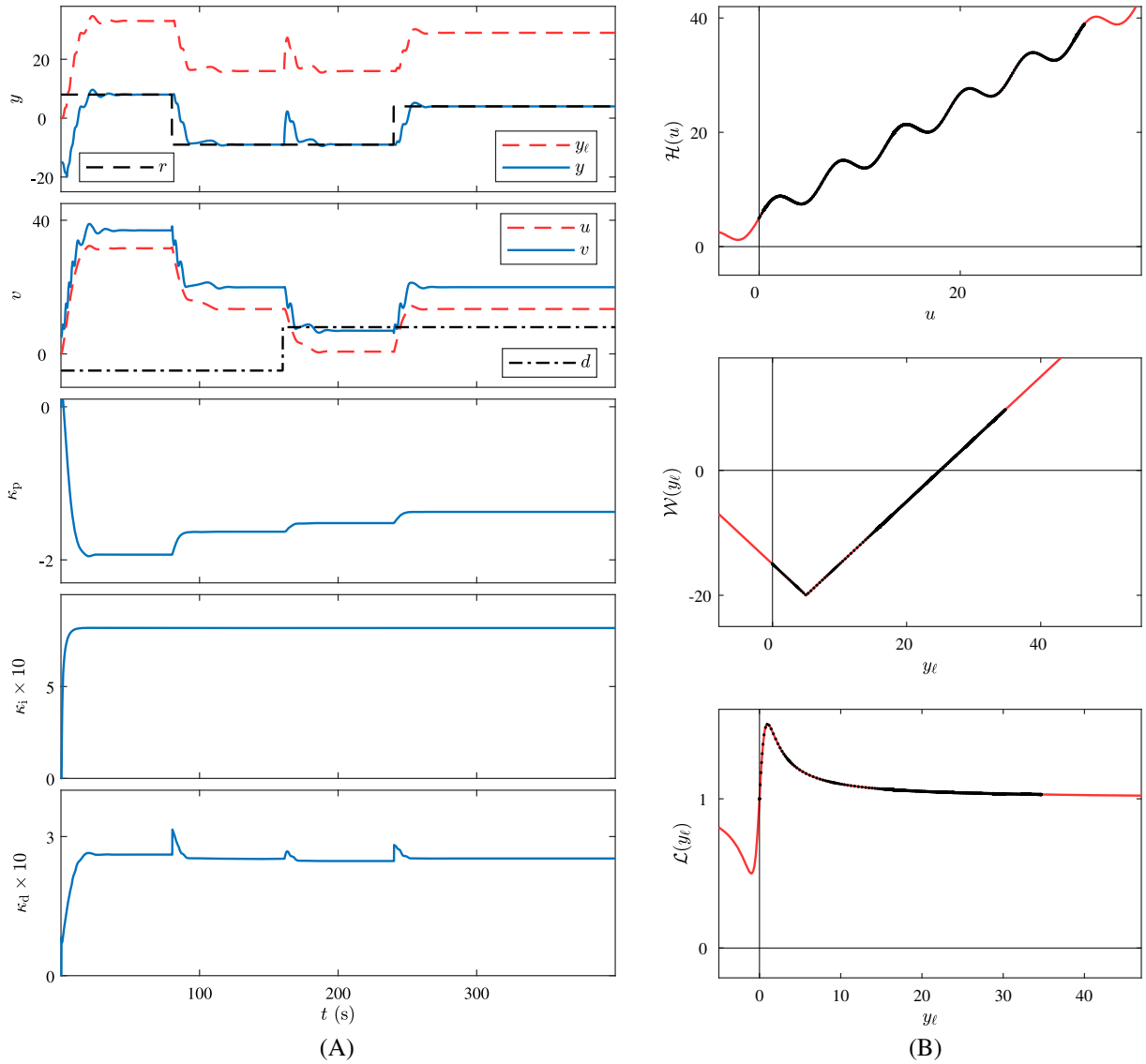

FIGURE 34 A, Example 41: Command following and disturbance rejection with nonmonotonic $\mathcal{H}$, $\mathcal{W}$, and $\mathcal{L}$; B, Example 41: $\mathcal{H}$ as a function of u, and $\mathcal{W}$ and $\mathcal{L}$ as functions of y_ℓ. Each black dot denotes a point $(u(t), \mathcal{H}(u(t)))$, $(y_\ell(t), \mathcal{W}(y_\ell(t)))$, and $(y_\ell(t), \mathcal{L}(y_\ell(t)))$ computed during the simulation

Figure 36A shows asymptotic command following and disturbance rejection for $\tau_d = 1, 5, 10$ s (ie, $n_d = 10, 50, 100$).

Example 44. *Undamped oscillator with dead time.* Consider the plant

$$G(s) = \frac{e^{-\tau_d s}}{2s^2 + 10}, \tag{61}$$

which represents an undamped oscillator with dead time. Let $\tau_d = n_d T_s$, where n_d is a positive integer. It follows from (58) that the discrete-time counterpart of $G(s)$ with sample time $T_s = 0.1$ s is

$$G_d(\mathbf{z}) = \frac{0.00249(\mathbf{z} + 1)}{(\mathbf{z}^2 - 1.95\mathbf{z} + 1)\mathbf{z}^{n_d}}. \tag{62}$$

Figure 36B shows asymptotic command following and disturbance rejection for $\tau_d = 1, 1.5, 2$ s (ie, $n_d = 10, 15, 20$).

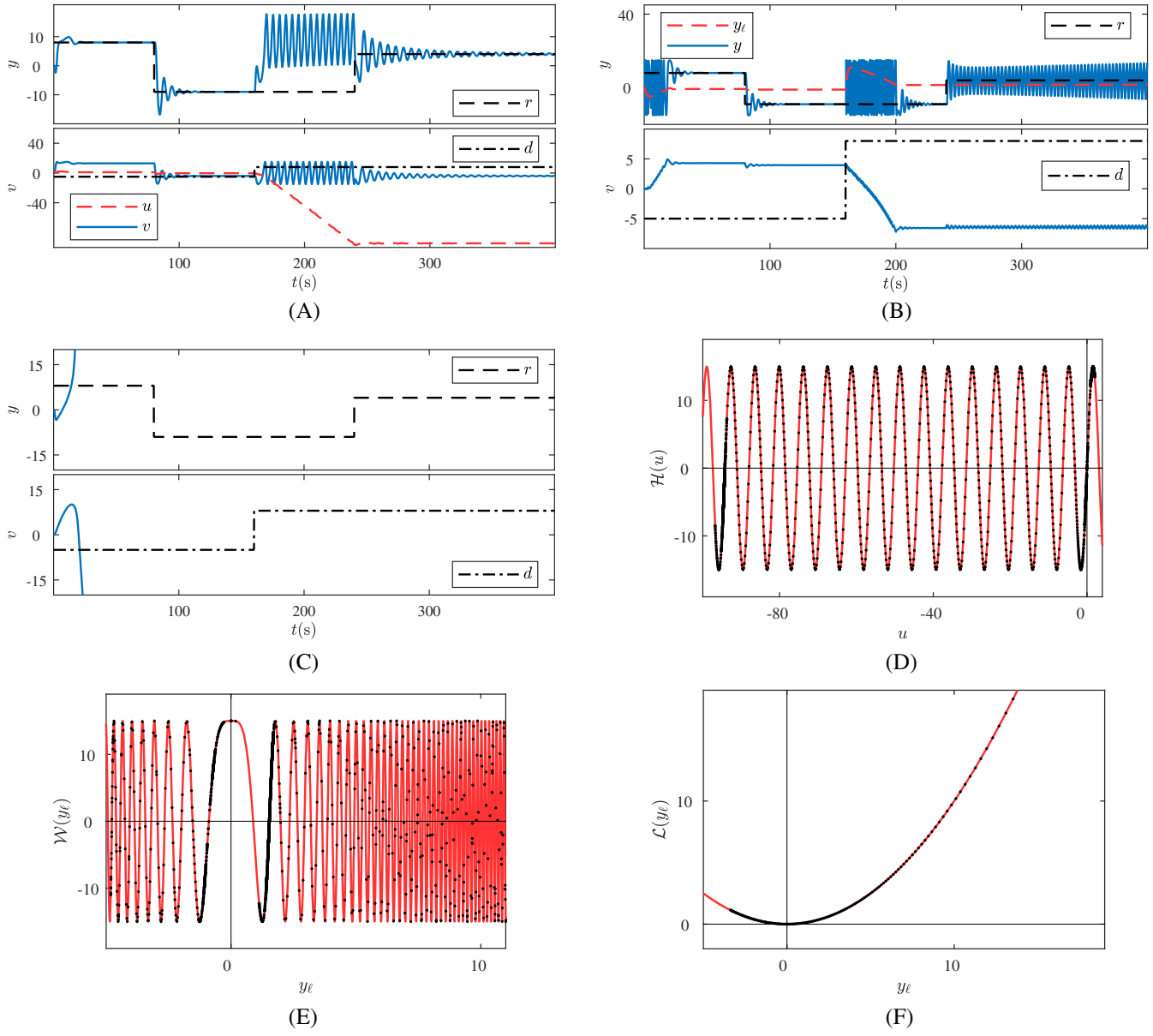

FIGURE 35 A, Example 42: Command following and disturbance rejection with nonmonotonic $\mathcal{H}$. The response diverges; B, Example 42: $\mathcal{H}$ as a function of u. Black dots denote $(u(t), \mathcal{H}(u(t)))$; C, Example 42: Command following and disturbance rejection with nonmonotonic $\mathcal{W}$. The response diverges; D, Example 42: $\mathcal{W}$ as a function of y_ℓ. Black dots denote $(y_\ell(t), \mathcal{W}(y_\ell(t)))$; E, Example 42: Command following and disturbance rejection with nonmonotonic $\mathcal{L}$. The response diverges; F, Example 42: $\mathcal{L}$ as a function of y_ℓ. Black dots denote $(y_\ell(t), \mathcal{L}(y_\ell(t)))$

Example 45. *Damped rigid body with dead time.* Consider the plant

$$G(s) = \frac{e^{-\tau_d s}}{2s^2 + 20s}, \tag{63}$$

which represents the dynamics of a damped rigid body with dead time. Let $\tau_d = n_d T_s$, where n_d is a positive integer. It follows from (58) that the discrete-time counterpart of $G(s)$ with sample time $T_s = 0.1$ s is

$$G_d(\mathbf{z}) = \frac{0.0018\mathbf{z} + 0.0013}{(\mathbf{z}^2 - 1.368\mathbf{z} + 0.3679)\mathbf{z}^{n_d}}. \tag{64}$$

Let $G_f(\mathbf{q}) = \mathbf{q}^{-30}$, $p_0 = 0.1$, $\mu = 10^3$, and $\nu = 1$, and assume that the control u saturates at ± 50. The choice of G_f, which is due to the largest dead time, is implemented using the extended adaptive digital PID controller described

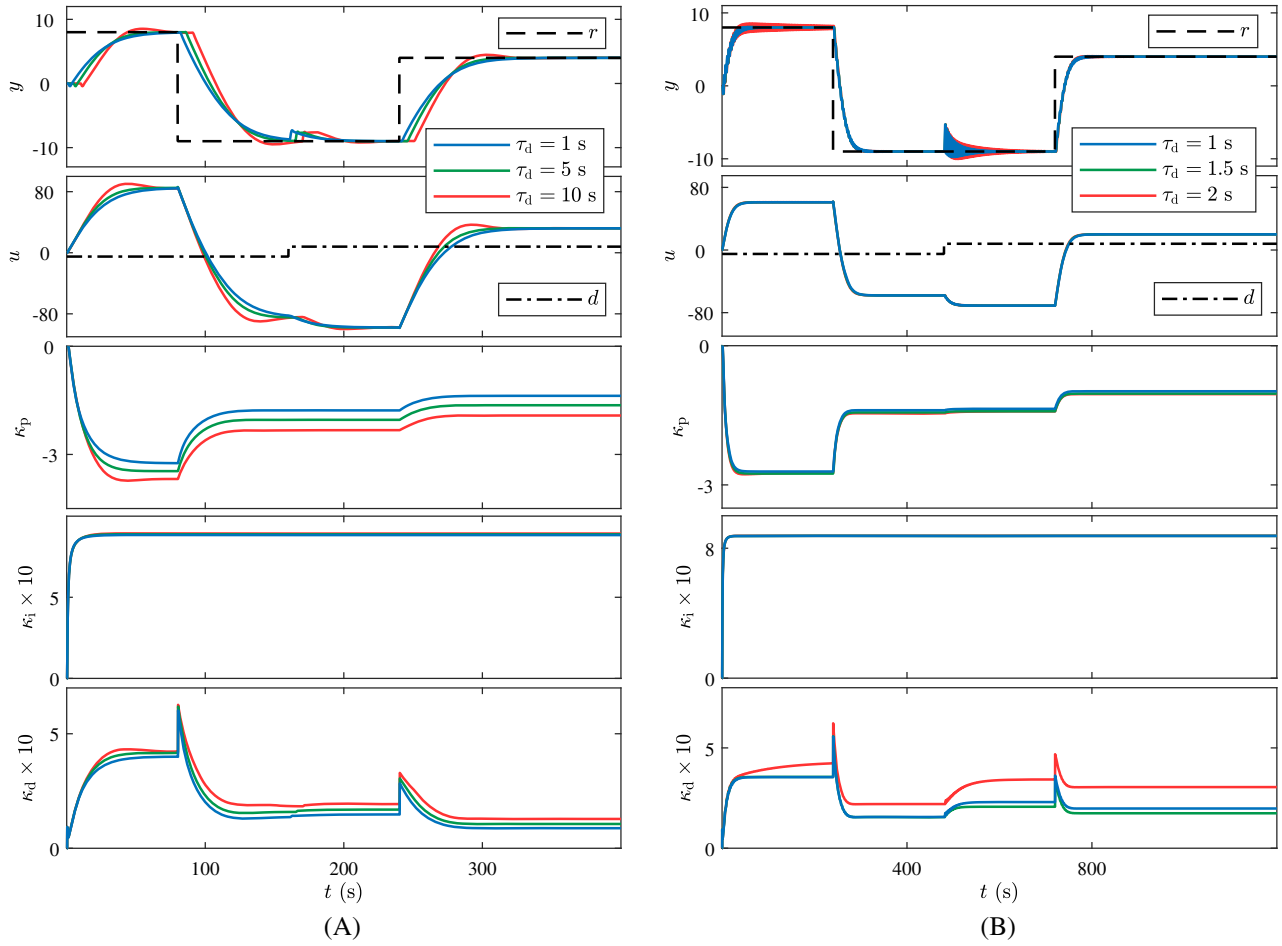

FIGURE 36 A, Example 43: Command following and disturbance rejection for the damped oscillator with various values of dead time; B, Example 44: Command following and disturbance rejection for an undamped oscillator with various values of dead time

in the next section. Figure 37A shows asymptotic command following and disturbance rejection for $\tau_d = 0.5, 1, 2$ s (ie, $n_d = 5, 10, 20$).

Example 46. *Undamped rigid body.* Consider the plant

$$G(s) = \frac{1}{s^2}, \tag{65}$$

which represents the dynamics of an undamped rigid body. Let $\tau_d = 0$. It follows from (58) that the discrete-time counterpart of $G(s)$ with sample time $T_s = 0.1$ s is

$$G_d(\mathbf{z}) = \frac{0.005(\mathbf{z}+1)}{(\mathbf{z}-1)^2}. \tag{66}$$

Let $G_f(\mathbf{q}) = \mathbf{q}^{-5}$, $p_0 = 10^3$, $\mu = 10^3$, and $\nu = 20$, and assume that the control u saturates at ± 50. Figure 37B shows asymptotic command following and disturbance rejection. For this example, dead time requires specialized tuning, and thus τ_d is chosen to be zero.

13 | EXTENDED ADAPTIVE DIGITAL PID CONTROLLER

The adaptive digital PID controller given by Proposition 2 is a specialization of the adaptive controller given in the work of Rahman et al.[55] A more general adaptive digital PID controller can be obtained by replacing (28) with the retrospective

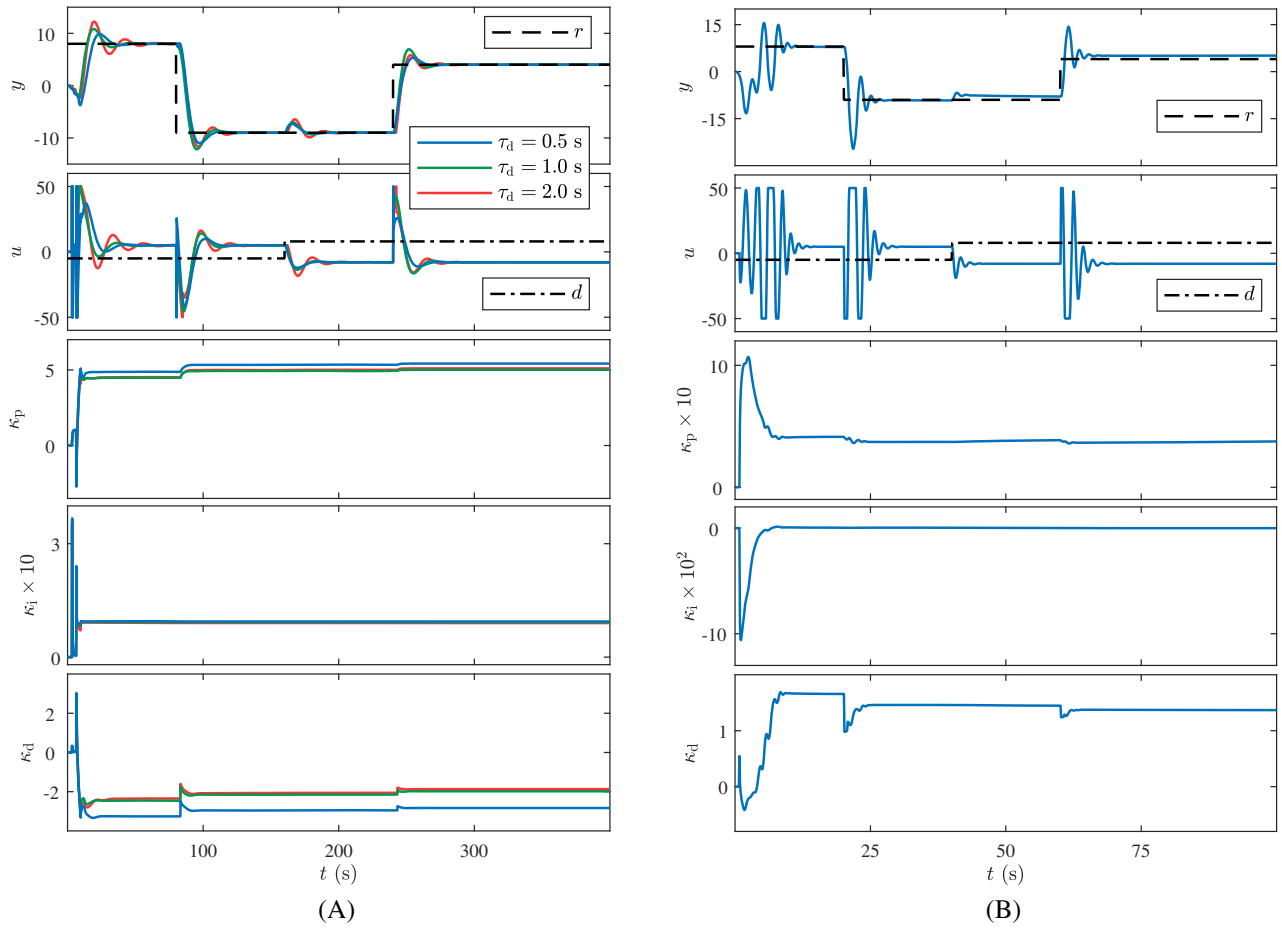

FIGURE 37 A, Example 45: Command following and disturbance rejection for the damped rigid body; B, Example 46: Command following and disturbance rejection for the undamped rigid body

performance variable

$$\hat{z}_k(\theta) \triangleq \bar{e}_k - G_f(\mathbf{q})(u_k - \phi_k\theta), \tag{67}$$

where G_f is a filter of order n_f in the forward-shift operator $\mathbf{q}$. By choosing G_f as

$$G_f(\mathbf{q}) = \sum_{i=1}^{n_f} \frac{N_i}{\mathbf{q}^i}, \tag{68}$$

(67) becomes

$$\hat{z}_k(\theta) = \bar{e}_k - N(U_k - \Phi_k\theta), \tag{69}$$

where

$$N \triangleq \begin{bmatrix} N_1 & \dots & N_{n_f} \end{bmatrix} \in \mathbb{R}^{1\times n_f}, \quad U_k \triangleq \begin{bmatrix} u_{k-1} \\ \vdots \\ u_{k-n_f} \end{bmatrix} \in \mathbb{R}^{n_f}, \quad \Phi_k \triangleq \begin{bmatrix} \phi_{k-1} \\ \vdots \\ \phi_{k-n_f} \end{bmatrix} \in \mathbb{R}^{n_f\times 3}. \tag{70}$$

With this extension, (31), (30) are replaced by

$$P_{k+1} = P_k - \frac{1}{1 + N\Phi_k P_k \Phi_k^{\mathrm{T}} N^{\mathrm{T}}} P_k \Phi_k^{\mathrm{T}} N^{\mathrm{T}} N \Phi_k P_k, \tag{71}$$

$$\theta_{k+1} = \theta_k + P_{k+1}\Phi_k^{\mathrm{T}} N^{\mathrm{T}}(\bar{e}_k - NU_k + N\Phi_k\theta_k). \tag{72}$$

In the case of a known delay of n_d samples, the filter $G_f(\mathbf{q}) = \frac{N_d}{\mathbf{q}^{n_d}}$ may be suitable. Finally, as shown in the work of Rahman et al,[55] including the nonminimum-phase zeros of the plant in the numerator of G_f helps to avoid unstable pole-zero cancelation.

14 | CONCLUSIONS AND FUTURE RESEARCH

A theoretical challenge arising from this numerical study is the need to prove the SBC. A reasonable starting point is to assume that $\mathcal{H}$, $\mathcal{W}$, and $\mathcal{L}$ are absent and that r is feasible so that antiwindup is not needed. In this case, it may be possible to construct a discrete-time Lyapunov function to prove asymptotic command following and disturbance rejection. A proof for the case involving $\mathcal{H}$, $\mathcal{W}$, and $\mathcal{L}$ under antiwindup control is likely to be significantly more challenging.

Assuming that SBC is true, an interesting problem is to determine the class of nonmonotonic $\mathcal{H}$, $\mathcal{W}$, and $\mathcal{L}$ under which command following and disturbance rejection can be achieved. In addition, the examples suggest that some of the assumptions, such as (A14), are necessary for asymptotic command following. Furthermore, for higher-order dynamics with zeros, the extension of Proposition 2 given in Section 13 provides a starting point for generalizing SBC to larger classes of SISO and MIMO plants.

As another extension of this work, variations of RLS may be useful for improving the performance and robustness of the adaptive digital PID algorithm. For example, variable-rate forgetting is a promising candidate.[85-89]

Finally, the numerical examples given in this paper to support SBC provide a systematic numerical exploration of the robustness of the adaptive digital PID controller under a wide range of conditions that may arise in practice. The next step in this research is to experimentally apply this technique to physical systems that are subject to real-world off-nominal conditions.

ACKNOWLEDGEMENTS

This research was supported by AFOSR under DDDAS grant FA9550-18-1-0171 and ONR under grants N00014-18-1-2211 and N00014-19-1-2273. The authors thank Mario Santillo for helpful suggestions and Nima Mohseni for providing (58).

ORCID

Mohammadreza Kamaldar https://orcid.org/0000-0002-4774-9794
Syed Aseem Ul Islam https://orcid.org/0000-0001-8075-2170
Dennis S. Bernstein https://orcid.org/0000-0003-0399-3039

REFERENCES

1. Francis B, Sebakhy OA, Wonham WM. Synthesis of multivariable regulators: the internal model principle. *Appl Math Optim*. 1974;1(1):64-86.
2. Silva GJ, Datta A, Bhattacharyya SP. New results on the synthesis of PID controllers. *IEEE Trans Autom Control*. 2002;47(2):241-252.
3. Ang KH, Chong G, Li Y. PID control system analysis, design, and technology. *IEEE Trans Control Syst Technol*. 2005;13(4):559-576.
4. Yu C-C. *Autotuning of PID Controllers: A Relay Feedback Approach*. London, UK: Springer; 2006.
5. Visioli A. *Practical PID Control*. London, UK: Springer Science & Business Media; 2006.
6. O'Dwyer A. *Handbook of PI and PID Controller Tuning Rules*. 3rd ed. London, UK: Imperial College Press; 2009.
7. Vilanova R, Visioli A. *PID Control in the Third Millennium*. London, UK: Springer; 2012.
8. Díaz-Rodríguez I, Han S, Bhattacharyya SP. *Analytical Design of PID Controllers*. Basel, Switzerland: Springer; 2019.
9. Maxim A, Copot D, Copot C, Ionescu C. The 5W's for control as part of industry 4.0: why, what, where, who, and when–a PID and MPC control perspective. *Inventions*. 2019;4(1):10.
10. Åström KJ, Hägglund T. *PID Controllers: Theory, Design, and Tuning*. Research Triangle Park, NC: Instrument Society of America (ISA); 1995.
11. Keel LH, Mitra S, Bhattacharyya SP. Data driven synthesis of three term digital controllers. *SICE J Control Meas Syst Integr*. 2008;1(2):102-110.
12. Mizumoto I, Ikeda D, Hirahata T, Iwai Z. Design of discrete time adaptive PID control systems with parallel feedforward compensator. *Control Eng Pract*. 2010;18(2):168-176.
13. Cuoghi S, Ntogramatzidis L. Direct and exact methods for the synthesis of discrete-time proportional–integral–derivative controllers. *IET Control Theory Appl*. 2013;7(18):2164-2171.
14. Seshagiri S, Khalil HK. Robust output feedback regulation of minimum-phase nonlinear systems using conditional integrators. *Automatica*. 2005;41(1):43-54.
15. Padula F, Visioli A. Tuning rules for optimal PID and fractional-order PID controllers. *J Process Control*. 2011;21(1):69-81.
16. Zhao C, Guo L. PID controller design for second order nonlinear uncertain systems. *Sci China Inf Sci*. 2017;60(2):022201.
17. Zhang J, Guo L. Theory and design of PID controller for nonlinear uncertain systems. *IEEE Control Syst Lett*. 2019;3(3):643-648.

18. Zaccarian L, Teel AR. *Modern Anti-Windup Synthesis: Control Augmentation for Actuator Saturation*. Princeton, NJ: Princeton University Press; 2011.
19. Penttinen J, Koivo HN. Multivariable tuning regulators for unknown systems. *Automatica*. 1980;16(4):393-398.
20. Nishikawa Y, Sannomiya N, Ohta T, Tanaka H. A method for auto-tuning of PID control parameters. *Automatica*. 1984;20(3):321-332.
21. Gawthrop P. Self-tuning PID controllers: algorithms and implementation. *IEEE Trans Autom Control*. 1986;31(3):201-209.
22. Wellstead P, Zarrop MB. *Self-Tuning Systems: Control and Signal Processing*. New York, NY: John Wiley & Sons; 1991.
23. Tomei P. Adaptive PD controller for robot manipulators. *IEEE Trans Robotics Autom*. 1991;7(4):565-570.
24. Åström KJ, Hägglund T, Hang CC, Ho WK. Automatic tuning and adaptation for PID controllers-a survey. In: Dugard MM L, Landau I, eds. *Adaptive Systems in Control and Signal Processing*. Oxford, UK: Pergamon Press; 1993:371-376.
25. Schei TS. Automatic tuning of PID controllers based on transfer function estimation. *Automatica*. 1994;30(12):1983-1989.
26. Poulin E, Pomerleau A, Desbiens A, Hodouin D. Development and evaluation of an auto-tuning and adaptive PID controller. *Automatica*. 1996;32(1):71-82.
27. Logemann H, Ryan EP. Time-varying and adaptive integral control of infinite-dimensional regular linear systems with input nonlinearities. *SIAM J Control Optim*. 2000;38(4):1120-1144.
28. Benaskeur AR, Desbiens A. Backstepping-based adaptive PID control. *IEE Proc Control Theory Appl*. 2002;149(1):54-59.
29. Chang W-D, Hwang R-C, Hsieh J-G. A self-tuning PID control for a class of nonlinear systems based on the Lyapunov approach. *J Process Control*. 2002;12(2):233-242.
30. Tan KK, Huang S, Ferdous R. Robust self-tuning PID controller for nonlinear systems. *J Process Control*. 2002;12(7):753-761.
31. Parra-Vega V, Arimoto S, Liu Y-H, Hirzinger G, Akella P. Dynamic sliding PID control for tracking of robot manipulators: theory and experiments. *IEEE Trans Robotics Autom*. 2003;19(6):967-976.
32. Chang W-D, Yan J-J. Adaptive robust PID controller design based on a sliding mode for uncertain chaotic systems. *Chaos Solit Fractals*. 2005;26(1):167-175.
33. Monje CA, Vinagre BM, Feliu V, Chen Y. Tuning and auto-tuning of fractional order controllers for industry applications. *Control Eng Pract*. 2008;16(7):798-812.
34. Leva A, Negro S, Papadopoulos AV. PI/PID autotuning with contextual model parametrisation. *J Process Control*. 2010;20(4):452-463.
35. Romero JA, Sanchis R, Balaguer P. PI and PID auto-tuning procedure based on simplified single parameter optimization. *J Process Control*. 2011;21(6):840-851.
36. Boubakir A, Labiod S, Boudjema F. A stable self-tuning proportional-integral-derivative controller for a class of multi-input multi-output nonlinear systems. *J Vib Control*. 2012;18(2):228-239.
37. Shen D, Sun W, Sun Z. Adaptive PID formation control of nonholonomic robots without leader's velocity information. *ISA Transactions*. 2014;53(2):474-480.
38. Butt WA, Yan L, Amezquita SK. Adaptive integral dynamic surface control of a hypersonic flight vehicle. *Int J Syst Sci*. 2015;46(10):1717-1728.
39. Jung J-W, Leu VQ, Do TD, Kim E-K, Choi HH. Adaptive PID speed control design for permanent magnet synchronous motor drives. *IEEE Trans Power Electron*. 2015;30(2):900-908.
40. De Keyser R, Muresan CI, Ionescu CM. A novel auto-tuning method for fractional order PI/PD controllers. *ISA Transactions*. 2016;62:268-275.
41. Song Y, Guo J, Huang X. Smooth neuroadaptive PI tracking control of nonlinear systems with unknown and nonsmooth actuation characteristics. *IEEE Trans Neural Netw Learn Syst*. 2017;28(9):2183-2195.
42. Mercader P, Åström KJ, Baños A, Hägglund T. Robust PID design based on qft and convex–concave optimization. *IEEE Trans Control Syst Technol*. 2017;25(2):441-452.
43. Berner J, Soltesz K, Hägglund T, Åström KJ. An experimental comparison of PID autotuners. *Control Eng Pract*. 2018;73:124-133.
44. Habibi H, Nohooji HR, Howard I. Adaptive PID control of wind turbines for power regulation with unknown control direction and actuator faults. *IEEE Access*. 2018;6:37464-37479.
45. De Keyser R, Muresan CI, Ionescu CM. Universal direct tuner for loop control in industry. *IEEE Access*. 2019;7:81308-81320.
46. Åström KJ, Wittenmark B. On self-tuning regulators. *Automatica*. 1973;9(2):185-199.
47. Clarke DW, Gawthrop PJ. Self-tuning controller. *Proc IEE*. 1975;122(9):929-934.
48. Isermann R. On advanced methods of process computer control for industrial processes. *IFAC Proc Vol*. 1978;11(1):411-421.
49. Wellstead PE, Prager D, Zanker P. Pole assignment self-tuning regulator. *Proc IEE*. 1979;126(8):781-787.
50. Clarke DW. Self-tuning control of nonminimum-phase systems. *Automatica*. 1984;20(5):501-517.
51. Radke F, Isermann R. A parameter-adaptive PID-controller with stepwise parameter optimization. *Automatica*. 1987;23(4):449-457.
52. Chen J, Huang T-C. Applying neural networks to on-line updated PID controllers for nonlinear process control. *J Process Control*. 2004;14(2):211-230.
53. Kurokawa R, Sato T, Vilanova R, Konishi Y. Closed-loop data-driven trade-off PID control design. *IFAC-PapersOnLine*. 2018;51(4):244-249.
54. Formentin S, Campi MC, Carè A, Savaresi SM. Deterministic continuous-time Virtual Reference Feedback Tuning (VRFT) with application to PID design. *Syst Control Lett*. 2019;127:25-34.
55. Rahman Y, Xie A, Bernstein DS. Retrospective cost adaptive control: pole placement, frequency response, and connections with LQG control. *IEEE Control Syst Mag*. 2017;37:28-69.
56. Bloemen H, Van Den Boom T, Verbruggen H. Model-based predictive control for Hammerstein? Wiener systems. *Int J Control*. 2001;74(5):482-495.

57. O'Dwyer A. PI and PID controller tuning rules for time delay processes: a summary. Part 2: PID controller tuning rules. In: Proceedings of the Irish Signals and Systems Conference; 1999; Galway, Ireland.
58. Åström KJ, Hägglund T. Revisiting the Ziegler–Nichols step response method for PID control. *J Process Control*. 2004;14(6):635-650.
59. Cogan B, de Paor AM, Quinn A. PI control of first-order lag plus time-delay plants: root locus design for optimal stability. *Trans Inst Meas Control*. 2009;31(5):365-379.
60. Gherfi K, Charef A, Abbassi HA. Proportional integral-fractional filter controller design for first order lag plus time delay system. *Int J Syst Sci*. 2018:1-20.
61. Luyben WL. Effect of derivative algorithm and tuning selection on the PID control of dead-time processes. *Ind Eng Chem Res*. 2001;40(16):3605-3611.
62. Xiang G, Yang Y, Yang Q. Twice optimum control for a kind of first order systems with dead-time. *Inf Control*. 1995;4.
63. Shinskey FG. PID-deadtime control of distributed processes. *Control Eng Pract*. 2001;9(11):1177-1183.
64. Roy A, Iqbal K. PID controller tuning for the first-order-plus-dead-time process model via Hermite-Biehler theorem. *ISA Transactions*. 2005;44(3):363-378.
65. Normey-Rico JE, Camacho EF. *Control of Dead-Time Processes*. London, UK: Springer Science & Business Media; 2007.
66. Yuan J, Chen Y, Fei S. Analysis of actuator rate limit effects on first-order plus time-delay systems under fractional-order proportional-integral control. *IFAC-PapersOnLine*. 2018;51(4):37-42.
67. Onat C. A new design method for PI–PD control of unstable processes with dead time. *ISA Transactions*. 2019;84:69-81.
68. da Silva LR, Flesch RCC, Normey-Rico JE. Controlling industrial dead-time systems: When to use a PID or an advanced controller. *ISA Transactions*. 2019.
69. Sato T, Hayashi I, Horibe Y, Vilanova R, Konishi Y. Optimal robust PID control for first-and second-order plus dead-time processes. *Applied Sciences*. 2019;9(9):1934.
70. Kurokawa R, Sato T, Vilanova R, Konishi Y. Discrete-time first-order plus dead-time model-reference trade-off PID control design. *Applied Sciences*. 2019;9(16):3220.
71. Birs I, Muresan C, Nascu I, Ionescu C. A survey of recent advances in fractional order control for time delay systems. *IEEE Access*. 2019;7:30951-30965.
72. Astrom KJ, Hang CC, Lim BC. A new Smith predictor for controlling a process with an integrator and long dead-time. *IEEE Trans Autom Control*. 1994;39(2):343-345.
73. Åström KJ, Hägglund T. The future of PID control. *Control Eng Pract*. 2001;9(11):1163-1175.
74. Tan F, Li H-X, Shen P. Smith predictor-based multiple periodic disturbance compensation for long dead-time processes. *Int J Control*. 2018;91(5):999-1010.
75. Porter B, Jones AH. Genetic tuning of digital PID controllers. *Electronics Letters*. 1992;28(9):843-844.
76. Keel LH, Rego JI, Bhattacharyya SP. A new approach to digital PID controller design. *IEEE Trans Autom Control*. 2003;48(4):687-692.
77. Åström KJ, Wittenmark B. *Computer-Controlled Systems: Theory and Design*. 3rd ed. Mineola, NY: Dover Publications; 2013.
78. Jury EI. *Inners and Stability of Dynamic Systems*. Malabar, FL: Krieger Publishing; 1982.
79. Franklin GF, Powell JD, Workman ML. *Digital Control of Dynamic Systems*. Boston, MA: Addison Wesley Longman; 1998.
80. Islam SAU, Bernstein DS. Recursive least squares for real-time implementation. *IEEE Control Syst Mag*. 2019;39:82-85.
81. Ljung L, Söderström T. *Theory and Practice of Recursive Identification*. Cambridge, MA: MIT Press; 1985.
82. Lennartson B, Soderstrom T. Investigation of the intersample variance in sampled-data control. *Int J Control*. 1989;50(5):1587-1602.
83. Shats S, Shaked U. Exact discrete-time modelling of linear analogue systems. *Int J Control*. 1989;49(1):145-160.
84. Osburn SL, Bernstein DS. An exact treatment of the achievable closed-loop H_2 performance of sampled-data controllers: from continuous-time to open-loop. In: Proceedings of the 32nd IEEE Conference on Decision and Control; 1993; San Antonio, TX.
85. Fortescue TR, Kershenbaum LS, Ydstie BE. Implementation of self-tuning regulators with variable forgetting factors. *Automatica*. 1981;17(6):831-835.
86. Canetti RM, España MD. Convergence analysis of the least-squares identification algorithm with a variable forgetting factor for time-varying linear systems. *Automatica*. 1989;25(4):609-612.
87. Dayal BS, MacGregor JF. Recursive exponentially weighted PLS and its applications to adaptive control and prediction. *J Process Control*. 1997;7(3):169-179.
88. Leung S-H, So CF. Gradient-based variable forgetting factor RLS algorithm in time-varying environments. *IEEE Trans Signal Process*. 2005;53(8):3141-3150.
89. Paleologu C, Benesty J, Ciochina S. A robust variable forgetting factor recursive least-squares algorithm for system identification. *IEEE Signal Process Lett*. 2008;15:597-600.

How to cite this article: Kamaldar M, Islam SAU, Sanjeevini S, Goel A, Hoagg JB, Bernstein DS. Adaptive digital PID control of first-order-lag-plus-dead-time dynamics with sensor, actuator, and feedback nonlinearities. *Adv Control Appl*. 2019;1:e20. https://doi.org/10.1002/adc2.0020